THESIS FOR THE DEGREE OF DOCTOR OF PHILOSOPHY (PhD)

Thermogenic regulation of human abdominal and neck area derived adipocytes by mitophagy, irisin and BMP7

by

Abhirup Shaw

Supervisor: Prof. Dr. László Fésüs

UNIVERSITY OF DEBRECEN

DOCTORAL SCHOOL OF MOLECULAR, CELL AND IMMUNE BIOLOGY

DEBRECEN, 2022

Table of contents

List of figures and tables

List of abbreviations

UCP1 - Uncoupling protein 1
WAT - White adipose tissue
BAT – Brown adipose tissue
ANOVA - Analysis of variance
ADP/ATP - Adenosine diphosphate/Adenosine triphosphate
β-GPA – β/3-Guanidinopropionic acid
BMI - Body mass index
BMP - Bone morphogenetic protein
cAMP - 3',5'-cyclic adenosine monophosphate
CIDEA - Cell Death-Inducing DFFA-Like Effector A
CKMT1/2 - Creatine Kinase, Mitochondrial ½
CNS - Central nervous system
CREB - cAMP Response Element Binding Protein
Ct - Threshold cycle
DMEM - Dulbecco's modified Eagle's medium
DMSO - Dimethyl sulfoxide
DNA – Deoxyribonucleic acid
ELISA - Enzyme-linked immunosorbent assay
FBS - Fetal bovine serum
FNDC5 - Fibronectin Type III Domain Containing 5
GAPDH - Glyceraldehyde-3-Phosphate Dehydrogenase
GLUT4 - Glucose transporter type 4
IBMX - 3-Isobutyl-1-methylxantin
IL - Interleukin
LSC - Laser-scanning cytometry
MAPK - Mitogen-activated protein kinase
MCP-1 - Monocyte Chemotactic Protein-1 (C-C Motif Chemokine Ligand 2)
NAD+/NADH - Nicotinamide adenine dinucleotide
NE – Norepinephrine
NST - Non-shivering thermogenesis
OCR - Oxygen consumption rate
PBS - Phosphate Buffered Saline
PCr – Phospho-creatine
PCR - Polymerase chain reaction
PET/CT - Positron emission tomography/computed tomography
PGC-1α - PPARγ Coactivator-1α
PKA/PKC - Protein Kinase A/C
PPARγ - Peroxisome Proliferator Activated Receptor Gamma
PRDM16 - PR Domain 16 PVDF - Polyvinylidene fluoride
RNA - Ribonucleic acid
SD - Standard deviation
SDS - Sodium dodecyl-sulphate
SNS - Sympathetic nervous system
SVF - Stromal-vascular fraction
T3 - 3,3′,5-Triiodo-L-thyronine
TGF-β - Transforming growth factor-beta
TOM20 – Translocase of outer mitochondrial membrane 20
TNFα - Tumour necrosis factor alpha
^{18}F-FDG - ^{18}F-fluorodeoxyglucose
^{123}I-MIBG - ^{123}I-meta-iodobenzylguanidine

Keywords

Obesity, adipocytes, thermogenesis, UCP1, creatine futile cycle, irisin, BMP7, cAMP, mitophagy, cytokines, CXCL1, angiogenesis

1. Introduction and theoretical background

1.1. Obesity and the role of thermogenic adipocytes

Obesity, defined by disproportionate body weight for height with an excessive accumulation of adipose tissue, is considered by many as a 21st century epidemic (González-Muniesa et al., 2017). Incidence of obesity is increasing globally over the past decades (Figure 1). It is the sixth important risk factor contributing to the overall disease burden worldwide. Obesity is a major risk factor for various metabolic diseases, type 2 diabetes, coronary heart disease and certain cancers (González-Muniesa et al., 2017; Park et al., 2011). Obese patients have up to 3 times higher risk for relative morbidity than people with normal body weight for other components of metabolic syndrome (Bényi et al., 2012).

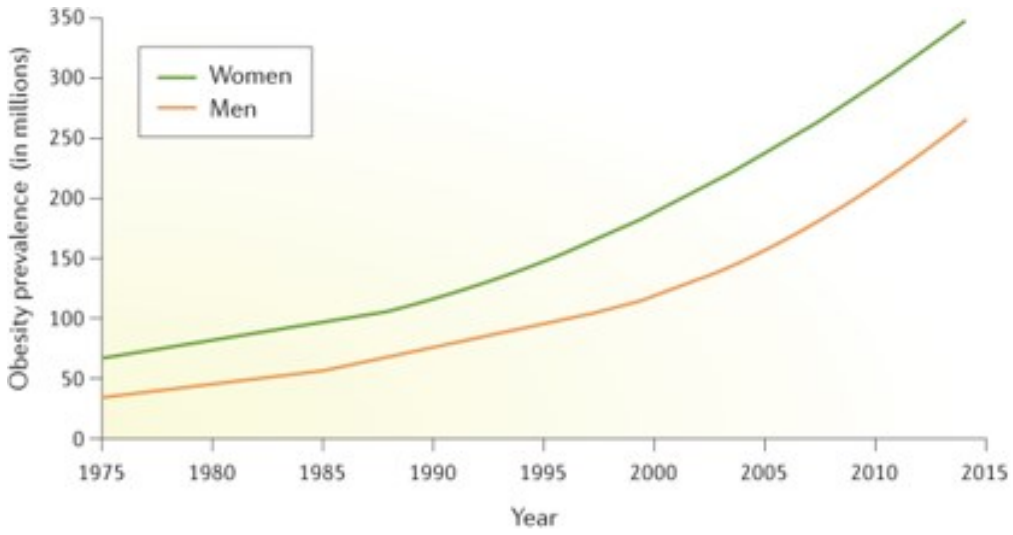

Figure 1: Prevalence of obesity worldwide. Global incidence of obesity has vastly increased over the past few decades, however effective therapeutic targets are limited. (González-Muniesa et al., 2017)

Although the prevalence of obesity is increasing worldwide, available effective therapeutic targets are limited. Thermogenic beige and brown adipocytes play an important role in combating obesity. Recent studies using radiolabelled substrates like ^{18}F-FDG and ^{123}I-MIBG identified metabolically active brown adipose tissue (BAT) in healthy humans that can dissipate energy into heat. PET/CT found these thermogenic fat depots to be interspersed into six anatomic depots: cervical, supraclavicular, axillary, paraspinal, mediastinal, and abdominal (Figure 2) (Admiraal et al., 2013; Cypess et al., 2009; Hany et al., 2002; Nedergaard et al.,

2007; Saito et al., 2009; van Marken Lichtenbelt et al., 2009; Virtanen et al., 2009). These thermogenic fat depots are predicted to account for up to 5% of basal metabolic rate in healthy adults that would result in 4kg of fat loss per year (Rosen & Spiegelman, 2014; van Marken Lichtenbelt & Schrauwen, 2011). Studies have also shown a strong negative corelation between obesity or glucose intolerance and amount of active BAT in humans (Chondronikola et al., 2014; Lee et al., 2010; Lee et al., 2014; Matsushita et al., 2014; Ouellet et al., 2011; Yoneshiro et al., 2013). Hence stimulation of BAT might be an important therapeutic application for obesity treatment (Lee et al., 2013; Lichtenbelt et al., 2014; Schrauwen et al., 2015; Whittle et al., 2011).

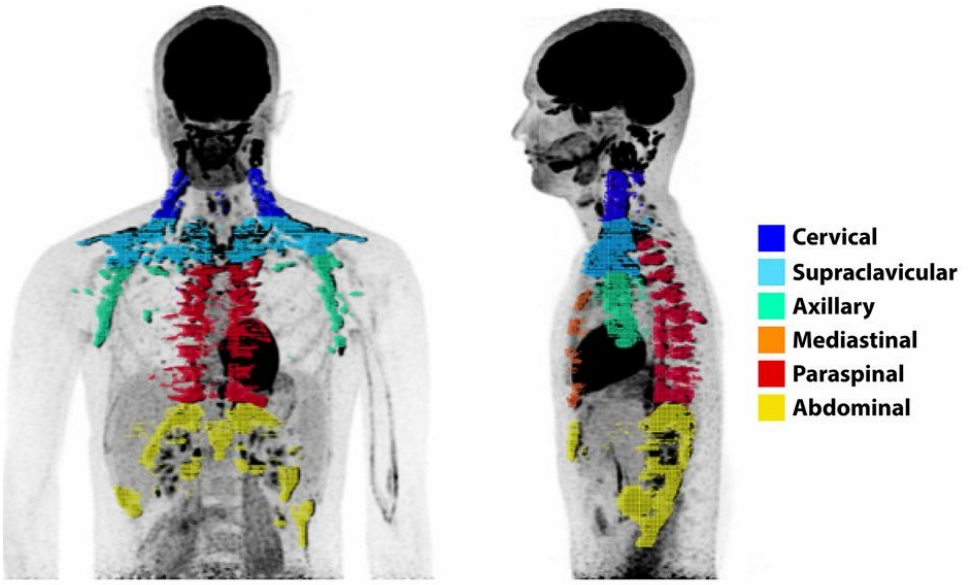

Figure 2: Distribution of active BAT in humans. Active BAT can be detected in six distinct anatomic depots. (Leitner et al., 2017)

1.2. Types of adipocytes

Adipocytes can be broadly classified into three types: white adipocytes, brown adipocytes, and beige adipocytes (Figure 3).

White adipocytes containing an unilocular lipid droplet are the most abundant type of adipocytes. They primarily function as a storehouse of excess energy in the form of lipid droplets (Sanchez-Gurmaches et al., 2016). Major white adipose tissue (WAT) depots in

humans are generally identified as subcutaneous and visceral. Excess of visceral WAT has been linked to various metabolic dysfunctions (Meisinger et al., 2006; Pischon et al., 2008).

Brown adipocytes are distinguished by their abundant mitochondria and presence of multilocular lipid droplets. White and brown adipocytes both accumulate triglycerides in their cytoplasm; while white adipocytes form unilocular lipid droplets, brown adipocytes form multilocular lipid droplets. Brown adipocytes have high expression of uncoupling protein 1 (UCP1), an inner mitochondrial membrane protein, that when activated is involved in non-shivering thermogenesis (Cannon & Nedergaard, 2004).

Studies have shown the presence of "brown adipocyte-like" cells in murine WAT depots upon cold exposure, that possessed multilocular morphology and mitochondria with high UCP1 content (Cinti, 2005; Cousin et al., 1992; Granneman et al., 2005; Himms-Hagen et al., 2000; Young et al., 1984). In the recent period considerable attention has been paid in understanding this group of adipocytes termed as "beige" adipocytes. Earlier formation of beige adipocytes was assumed to be reversible transdifferentiation of white to brown adipocytes (De Matteis et al., 2002; Granneman et al., 2005; Himms-Hagen et al., 2000). However recent studies using mouse models showed that beige adipocytes arose from a distinct precursor in response to stimuli like cold, diet, exercise, and it was partially regulated by the β3-adrenergic signalling pathway (Harms & Seale, 2013; Lee et al., 2012; Petrovic et al., 2010; Seale et al., 2011; Wang et al., 2013; Wu et al., 2012).

Beige and white adipocytes are derived from the same mesenchymal precursors, but the beige adipocytes exist in a masked condition in subcutaneous WAT depots when adrenergic stimulation is absent (Kajimura et al., 2015). Studies have shown that certain genetic factors like rs1421085 T-to-C single-nucleotide variant can influence the differentiation of mesenchymal precursors into either beige or white adipocytes (Claussnitzer et al., 2015). Obese individuals possess less BAT, but high amount of brownable fat enriched with beige adipocytes (Leitner et al., 2017). However, these beige adipocytes are undergoing transition to white adipocytes as a result of high level of ongoing autophagy/mitophagy, as indicated by the higher expression of ATG genes in subcutaneous WAT of obese individuals (Haim et al., 2015; Kosacka et al., 2015). A recent study has shown that beige adipocytes can transition to white upon removal of adrenergic stimulus and mitophagy plays an important role in the transition (Altshuler-Keylin et al., 2016).

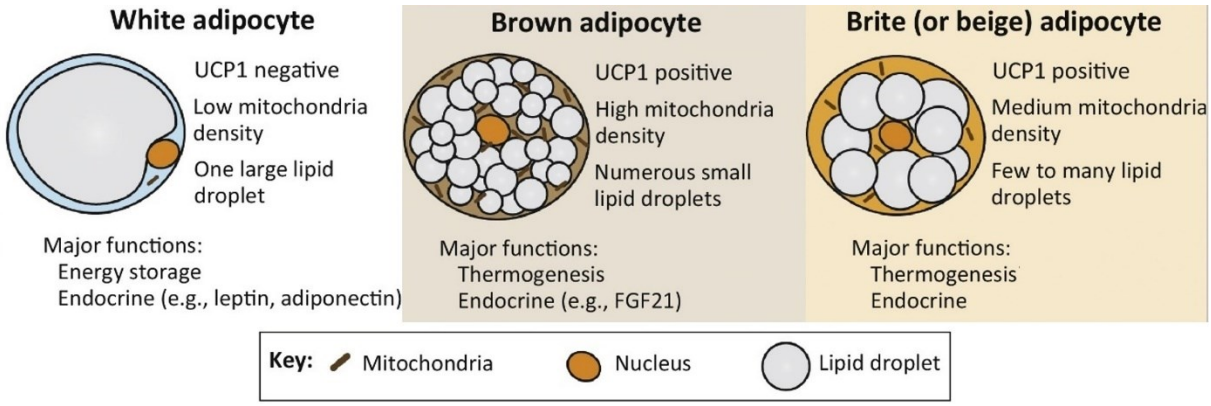

Figure 3: Types of adipocytes (summary). Differentiated adipocytes can be broadly classified into three subtypes like white, brown or beige adipocytes. Brown and beige adipocytes serve as an important tool to release excess stored energy via thermogenesis. (Sanchez-Gurmaches et al., 2016)

1.3. Uncoupling protein 1 (UCP1) mediated thermogenesis

UCP1 is an inner mitochondrial membrane protein that is primarily responsible for the thermogenic function of BAT (Heaton et al., 1978). The mitochondrial electron transport chain transports protons to the intermembrane space, thereby creating a proton gradient across the inner membrane, which drives ATP synthesis (Figure 4A). UCP1 is a member of mitochondrial carrier protein family that can uncouple mitochondrial ATP synthesis from the respiratory chain, thereby decreasing the proton gradient across the inner mitochondrial membrane and generating heat (Figure 4B) (Jacobsson et al., 1985; Lin & Klingenberg, 1980; Nicholls, 1976; Nicholls & Locke, 1984; Ricquier et al., 1979). β3-adrenergic stimulation triggers the formation of long-chain fatty acids from triglycerides upon cleavage by hormone sensitive lipase, that in turn leads to activation of UCP1 (Chaudhry & Granneman, 1999; Matthias et al., 2000; Prusiner et al., 1968; Shih & Taberner, 1995). Fatty acids permanently associated with UCP1 by hydrophobic interactions function as proton carriers though UCP1 across the inner mitochondrial membrane. The protons are released in the mitochondrial matrix; however, the fatty acid anion stays associated with UCP1 to continue the proton transfer cycle (Fedorenko et al., 2012). Thus, UCP1 leads to energy dissipation as heat generated from β-oxidation of fatty acids.

1.4. Futile creatine cycle mediated thermogenesis and other UCP1-independent thermogenic mechanisms

UCP1 has been well established as an important component of non-shivering thermogenesis. However, UCP1 knockout mice were seen to be able to tolerate chronic cold exposure, if the temperature change was gradual (Golozoubova et al., 2001). This created a gap in understanding the mechanisms of thermogenesis. Recent studies indicated that proteins involved in creatine synthesis and phosphorylation were elevated in beige fat mitochondria (Kazak et al., 2015; Kazak & Cohen, 2020; Roesler & Kazak, 2020). The findings hinted towards a futile creatine phosphorylation and dephosphorylation cycle that has the capacity to mediate thermogenesis in beige fat. In this cycle, first creatine is phosphorylated by creatine kinase using ATP. Following that, the high energy phosphate is immediately hydrolysed generating heat (Figure 4C). Recent studies indicated that the phosphatase involved in the dephosphorylation may most likely be the tissue-nonspecific alkaline phosphatase (TNAP) (Sun et al., 2021). Studies showed that the level of mitochondrial creatine kinase 2 (CKMT2) was elevated in beige fat (Kazak et al., 2015). A very recent study indicated that the cytosolic creatine kinase B (CKB) is targeted to mitochondria and plays a vital role in the creatine cycle (Rahbani et al., 2021). Further research is necessary to identify all the components involved in this newly discovered mechanism for thermogenesis.

A similar thermogenic futile cycle is mediated by the calcium ion (Ca^{2+}) cycling by the Ca^{2+} ATPase SERCA. SERCA pumps calcium ions into the sarcoplasmic reticulum that is followed by leakage of Ca^{2+} into the cytoplasm (Block, 1994; Block et al., 1994). Sarcolipin uncouples SERCA-mediated ATP hydrolysis from calcium ion pumping resulting in generation of heat. Although SERCA mediated thermogenesis is mostly active in skeletal muscle cells, studies have shown this mechanism to be active in BAT as well (Bal et al., 2012; de Meis et al., 2006).

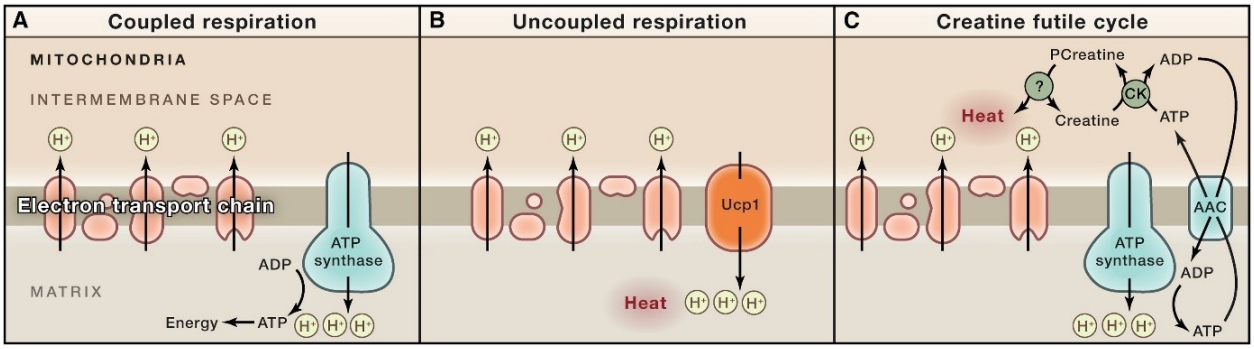

Figure 4: Types of mitochondrial respiration. (A) Coupled respiration, (B) Uncoupled respiration and (C) Creatine futile cycle. Both uncoupled respiration and futile creatine cycle plays an important role in mediating non-shivering thermogenesis. (Reilly & Saltiel, 2015)

1.5. Mitophagy and maintenance of thermogenic beige adipocytes

Mitochondria plays an important role in driving thermogenesis of beige and brown adipocytes. Mitochondria can change their morphology via fusion or fission to shift between large networks of elongated and fragmented units (Liesa & Shirihai, 2013). Rodent brown adipocytes develop high rate of mitochondria fragmentation upon adrenergic stimulation that results in enhanced mitochondrial uncoupling mediated energy expenditure (Liesa & Shirihai, 2013; Wikstrom et al., 2014). UCP1 enriched mitochondria in humans are mostly fragmented (Pisani et al., 2018). Mitochondrial turnover is essential for maintaining cellular homeostasis, that is tightly regulated by biogenesis and selective degradation (Palikaras & Tavernarakis, 2014). Mitochondrial biogenesis is precisely controlled by several nuclear-coded transcriptional regulators, like the peroxisome proliferator–activated receptor γ coactivator 1α (PGC-1α), the mitochondrial transcription factor A (Tfam), the nuclear respiratory factor (Nrf) 1 and Nrf2 (Kelly & Scarpulla, 2004).

Autophagy is an evolutionary conserved mechanism by which unwanted and damaged cellular components are digested and recycled intracellularly in eukaryotic cells. During autophagy, unwanted or damaged proteins or organelles are engulfed by a double membrane vesicle called autophagosome, in order to be delivered to the lysosome for degradation (Füllgrabe et al., 2014). Autophagosome biogenesis is mediated by proteins encoded by autophagy-related genes (ATG). During autophagosome formation the most important step is the conjugation of microtubule-associated protein 1 light chain 3 (LC3-I) to the phosphatidylethanolamine (PE), that results in the formation of the lipidated LC3-II, which is then inserted into autophagosomes.

LC3 is the most commonly used marker for autophagosomes, as the amount of LC3-II corelates with the number of autophagosomes (Figure 5) (Lamb et al., 2013). A well accepted method to monitor autophagic activity is the conversion of LC3-I to LC3-II by western blot analysis. Increased ratio of LC3-II/LC3-I indicates a high level of ongoing autophagy (Mizushima et al., 2010). Autophagic flux is a measure of the autophagic degradation activity. Chloroquine (CQ) inhibits the last stage of autophagy, hence preventing the degradation of autophagic cargo and LC3-II. Thus, application of CQ is a convenient tool to measure autophagic flux (Yoshii & Mizushima, 2017). p62 is an autophagy adapter protein that functions as a link between LC3 and the ubiquitinated targets. p62 is continuously degraded during autophagy, hence a lower level of p62 indicates higher autophagic activity and vice versa (Pankiv et al., 2007).

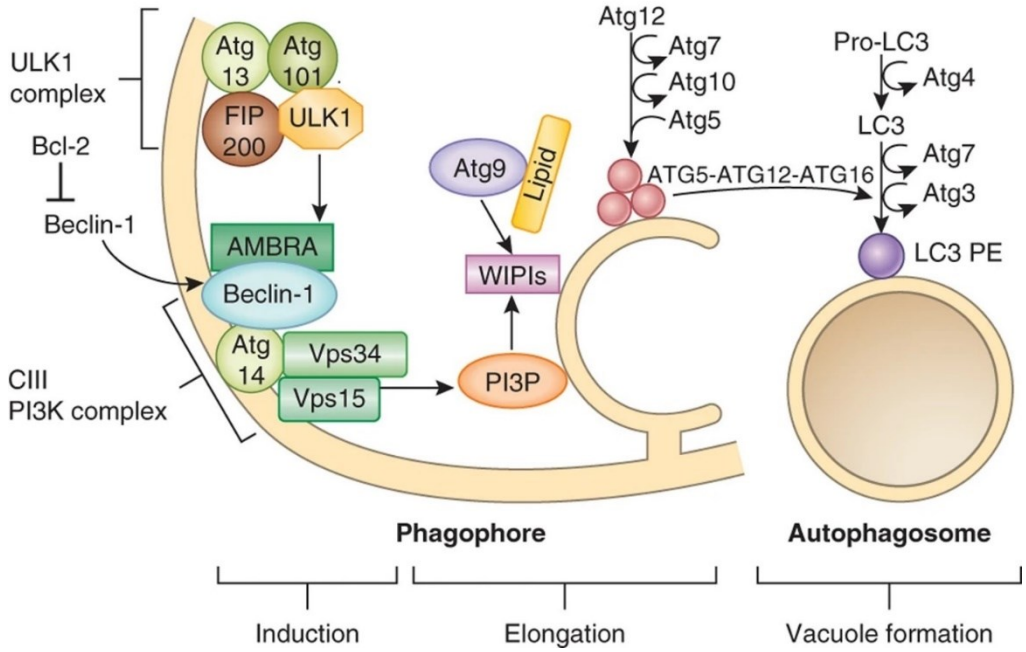

Figure 5: Overview of the autophagy machinery. ATG genes play an important role in the induction and elongation phase. Lipidated LC3 is recruited on the outer wall of autophagosome that marks it for lysosomal degradation. (Nixon, 2013)

Mitophagy or the selective degradation of unwanted and damaged mitochondria by autophagy is an essential quality control mechanism that helps to maintain a healthy and functional mitochondrial network (Kim et al., 2007; Palikaras et al., 2018). Mitophagy is triggered by the reduction of mitochondrial membrane potential and occurs primarily via parkin dependent and independent mechanisms (Figure 6). The parkin mediated mitophagy mechanism is initiated by stabilization of PINK1 (PTEN (phosphatase and tensin homolog)-induced putative kinase 1) on

the outer mitochondrial membrane (OMM). This is followed by the recruitment of parkin, that in turn ubiquitinates OMM proteins (Matsuda et al., 2010; Narendra et al., 2008). Selective autophagy adaptor proteins, like NBR1 (neighbour of Brca1 gene 1), p62 (SQSTM1), OPTN (optineurin) and NDP52 (nuclear dot protein 52) act as bridges between the ubiquitinated mitochondrial proteins and LC3 to mediate the engulfment of mitochondria into autophagosomes (Figure 6A) (Lazarou et al., 2015). Mitophagy can also occur independent of parkin mediated ubiquitination through the direct interaction of LC3 with mitochondria-localized proteins, (Figure 6B) like FUNDC1 (FUN14 domain-containing protein1), BNIP3 (BCL2 Interacting Protein 3), BCL2L13 (Bcl-2-Like Protein 13) and NIX (BNIP3 homology NIP3-like protein X) (Hamacher-Brady & Brady, 2016). Recent studies in mice have indicated that beige adipocytes can convert to white upon removal of adrenergic stimulation via mitophagy mediated selective clearance of the mitochondria (Altshuler-Keylin et al., 2016).

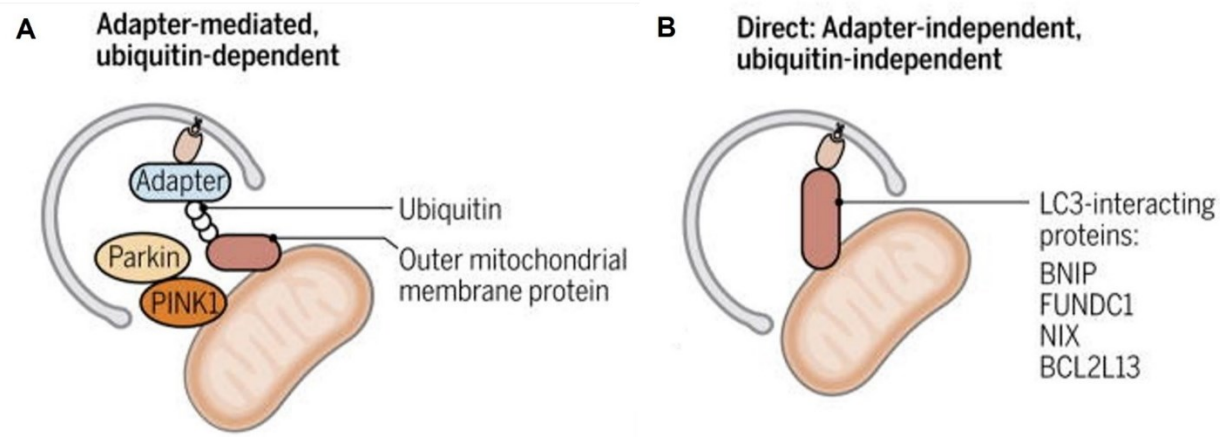

Figure 6: Types of mitophagy.

Mitophagy is mediated via two distinct mechanisms. (A) Parkin dependent (adapter-mediated) and (B) Parkin independent (adapter-independent) pathways (Altshuler-Keylin & Kajimura, 2017)

1.6. Brown adipose tissue as an endocrine organ

BAT is an important mediator of adaptive thermogenesis and increased BAT activity has been shown to exert a protective role against obesity and other metabolic disorders like type 2 diabetes. Recent studies suggest a secretory role of BAT that can contribute to the systemic effects of BAT activity (Villarroya et al., 2019). Specific adipokines released by BAT, termed as batokines, mediate their effects in autocrine, paracrine or endocrine manner (Villarroya et al., 2019). Batokines have been shown to promote hypertrophy and hyperplasia of BAT, vascularization, innervation and blood flow that will assist in improving thermogenesis (Villarroya et al., 2017; Villarroya et al., 2019). Vascular endothelial growth factor A (VEGFA), secreted by brown adipocytes promotes angiogenesis and vascularization of BAT (Mahdaviani et al., 2016; Sun et al., 2014; Xue et al., 2009). Fibroblast growth factor (FGF) 21 is another important batokine that enhances the beiging of WAT in animal studies (Cuevas-Ramos et al., 2019) and improves BAT thermogenesis (Hondares et al., 2011; Ruan et al., 2018; Wang et al., 2015).

1.7. Browning inducers and thermogenic activators

Upon cold exposure in animals, the cold is perceived by transient receptor potential (TRP) channels. TRPs are membrane proteins whose major function is to communicate the changes in the environment (Dhaka et al., 2006). Cold activated TRPs activate the sympathetic nerves entering BAT (Nakamura, 2011). Noradrenaline (NA) is then released from the sympathetic nerve endings which activates the β-adrenoreceptors, which in turn activates the adenyl cyclase leading to increased intracellular cAMP levels. cAMP activates intracellular events like hydrolysis of triglyceride, oxidation of fatty acids and activation of UCP1 leading to improved thermogenesis in both mouse and humans (Inokuma et al., 2005; Saito et al., 2020).

Insulin signalling has been shown to play a crucial role in glucose uptake and storage of lipid droplets in both white and brown adipocytes, which occurs via the upregulation and transfer of Glucose transporter type 4 (GLUT4) to the plasma membrane (Omatsu-Kanbe et al., 1996; Slot et al., 1991; Teruel et al., 1996). Leptin that acts as an appetite supressing hormone secreted by adipocytes, has been shown to enhance BAT thermogenesis by activating SNS via the release of melanocyte-stimulating hormone in the hypothalamus (Commins et al., 2001; Halaas et al., 1995; Minokoshi et al., 1999; Pelleymounter et al., 1995; Satoh et al., 1998). Thyroid hormones have also shown to elevate heat production that was suggested to be peripherally mediated (Abelenda & Puerta, 1992; Branco et al., 1999; Heick et al., 1973; Sundin, 1981). However,

recent studies indicated that T3 inhibits AMPK in the ventromedial hypothalamus resulting in SNS activation leading to improved thermogenic capacity in mice. The central effects of thyroid hormones seem to be more significant than their peripheral action on non-shivering thermogenesis mediated regulation of energy balance (Alvarez-Crespo et al., 2016; López et al., 2010; Nedergaard et al., 1997).

1.8. Irisin

Physical exercise has been shown to mediate beneficial metabolic effects and offer protection against various pathological conditions, neurodegenerative disorders and certain cancers (Brandt & Pedersen, 2010; Mathur & Pedersen, 2008). Physical exercise stimulates the release of certain hormones from skeletal and cardiac muscles termed "myokines" that mediates the crosstalk between brain, muscle, adipose tissue, and in turn regulates browning (Contreras et al., 2015; Febbraio & Pedersen, 2002; Gamas et al., 2015; Pedersen & Febbraio, 2012). Irisin was discovered as a myokine that is cleaved from Fibronectin Type III Domain Containing 5 (FNDC5) transmembrane protein and was able to induce a beige differentiation program in mice WAT (Figure 7) (Boström et al., 2012). Physical exercise upregulates PGC-1α in skeletal myocytes, that in turn upregulates FNDC5; cleavage of FNDC5 leads to the release of irisin in circulation (Boström et al., 2012). A recent study has indicated that irisin exerts its effect via the integrin receptors: integrin subunit alpha V (ITGAV) and integrin subunit beta (ITGB) 1/3/5 (ITGB1/3/5) (Kim et al., 2018). Irisin mediates its positive effects on browning via the p38 MAPK and ERK pathways (Zhang et al., 2014).

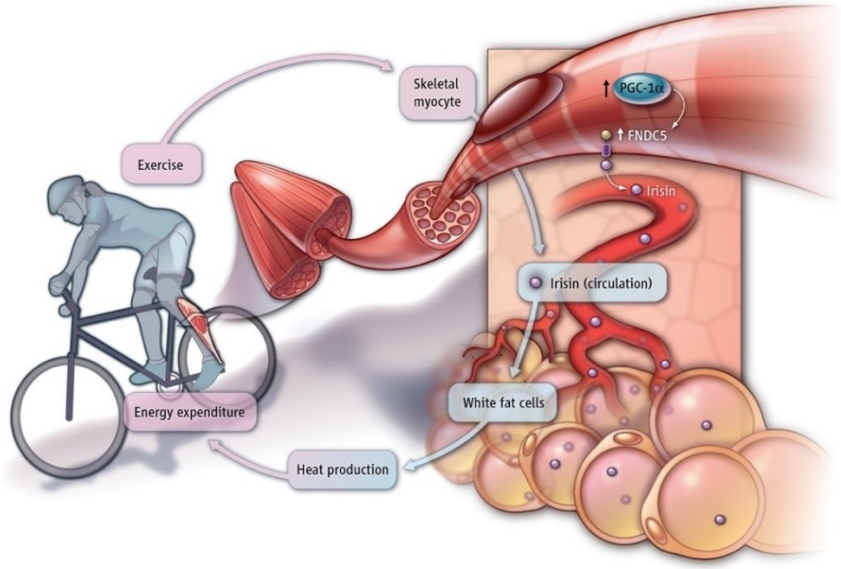

Figure 7: Irisin acts as an inducer of browning in human subcutaneous WAT (Kelly, 2012)

1.9. BMP7

Bone morphogenic protein (BMP) 7 acts as an auto/paracrine mediator that drives classical brown adipocyte differentiation in mice (Tseng et al., 2008). BMP7 has been shown to promote differentiation of brown preadipocytes from embryonic stem cells even in absence of an adipogenic differentiation medium (Figure 8). BMPs exert its effect via heterotetrametric complexes of transmembrane receptors, which are type I or type II serine/threonine kinase receptors (Gámez et al., 2013; Katagiri & Watabe, 2016; Mueller & Nickel, 2012). Type I BMP receptors can be classified into BMPR1A, BMPR1B, Activin A Receptor (ACVR)-like (L) 1, and ACVR1. Studies showed BMP7 to interact with BMPR1A, BMPR1B, and ACVR1. BMP7 also interacts with Type II BMP receptors, like BMPR2, ACVR2A, and ACVR2B (Gomez-Puerto et al., 2019; Hinck, 2012; Liu et al., 1995). BMP7 increases the expression of UCP1, PGC1α, and PRDM16 via the activation of p38 MAPK pathway (Tseng et al., 2008). Previous studies indicated BMP7 can upregulate UCP1 expression in selected clones of human neck derived immortalized white and brown preadipocytes (Xue et al., 2015).

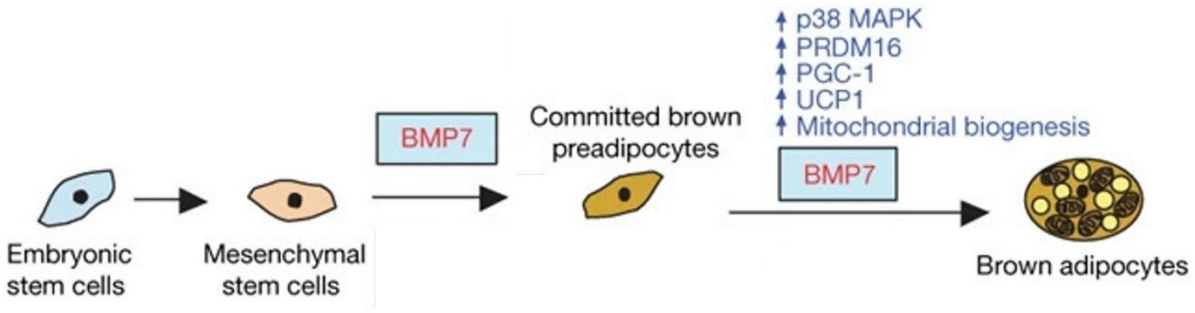

Figure 8: BMP7 drives classical brown adipocyte differentiation in mice (Tseng et al., 2008)

2. Aim of the study

- **Recent studies indicated that mitophagy is elevated during beige to white adipocyte transition in mice upon removal of adrenergic stimulation. So, I aim to understand how autophagy/mitophagy is regulated during the thermogenic response associated with a cAMP mediated adrenergic stimulus.**

- **Irisin has been shown to induce a beige differentiation program in mouse subcutaneous white adipose tissue. It can also induce a thermogenic response in human subcutaneous abdomen derived differentiating adipocytes. Hence, I intend to elucidate the effect of irisin in human subcutaneous and deep neck derived differentiating adipocytes.**

- **BMP7 is a potent browning inducer and has been shown to drive classical thermogenic brown adipocyte differentiation in mice. BMP7 can promote brown adipocyte like differentiation in human subcutaneous abdomen derived differentiating adipocytes. Hence, I intend to elucidate the effect of BMP7 in human subcutaneous and deep neck derived differentiating adipocytes.**

3. Material and methods

3.1. Source of cells and ethics statement

Human adipose derived mesenchymal stem cells (hADMSCs) were isolated from the stromal vascular fractions (SVF) of subcutaneous abdominal adipose tissue of healthy volunteers undergoing planned liposuction for experiments evaluating the regulation of mitophagy upon thermogenic stimulus (Kristóf et al., 2015; Szatmári-Tóth et al., 2020). In case of treatments with Irisin and BMP7, hADMSCs were obtained from SVFs of subcutaneous neck (SC) and deep neck (DN) tissues of healthy volunteers (Kristóf et al., 2019; Sárvári et al., 2015; Shaw, Tóth, Arianti, et al., 2021; Shaw, Tóth, Király, et al., 2021; Tóth et al., 2020). A pair of biopsies was obtained from SC and DN areas of same donor to avoid inter-individual variations. Isolations were performed from donors aged between 18-65 years.

The study protocol was approved by the Medical Research Council of Hungary via approval number: 20571-2/2017/EKU. All experiments were carried out strictly under approved ethical guidelines and regulations.

3.2. Materials

All materials were obtained from Sigma-Aldrich (Munich, Germany) unless stated otherwise.

3.3. Isolation, cultivation, and differentiation of human adipose-derived mesenchymal stem cells (hADMSCs) ex vivo

Adipose tissue biopsies were transported immediately to our laboratory following elective surgeries. Fibrous material and blood vessels were removed from the biopsies, then minced into small pieces, and digested with collagenase (120 U/ml) in PBS (1 hour, 37°C) with gentle agitation. hADMSCs were centrifuged down from the cell suspension at 1300rpm for 10 minutes; then resuspended and cultured in T75 flasks with DMEM-F12 medium containing 10% FBS (Thermo Fisher Scientific, MA, USA), 100 U/ml penicillin-streptomycin, 33 µM biotin and 17 µM panthothenic acid at 37°C in 5% CO_2 (Shaw, Tóth, Arianti, et al., 2021; Shaw, Tóth, Király, et al., 2021). Absence of mycoplasma was confirmed by PCR analysis (PCR Mycoplasma Test Kit I/C, PromoCell Gmbh, Germany). hADMSCs from fully confluent flasks were trypsinized and seeded (15000 cells/cm^2) to 6 well, 12 well, µ-Ibidi or 96 well Seahorse plates in the same medium under identical conditions.

Once the cell culture became confluent, differentiation was initiated by either the white or beige adipogenic differentiation medium for a period of 14 days (unless indicated otherwise). The white adipogenic differentiation medium consisted of DMEM-F12 supplemented with 33 μM biotin, 17 μM panthothenic acid, 10 μg/ml human apo-transferrin, 20 nM human insulin, 100 nM hydrocortisone, 200 pM T3, 2 μM rosiglitazone, 25 nM dexamethasone and 500 μM IBMX for the first four days, following which rosiglitazone, dexamethasone and IBMX were omitted from the differentiation medium (Kristóf et al., 2015). The beige adipogenic differentiation medium consisted of DMEM-F12 containing 33 μM biotin, 17 μM panthothenic acid, 10 μg/ml apo-transferrin, 0.85 μM human insulin, 200 pM T3, 1 μM dexamethasone and 500 μM IBMX for the first four days, after that, dexamethasone and IBMX were omitted, and 500 nM rosiglitazone was added to the differentiation medium (Klusóczki et al., 2019). The medium was replaced every fourth day till the end of the 14-day differentiation period.

3.4. Treatments of differentiating hADMSCs and mature adipocytes with browning-inducers or activators

Where indicated, SC and DN derived preadipocytes were differentiated following the white adipogenic differentiation protocol in the presence of known browning inducers: human recombinant irisin (Cayman Chemicals, MI, USA, 11451) at 250 ng/mL (Shaw, Tóth, Király, et al., 2021) or human recombinant BMP7 (R&D Systems, MN, USA, 354-BP) at 50 ng/mL (Shaw, Tóth, Arianti, et al., 2021) throughout the 14-day differentiation period (unless indicated).

Human subcutaneous abdominal derived preadipocytes were differentiated following the white or beige adipogenic differentiation protocol for 14 days. The differentiated adipocytes were subjected to dibutyryl-cAMP (500μM) treatment for 6, 10 or 14 hours respectively (Cypess et al., 2013).

3.5. Gene silencing treatments in subcutaneous abdominal differentiated hADMSCs

Transfection and gene silencing were performed on differentiated white and beige adipocytes of abdominal origin using DharmaFECT1 transfection reagent (Dharmacon, CO, USA, T-2001-03). Differentiated adipocytes were incubated with a mixture of DharmaFECT1 and 50 nM of PARK2-targeted siRNA (Dharmacon, ON-TARGETplus SMARTpool Human Parkin siRNA, L-003603-00-0005) or non-targeted negative control siRNA (Dharmacon, ON-TARGETplus Non-targeting Control Pool, D-001810-10-05) for 4 days in white or beige differentiation medium devoid of penicillin/streptomycin (Szatmári-Tóth et al., 2020).

3.6. RNA Isolation, RT-qPCR, and RNA-Sequencing

For RNA isolation, following differentiation and treatments, adipocytes were collected using TRI Reagent. Total cellular RNA was isolated manually by chloroform extraction and isopropanol precipitation (Klusóczki et al., 2019; Kristóf et al., 2015).

For RT-PCR, RNA quality was ascertained by spectrophotometry, followed by cDNA generation using TaqMan reverse transcription reagents kit (Thermo Fisher Scientific). qPCR was performed with LightCycler 480 (Roche Diagnostics, IN, USA) using the probes (Applied Biosystems, MA, USA) listed in Table 1. Human GAPDH was used as the endogenous control. Samples were run in triplicate and gene expression values were calculated by the comparative cycle threshold (Ct) method. ΔCt values were obtained by deducting GAPDH Ct from the Ct of target; the normalized gene expression values were calculated by $2^{-\Delta Ct}$ (Czimmerer et al., 2018; Gyurina et al., 2019).

Table 1: List of TaqMan probes used in the study

Gene name	Assay ID
ITGAV	Hs00233808_m1
CXCL1	Hs00236937_m1
NFKB1	Hs00765730_m1
RELA	Hs00153294_m1
IL6	Hs00985639_m1
CCL2	Hs00234140_m1
CX3CL1	Hs00171086_m1
IL32	Hs00992441_m1
GAPDH	Hs99999905_m1
ID1	Hs00357821_g1
CKMT2	Hs00176502_m1
UCP1	Hs00222453_m1
ACAN	Hs00153936_m1
CRYAB	Hs00157107_m1
PPARGC1A	Hs01016719_m1
PARK2	Hs01038322_m1
SQSTM1	Hs00177654_m1
OPTN	Hs00184221_m1
NDP52	Hs00977443_m1
BNIP3	Hs00969291_m1
BNIP3L	Hs00188949_m1
FKBP8	Hs01014664_m1
BCL2L13	Hs00209789_m1
FUNDC1	Hs00697693_m1

For RNA-Sequencing, RNA sample quality was validated by Agilent Bioanalyzer using Eukaryotic Total RNA Nano Kit and samples with RNA integrity number >7 were used for library preparation. Libraries were prepared by NEBNext Ultra II RNA Library Prep (New England BioLabs, MA, United States), followed by sequencing runs on Illumina NextSeq500 using single-end 75 cycles sequencing (Tóth et al., 2020). The reads were aligned to GRCh38 (with EnsEMBL 95 annotation) by STAR aligner (Dobin et al., 2013). Reads were quantified by featureCounts (Liao et al., 2014) and R was used for gene expression analysis. Outlier genes, having Cook's distance>1 were removed from further analysis. After removal of the outlier genes, the obtained expression profile of the transcripts is considered as normalized RNA counts. PCA analysis could not show any batch effect considering donor, sex or tissue origin. Differentially expressed genes were obtained using DESeq2 algorithm with a log2 fold change threshold of more than 0.85. Pathway analysis was performed using PANTHER Reactome pathways and heatmaps were visualized using Morpheus Webtool based on calculated z-scores (Tóth et al., 2020). The interaction networks were determined using STRING and constructed using Gephi 0.9.2; node size illustrated the fold change (Tóth et al., 2020).

3.7. Quantification of mitochondrial DNA by qPCR

Total DNA was isolated by manual phenol–chloroform extraction from trizolyzed samples. mtDNA was quantified by qPCR in triplicates on diluted DNA using Ct method (Klusóczki et al., 2019; Kristóf et al., 2015). qPCR was performed using Maxima SYBR Green/ROX qPCR Master Mix (Thermo Fisher Scientific) with the following primers:

i) **mtDNA specific PCR**

forward 5'-CTATGTCGCAGTATCTGTCTTTG-3',

reverse 5'-GTTATGATGTCTGTGTGGAAAG-3'

ii) **nuclear specific PCR (SIRT1 gene),**

forward 5'-CTTTGTGTGCTATAGATGATATGGTAAATTG-3',

reverse 5'-GATTAAACAGTGTACAAAAGTAG-3'

3.8. Western blotting and antibodies

Cells were collected in 1x Laemmli loading buffer, boiled at 100°C for 10 min, separated by SDS-PAGE and finally transferred to PVDF Immobilon-P transfer membrane (Merck-Millipore, Germany). Following transfer, membrane was blocked by 5% skimmed milk for 1 hour and then kept for primary antibody incubation overnight in 1% milk solution (Klusóczki et al., 2019; Szatmári-Tóth et al., 2020). The primary antibodies used are listed in Table 2.

Table 2: List of primary antibodies used in the study

Primary antibody	Dilution	Manufacturer
anti-p50	1:1000	Cayman Chemicals, 13755
anti- IκBα	1:1000	Cell Signalling Technology, 4812
anti-β-actin	1:5000	Novus Biologicals, A2066
anti-UCP1	1:750	R&D Systems, MAB6158
anti-pCREB	1:1000	Merck-Millipore, 05-667
anti-CREB	1:1000	Abcam, ab31387
anti-PGC1α	1:1000	Santa Cruz Biotechnology, H-300
anti-CKMT2	1:1000	Novus Biologicals, NBP2-13841
anti-CKB	1:1000	Novus Biologicals, A2066
anti-OXPHOS	1:1000	Abcam, ab110411
anti-Aggrecan	1:1000	Novus Biologicals, NB100-74350
anti-ID1	1:1000	Novus Biologicals, JM92-13
anti-p62	1:5000	Novus Biological, NBP1-49956
anti-LC3	1:2000	Novus Biological, NB100-2220
anti-Parkin	1:750	Santa Cruz Biotechnology, sc-32282

HRP-conjugated goat anti-rabbit IgG antibody (1:10,000, Advansta, CA, USA, R-05072-500) and HRP-conjugated goat anti-mouse IgG antibody (1:5000, Advansta, R-05071-500) were used as the respective secondary antibodies. Immobilon western chemiluminescence substrate (Merck-Millipore) was used to visualize the immunoreactive proteins. Densitometry was performed by FIJI (ImageJ).

3.9. Immunostaining and image acquisition by laser scanning cytometry (LSC) and confocal microscopy

Preadipocytes were plated and differentiated in 8-well Ibidi µ-slides followed by the mentioned treatments. Cells were washed once with PBS and fixed by 4% PFA for 5 minutes. 0.1% saponin was used for membrane permeabilization, followed by blocking with 5% skimmed milk. Incubations were kept overnight with the following primary antibodies: anti-LC3 (1:200, Novus Biological, NB100-2220), anti-TOM20 (1:75, WH0009804M1), anti-CXCL1 (1:100, 712317, Thermo Fisher Scientific) or anti-UCP1 (1:200, U6382). Secondary antibody incubation was kept for 3 hours with the following antibodies: Alexa 647 goat anti-mouse IgG (1:1000, Thermo Fischer Scientific, A21236) and Alexa 488 goat anti-rabbit IgG (1:1000, Thermo Fischer Scientific, A11034). Propidium Iodide (1.5 µg/mL, 1 h) was used to label the nuclei. Images were acquired either with Olympus FluoView 1000 confocal microscope or iCys Research Imaging Cytometer (Shaw, Tóth, Arianti, et al., 2021; Shaw, Tóth, Király, et al., 2021; Szatmári-Tóth et al., 2020).

3.10. Image analysis

i) CXCL1 immunostaining intensity: The boundaries of preadipocytes and differentiated adipocytes were marked based on brightfield (BF) images and nuclear staining. The intensity of CXCL1 immunostaining was determined for each cell type manually using FIJI (Shaw, Tóth, Király, et al., 2021). The fluorescence intensity was normalized to per cell.

ii) LC3 punctae and fragmented mitochondria content (TOM20): LC3 punctae was quantified using FIJI with size (pixel^2): 50–infinity AU. Fragmented mitochondria were quantified from TOM20 immunostaining using FIJI with size (pixel^2): 0–100 AU. Both LC3 punctae and fragmented mitochondria content were normalized to per nucleus (Shaw, Tóth, Arianti, et al., 2021; Szatmári-Tóth et al., 2020).

iii) Co-localization of LC3 and TOM20 immunostaining: Colocalization was quantified by Pearson's correlation coefficients (PCC) between the pixel intensities of the two detection channels (Szatmári-Tóth et al., 2020).

iv) UCP1 immunostaining intensity, differentiation rate and texture sum variance calculation: Images were obtained by iCys Research Imaging Cytometer and analysed by high throughput automatic cell recognition protocol using the iCys companion software (iNovator Application Development Toolkit, CompuCyte Corporation) and CellProfiler (The Broad

Institute of MIT). The analysis was performed using technology developed by Dr. Endre Kristóf, Dr. Quang-Minh Doan-Xuan and Dr. Zsolt Bacsó of University of Debrecen (Doan-Xuan et al., 2013; Kristóf et al., 2015).

3.11. Determination of cellular oxygen consumption rate (OCR) and extracellular acidification rate (ECAR)

Cells were seeded and differentiated on XF96 (Seahorse Biosciences, MA, USA) assay plates and OCR, ECAR were measured by XF96 oximeter (Seahorse Biosciences). Baseline respiration and acidification were measured for 30 mins followed by cAMP stimulated values. A single bolus dose of dibutyryl-cAMP (at 500 μM final concentration) was added to mimic adrenergic stimulation leading to the stimulated OCR and ECAR values, that were measured every 30 mins. Oligomycin at 2 μM final concentration was added 3 hours post treatment to block ATP synthase activity for proton leak OCR measurement. Creatine cycle related OCR was measured by addition of β-GPA (2mM) after cAMP stimulation (Kazak et al., 2015). Antimycin A (10 μM) was added at the end for baseline correction. OCR was normalized to protein content (Arianti et al., 2021; Shaw, Tóth, Arianti, et al., 2021).

3.12. Determination of released factors

Supernatants were collected from cell culture experiments during regular replacement of media on days 4,12,18,21 of the differentiation period, as indicated. For SC and DN differentiating adipocytes, supernatants collected from the same set of donors were considered as one repetition. In case of tissue biopsies, 10-20 mg of SC and DN tissue samples from the same donor were floated for 24 hours in DMEM-F12-HAM medium in the presence or absence of 250 ng/mL irisin. The release of CXCL1, CX3CL1, IL-32, TNFα, and IL1-β were analysed using ELISA Kits (R&D systems) following manufacturer's instructions (Kristóf et al., 2019; Shaw, Tóth, Király, et al., 2021).

3.13. Human umbilical vein endothelial cell (HUVEC) adhesion assay

The HUVEC cell line was generated from endothelial cells isolated from human umbilical cord vein of a healthy newborn by collagenase treatment (Palatka et al., 2006). M199 medium (Biosera, France) supplemented with 10% FBS (Thermo Fisher Scientific), 10% EGM2 (Lonza, Switzerland), 20 mM HEPES, 100 U/mL Penicillin, 100 μg/mL Streptomycin and 2.5 μg/mL Amphotericin B (Biosera) was used for cell culture. Cells were immortalized by viral delivery of telomerase gene using pBABE-neo-hTERT (Counter et al., 1998). Prior to the assay, EGM2

was omitted from the medium and FBS content was reduced to 1% and maintained for 24 hours, this will make proliferation unlikely (hereafter starvation media). 96-well plate was precoated with fibronectin (1.25 μg/mL) for 1 hour at 37°C, washed twice with PBS and seeded with HUVEC cells at 1000 cells/well density. Cells were allowed to adhere for 2 hours at 37°C and 5% CO_2 with the medium consisting of starvation media and conditioned media (collected during Day 12 of differentiation period) in 1:1 ratio. Recombinant human CXCL1 (R&D Systems, 275-GR) was added to the starvation media at 2500 pg/mL for its respective assay. Unattached cells were removed by PBS wash and adhered cells were incubated with starvation media containing CellTiter-Blue Cell Viability reagent (resazurin; Promega, WI, USA; 36 times dilution). To determine the ratio of attached cells in various conditions, the fluorescence intensity change of each well (Ex:530 nm/Em:590 nm), due to the conversion of resazurin to resorufin by cellular metabolism, was measured 2, 4, 6, 18, and 24 hours after adding resazurin. Slope of fluorescence intensity values plotted against time showed a linear slope, suggesting negligible cell proliferation. The relative adhesion values were obtained after subtraction of control values (wells containing only starvation media without cells) (Shaw, Tóth, Király, et al., 2021).

3.14. Statistical analysis and figure preparation

Results are expressed as mean ± SD for the number of independent repetitions indicated. For multiple comparisons, statistical significance was determined by one- or two-way ANOVA followed by Tukey post hoc test. For comparisons between two groups two-tailed t-test was used. Graphpad Prism 9 was used for figure preparation and evaluation of statistics.

4. Results

4.1. Regulation of thermogenesis via mitophagy

4.1.1. Adrenergic stimulus elevates expression of thermogenic genes in human primary abdominal preadipocytes differentiated to mature white and beige adipocytes

hADMSCs isolated from the SVFs of abdominal subcutaneous adipose tissue were differentiated to mature white and beige adipocytes following the respective white or beige differentiation protocol for a period of 14 days. Differentiated white and beige adipocytes were subjected to cAMP mediated adrenergic stimulus for a period of 6,10 and 14 hours respectively. Beige adipocytes possessed significantly higher UCP1 protein expression than white adipocytes (Figure 9A, right panel). Adrenergic stimulus elevated UCP1 gene expression starting 6 hours post treatment and was found to be significantly elevated at 10 hours post treatment in both white and beige differentiated adipocytes (Figure 9A, left panel). A similar pattern was observed for the UCP1 protein expression upon adrenergic stimulus with significant upregulation at 14 and 6 hours post treatment in white and beige differentiated adipocytes (Figure 9A, right panel). Blocking lysosomal degradation by chloroquine (CQ) did not affect UCP1 protein expression.

cAMP stimulus further upregulated the total mitochondrial content, that was found to be significantly upregulated 6 hours post treatment in white and beige differentiated adipocytes (Figure 9B). The gene expression of PGC1α, a mitochondrial biogenesis regulator (Kelly & Scarpulla, 2004) was also significantly elevated 6 hours post cAMP treatment in both white and beige differentiated adipocytes (Figure 9C). Hence, cAMP mediated adrenergic stimulus elevated the thermogenic potential of human primary abdomen derived white and beige differentiated adipocytes.

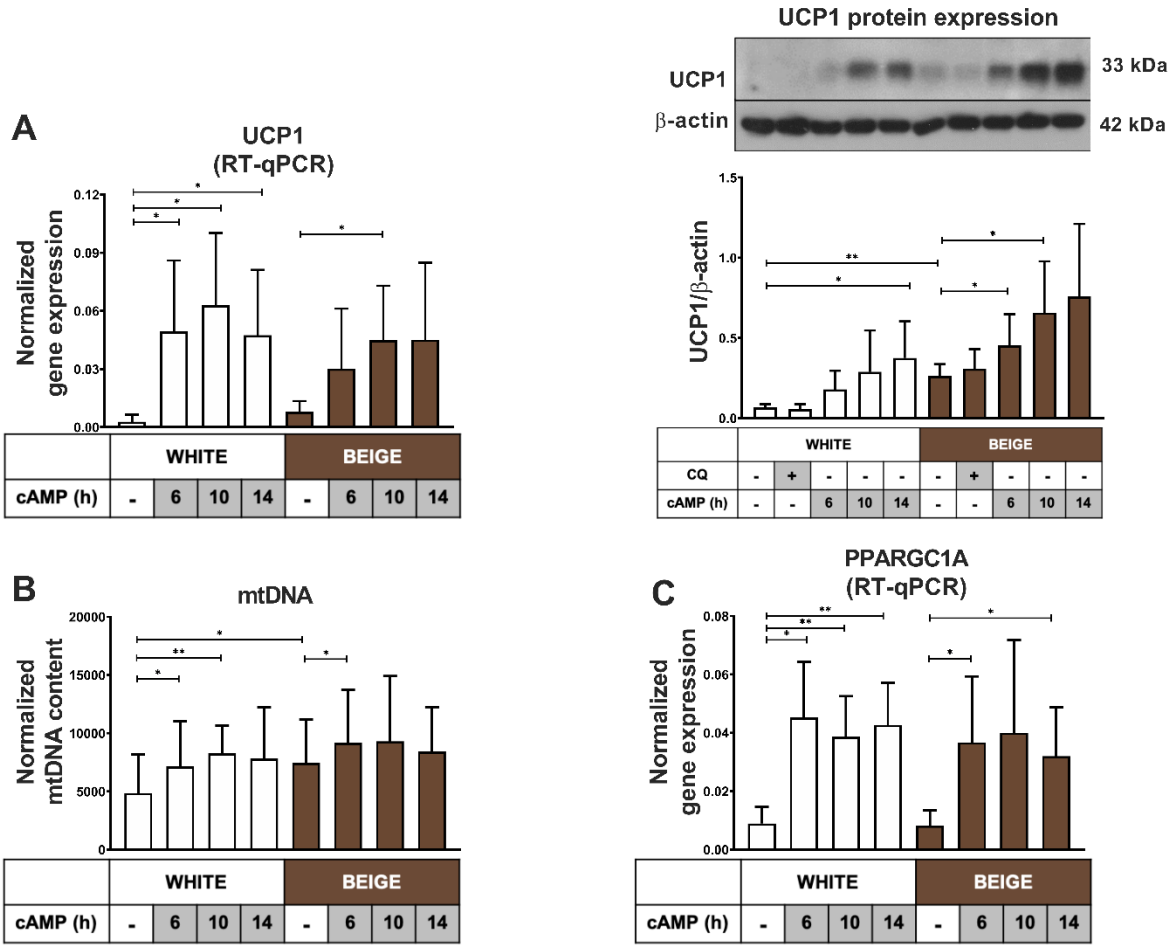

Figure 9: Adrenergic stimulus elevates expression of thermogenic genes in human primary abdominal derived differentiated adipocytes. hADMSCs of subcutaneous abdominal origin was differentiated to mature white and beige adipocytes following the respective differentiation protocol for a period of 14 days. CQ treatment (25 µM, 1hour) to block the lysosomal degradation activity and cAMP treatment (500 µM, 6-14hours) were performed as indicated. (A) Quantification of UCP1 gene and protein expression (n=5), (B) Quantification of total mitochondrial DNA content by qPCR (n=6), (C) PPARGC1A gene expression (n=5). Results are expressed as mean ± SD. Gene expression data was normalized to GAPDH and protein expression was normalized to β-actin. mtDNA was normalized to SIRT1. *p<0.05, **p<0.01. Statistics: paired t-test.

4.1.2. The high mitophagy rate in human abdominal derived white and beige differentiated adipocytes is downregulated upon adrenergic stimulus

A recent study in mice showed that autophagy-dependent mitochondrial clearance was low in beige adipocytes, that was upregulated during whitening upon removal of the β3-AR agonist (Altshuler-Keylin et al., 2016). Our study intended to investigate how autophagy is regulated upon adrenergic stimulation by cAMP. Gene expression of general autophagy markers ATG5, ATG7 and ATG12 were significantly reduced 6 hours post cAMP mediated adrenergic stimulus in both white and beige differentiated adipocytes (Figure 10A). LC3-II/ LC-I ratio is a well-accepted method for monitoring ongoing autophagic activity; an increased ratio indicates a high level of ongoing autophagy (Mizushima et al., 2010). CQ was administered to measure the autophagic flux (Yoshii & Mizushima, 2017). Under basal conditions a high LC3-II/LC3-I ratio was obtained for white differentiated adipocytes as compared to beige, that was further elevated upon CQ treatment, which indicated an increased autophagic flux in the white adipocytes (Figure 10B). The cAMP mediated adrenergic stimulus significantly reduced the LC3-II/LC3-I ratio in both white and beige differentiated adipocytes starting 6 and 10 hours post treatment, respectively (Figure 10B). This clearly indicated an inhibition of autophagy following adrenergic stimulus. Protein expression of p62, a well-known autophagy adapter protein (Pankiv et al., 2007), was significantly elevated following 6 hours cAMP treatment in both types of adipocytes that indicated reduced autophagy (Figure 10C). Together, the data suggested that cAMP mediated adrenergic stimulus downregulates the ongoing autophagic activity in both white and beige differentiated adipocytes.

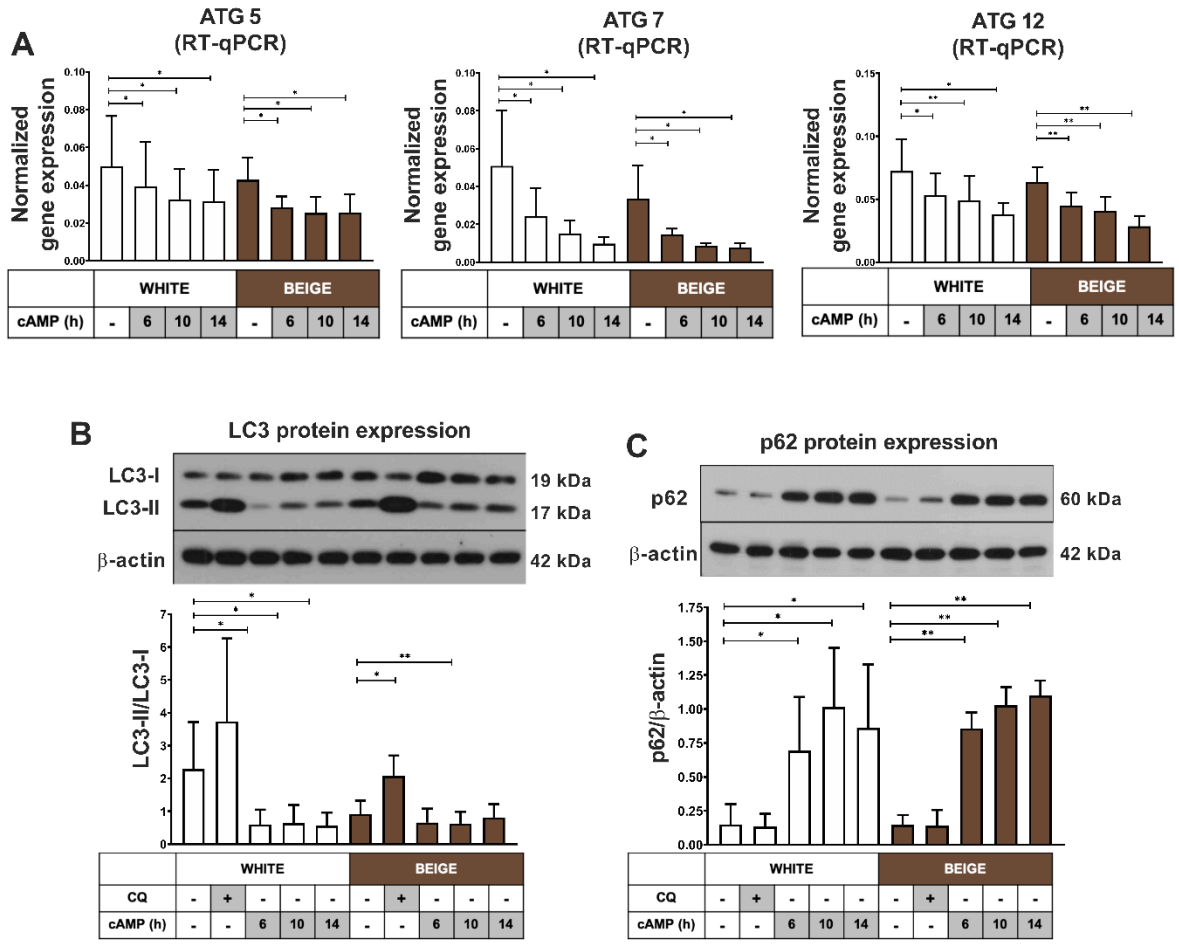

Figure 10: General autophagy markers are repressed upon adrenergic stimulus of adipocytes. hADMSCs were differentiated as in figure 9. CQ treatment (25 µM, 1hour) and cAMP treatment (500 µM, 6-14hours) were performed as indicated. (A) Quantification of gene expression for ATG 5/7/12 (n=5), (B) Representative immunoblot image for LC3-II, LC3-I followed by quantification of LC3-II:LC3-I (n=5), (C) p62 protein expression (n=5). Results are expressed as mean ± SD. Gene expression data was normalized to GAPDH and protein expression was normalized to β-actin. *p<0.05, **p<0.01. Statistics: paired t-test.

Next, co-immunostaining of LC3 (labelling autophagosomes) and TOM20 (labelling mitochondria) were performed in white and beige differentiated adipocytes without treatment or with cAMP and CQ treatments. Quantification of LC3 punctae counts is an important measure of ongoing autophagy and colocalization of LC3, TOM20 identifies mitophagy. CQ treatment increased the number of LC3 punctae count in white differentiated adipocytes indicating a higher autophagic flux (Figure 11). cAMP mediated adrenergic stimulus significantly reduced LC3 punctae count in both white and beige differentiated adipocytes further confirming that autophagy is repressed following the stimulus (Figure 11). Co-localization measurements for LC3 and TOM20 revealed that CQ increased co-localization in white and beige differentiated adipocytes indicating an enhanced mitophagic flux, whereas

cAMP treatment led to a significant reduction in co-localization, further indicating repressed mitophagy upon its stimulus (Figure 11).

A recent study revealed that mitochondria with fragmented morphology are mostly abundant in UCP1 (Pisani et al., 2018). Quantification of fragmented mitochondria content from TOM20 immunostaining showed that, cAMP treatment significantly increased the content of fragmented mitochondria in both white and beige differentiated adipocytes (Figure 11). These data collectively suggest that in unstimulated adipocytes, most of the fragmented mitochondria are eliminated because of the high mitophagy rate, which is rescued upon adrenergic stimulus, leading to a greater availability of UCP1 rich fragmented mitochondria capable of increased thermogenesis.

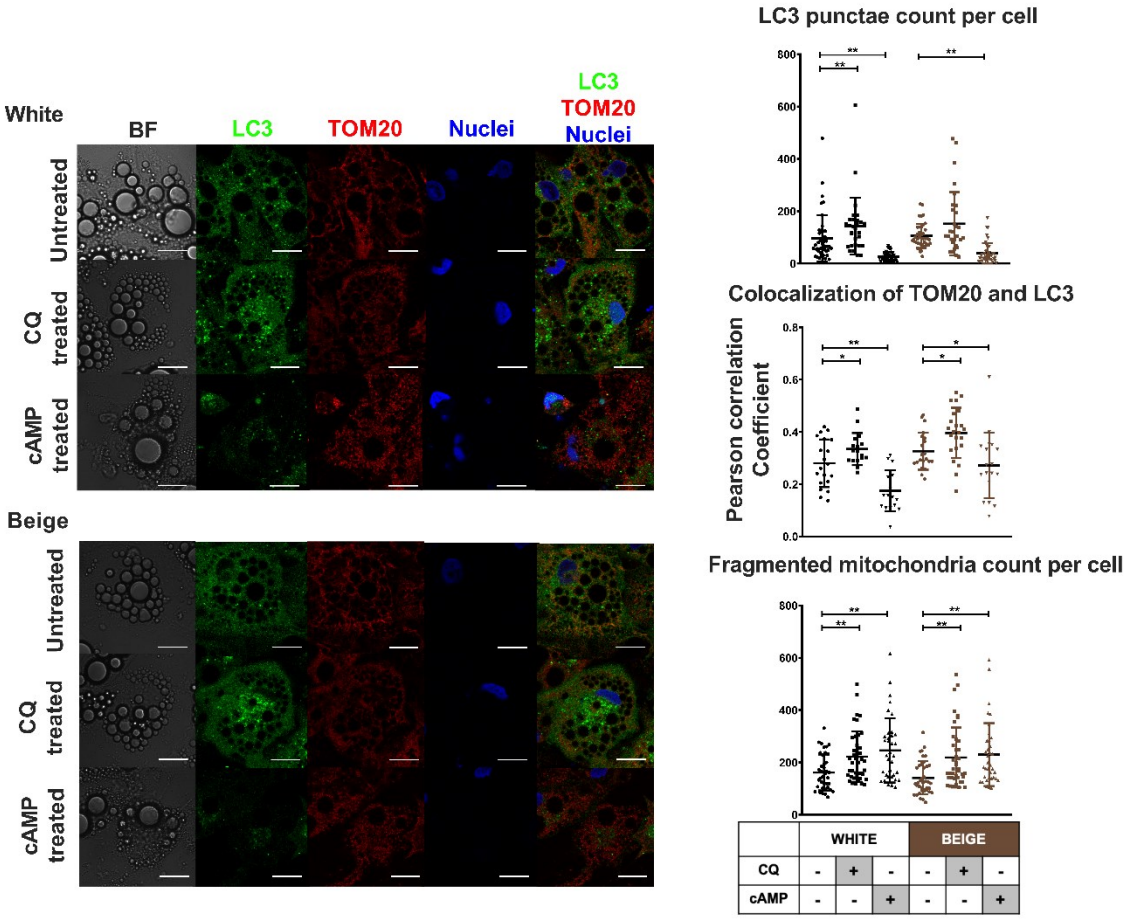

Figure 11: Mitophagy is downregulated upon cAMP mediated adrenergic stimulus of adipocytes. hADMSCs were differentiated as in figure 9-10. CQ treatment (25 µM, 1hour) and cAMP treatment (500 µM, 8hours) were performed as indicated. Representative confocal microscopy images of LC3 and TOM20 immunostaining are illustrated on left, followed by quantification of LC3 punctae, co-localization of TOM20 and LC3 and fragmented mitochondria count on right (n= 40-60 cells from 3 donors). Scalebars represent 5 µm. Nuclei were stained by propidium-iodide. LC3 punctae and fragmented mitochondria count were normalized to per cell. Results are expressed as mean ± SD. * $p < 0.05$, ** $p < 0.01$. Statistics: Mann–Whitney U test.

4.1.3. Adrenergic stimulus downregulates mitophagy via both parkin dependent and independent mechanisms

Mitophagy occurs in both parkin dependent and independent mechanisms (Altshuler-Keylin & Kajimura, 2017). cAMP mediated adrenergic stimulus significantly downregulated PARK2 gene expression starting 10 hours post treatment in both white and beige differentiated adipocytes (Figure 12A). Parkin protein expression was significantly downregulated 6 and 14 hours post cAMP treatment in beige differentiated adipocytes (Figure 12A). Significant reduction in gene expression of OPTN and CALCOCO2 (NDP52), the most prominent adapters of parkin-dependent pathway, was observed following the cAMP treatment (Figure 12 B,C). These results indicated prompt repression of parkin dependent mitophagy pathway upon adrenergic stimulus.

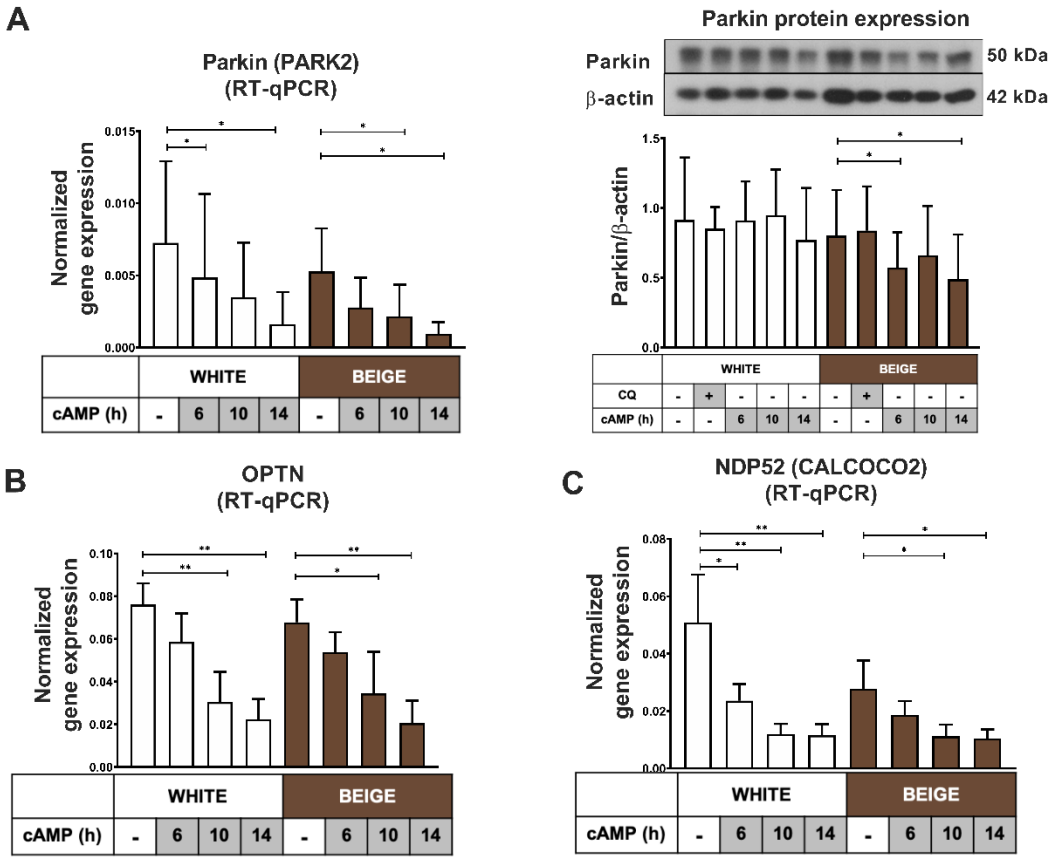

Figure 12: Adrenergic stimulus downregulates parkin dependent mitophagy pathway in adipocytes. hADMSCs were differentiated as in figure 9-11. CQ treatment (25 µM, 1hour) and cAMP treatment (500 µM, 6-14hours) were performed as indicated. (A) Quantification of Parkin gene and protein expression (n=5), Quantification of gene expression of (B) OPTN and (C) NDP52 (n=5). Results are expressed as mean ± SD. Gene expression data was normalized to GAPDH and protein expression was normalized to β-actin. *p<0.05, **p<0.01. Statistics: paired t-test.

Hence, as a next step, silencing of Parkin by siRNA was performed after white and beige differentiation, to check if it results in a stronger thermogenic response. The silencing resulted in 60% reduction of Parkin protein expression in both white and beige differentiated adipocytes (Figure 13A). The Parkin silencing by itself did not alter the levels of LC3-II/LC3-I ratio or the p62 protein expression, indicating that the ongoing mitophagy rate remained largely unchanged (Figure 13 B,C). The silencing resulted in increased UCP1 protein expression only in beige differentiated adipocytes (Figure 13D). cAMP could similarly upregulate UCP1 protein expression in cells incubated with Parkin and control siRNA, indicating that Parkin deficiency did not lead to the appearance of a more active beige phenotype.

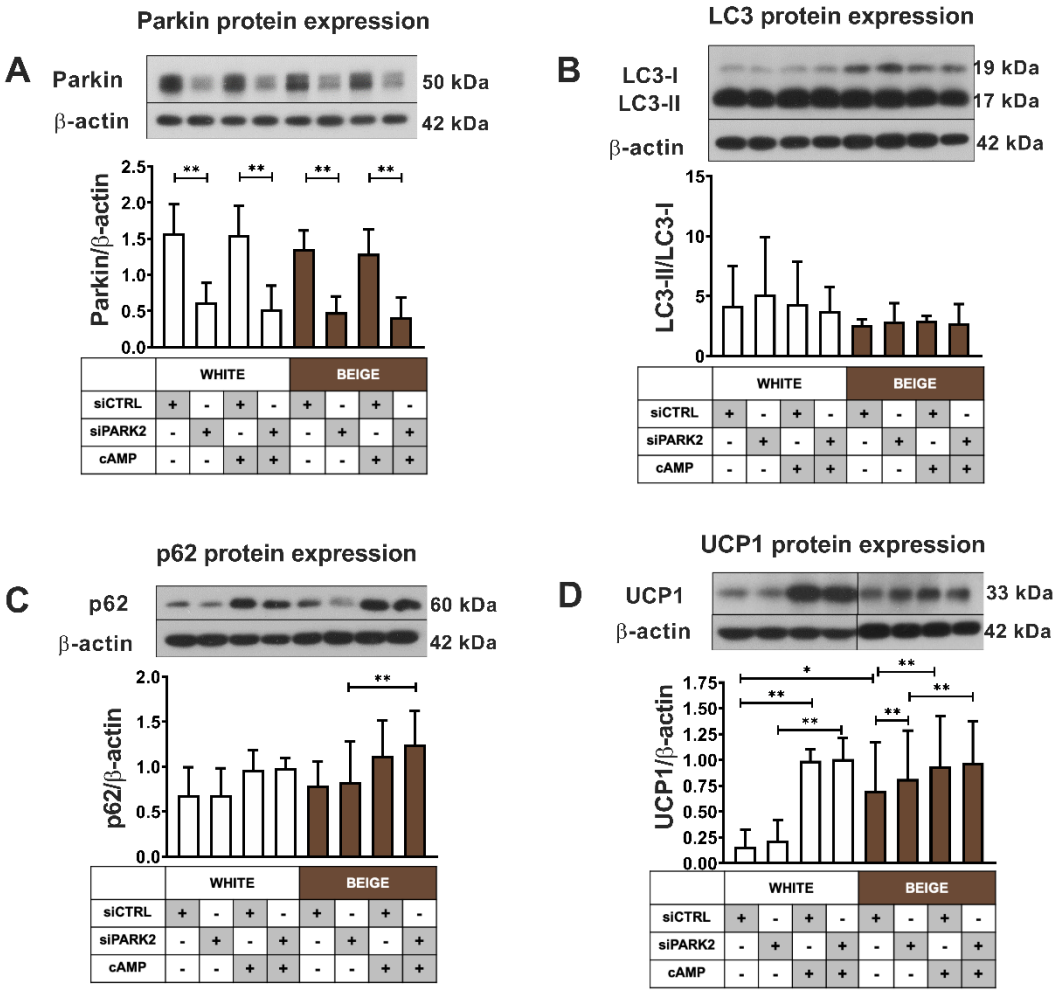

Figure 13: Impact of parkin silencing on autophagy and UCP1-dependent thermogenesis of adipocytes. hADMSCs were differentiated as in figure 9-12. cAMP treatment (500 µM, 10hours) was performed as indicated. Representative immunoblot followed by quantification of protein expression for (A) Parkin, (B) LC3-II, LC3-I (expressed as LC3-II:LC3-I), (C) p62 and (D) UCP1 in differentiated white and beige adipocytes silenced with either siCTRL or siPARK2 (n=4). Results are expressed as mean ± SD. Protein expression was normalized to β-actin. *p<0.05, **p<0.01. Statistics: paired t-test.

Since silencing of parkin alone could not repress autophagy or improve the cAMP mediated thermogenic response, the expression of parkin-independent mitophagy genes were also evaluated. In response to adrenergic stimulus, the gene expression of BCL2L13, FKBP8, FUNDC1 and BNIP3 was promptly repressed (Figure 14). Together, these results indicated a complex mechanism involving both parkin-dependent and independent mitophagy pathways by which mitophagy is repressed in white and beige differentiated adipocytes following adrenergic stimulus.

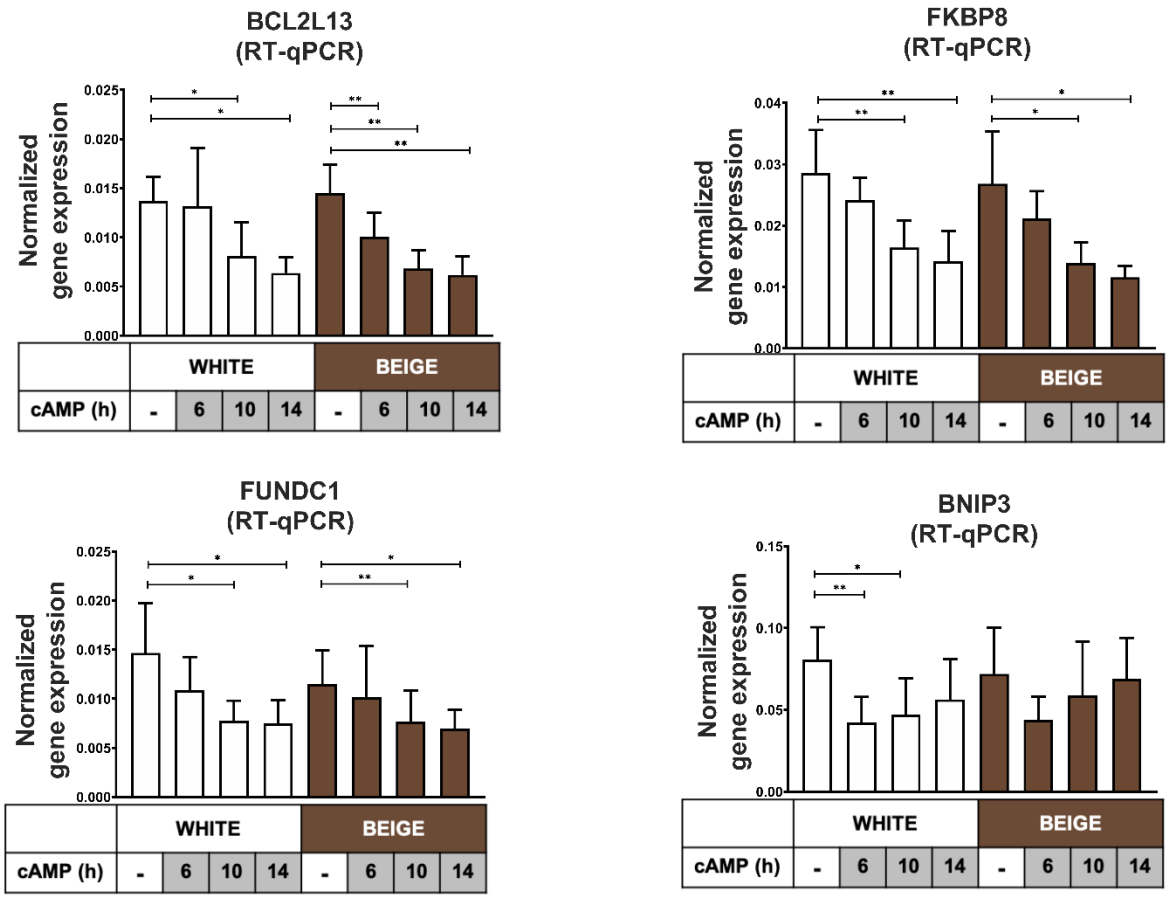

Figure 14: Adrenergic stimulus represses parkin-independent mitophagy pathway in adipocytes. hADMSCs were differentiated as in figure 9-13. CQ treatment (25 µM, 1hour) and cAMP treatment (500 µM, 6-14hours) were performed as indicated. Quantification of gene expression for BCL2L13, FKBP8, FUNDC1 and BNIP3 normalized to GAPDH (n=5). Results are expressed as mean ± SD. *p<0.05, **p<0.01. Statistics: paired t-test.

4.2. Effect of irisin on neck depot derived adipocytes

4.2.1. Human primary subcutaneous neck (SC) and deep neck (DN) derived preadipocytes differentiated equally to mature white adipocytes irrespective of irisin treatment

hADMSCs were isolated from SVFs of SC and DN biopsies of nine independent donors, maintained and then differentiated following the white adipogenic differentiation protocol (Tóth et al., 2020) with or without the presence of irisin for 14 days. Samples were collected, followed by RNA isolation and RNA-Sequencing (Tóth et al., 2020). Heatmap illustrating gene expression patterns of general adipocyte markers like FABP4, PLIN1 and ADIPOQ were elevated in all differentiated adipocytes compared to preadipocytes (Figure 15A). Adipocyte differentiation rate quantification by laser scanning cytometry (Kristóf et al., 2015) showed that more than 50% cells were differentiated following the 14-day differentiation and irisin did not exert any effect on the differentiation rate (Figure 15B). Gene expression of the proposed irisin receptors, ITGAV and ITGB1,3,5 (Kim et al., 2018) were expressed at a high extent at preadipocyte level and in all differentiated adipocytes (Figure 16). Hence SC and DN derived preadipocytes differentiated equally irrespective of the irisin treatment.

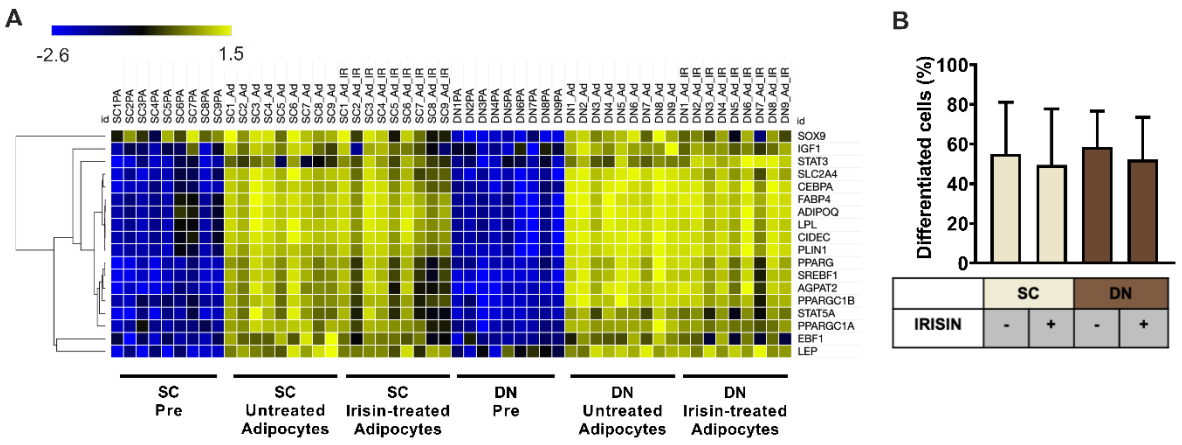

Figure 15: SC and DN derived preadipocytes differentiate to a similar extent irrespective of the presence of irisin. SC and DN preadipocytes were differentiated for 2 weeks following the white adipogenic differentiation protocol. Irisin (250 ng/mL) was administered during the whole differentiation period as indicated. (A) Heatmap showing the expression pattern of general adipogenic differentiation marker genes in samples used for Global RNA Sequencing (n=9), (B) Differentiation rate quantification by laser-scanning cytometry (n=9). Results are expressed as mean ± SD.

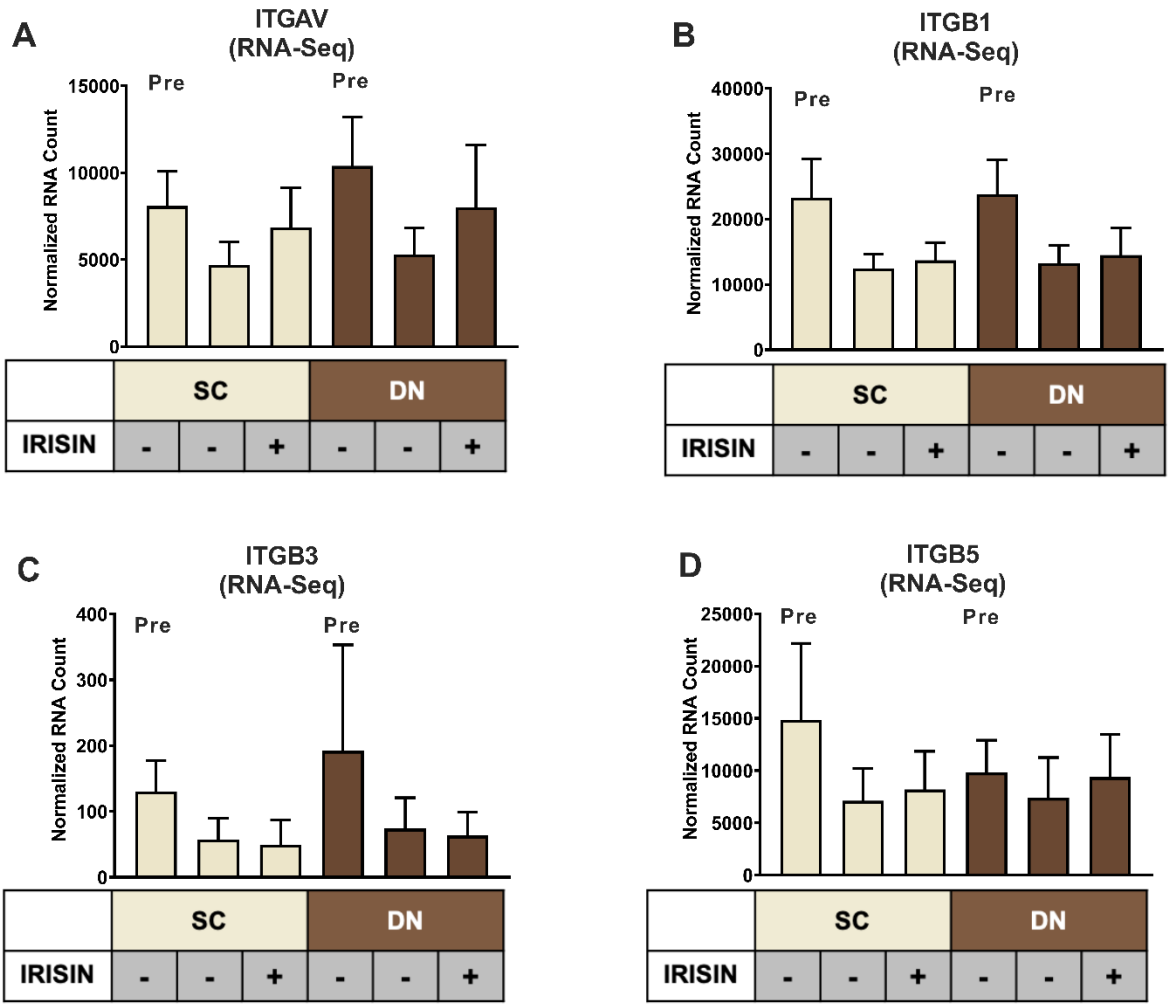

Figure 16: Gene expression of proposed irisin receptors in differentiated adipocytes. SC and DN preadipocytes were differentiated and treated as per figure 15. Quantification of ITGAV (A), ITGB1 (B), ITGB3 (C) and ITGB5 (D) gene expression as per RNA Sequencing data (n=9). Results are expressed as mean ± SD.

4.2.2. Irisin treatment cannot upregulate characteristic thermogenic genes in SC and DN derived differentiating adipocytes in contrast to adipocytes obtained from abdominal subcutaneous tissue depot

RNA Sequencing identified 79 upregulated genes upon irisin treatment that are visualized by Volcano Plot (Figure 17A). 50 and 66 genes were significantly upregulated in SC and DN adipocytes in response to irisin, 37 of which are commonly upregulated between the depots (Figure 17B). A list of all genes upregulated upon irisin treatment in SC and DN adipocytes are listed in Table 3.

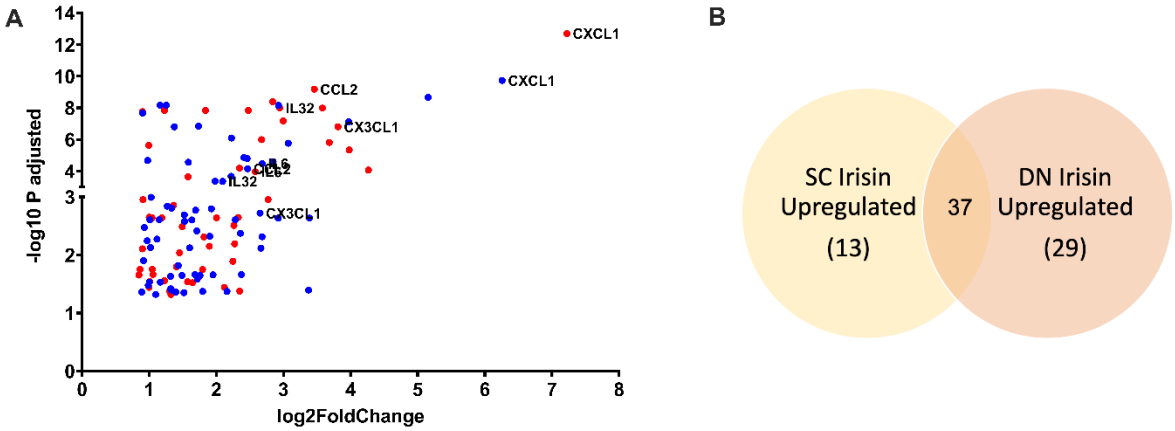

Figure 17: Irisin upregulates similar sets of genes in SC and DN depot derived differentiating adipocytes. SC and DN preadipocytes were differentiated and treated as per figure 15-16. (A) Volcano plot representing each of the upregulated genes in SC (red) and DN (blue) depots upon irisin treatment, (B) Venn diagram showing the commonly upregulated genes by irisin treatment in SC and DN depots.

Table 3: List of genes upregulated upon irisin treatment in SC and DN derived differentiated adipocytes

SC Irisin Upregulated			
Gene-symbol	**log2FoldChange**	**Gene-symbol**	**log2FoldChange**
CXCL1	7.224	CPXM2	1.794
CXCL3	4.266	AC245100.8	1.645
CXCL5	3.979	CYP7B1	1.579
CX3CL1	3.813	POU2F2	1.572
CXCL2	3.684	SLC39A8	1.493
TNFAIP6	3.581	KIRREL3	1.452
CCL2	3.46	IL34	1.405
CFB	2.997	NFKBIZ	1.361
IL32	2.945	DPYSL3	1.324
BIRC3	2.838	SORCS2	1.302
COL4A4	2.771	APOL1	1.228
ICAM1	2.673	RELB	1.227
IL6	2.581	TYMP	1.187
SOD2	2.478	RPL29P19	1.056
CLDN1	2.349	IL15RA	1.048
TRPA1	2.345	NFKBIA	1.042
RFLNA	2.327	NNMT	1.009
LRRC15	2.272	JUNB	0.999
ELOVL2	2.262	DGKI	0.999
IL18	2.247	NFKBIE	0.995
LINC02015	2.119	CNTNAP1	0.908
MT2A	2.002	ZC3H12A	0.901

RGS16	1.897	NFKB2	0.899
TNFAIP3	1.837	PLA2G4C	0.862
PDZK1IP1	1.818	SLC39A14	0.849

DN Irisin Upregulated			
Gene-symbol	**log2FoldChange**	**Gene-symbol**	**log2FoldChange**
CXCL1	6.258	SERPINE1	1.68
CXCL5	5.154	MXRA5	1.635
CXCL2	3.97	PDZK1IP1	1.604
CXCL3	3.387	NFKBIZ	1.583
HCK	3.374	KIRREL3	1.527
TNFAIP6	3.073	SLC39A8	1.523
CFB	2.926	SERPINE2	1.518
SLC7A2	2.922	ITGB2	1.49
RFLNA	2.847	ADCY4	1.434
CLDN1	2.683	CEMIP	1.396
IL6	2.682	SLC39A14	1.374
CCL11	2.664	LINC01503	1.336
CX3CL1	2.652	PODNL1	1.332
CCL2	2.465	PTX3	1.32
ICAM1	2.46	IL34	1.317
TRPA1	2.411	RPL29P19	1.269
MT1F	2.375	RELB	1.255
LRRC15	2.36	CYP7B1	1.166
ELOVL2	2.282	NFKBIE	1.162
SOD2	2.228	MT1E	1.15
MT2A	2.22	NNMT	1.115
AL356417.2	2.159	SH3BP1	1.097
IL32	2.094	JUNB	1.03
MXRA5Y	1.982	RARRES2	1.02
FNDC1	1.95	TNFAIP2	1.01
POU2F2	1.926	DRAM1	1.001
CH25H	1.902	SLC12A8	0.986
ANKRD1	1.798	SLCO3A1	0.977
RGS16	1.757	NFKBIA	0.97
TNFAIP3	1.735	ZC3H12A	0.926
IL7R	1.717	FTH1P8	0.916
BIRC3	1.711	NFKB2	0.902
KCNJ15	1.691	NTNG2	0.888

Previously our research group has shown that irisin treatment at 250 ng/mL can upregulate UCP1 gene expression in human primary subcutaneous abdominal differentiating adipocytes (Kristóf et al., 2015). Now, we have confirmed that irisin treatment can significantly upregulate UCP1 protein expression in abdominal differentiating adipocytes (Figure 18). Strikingly, irisin treatment could not upregulate characteristic thermogenic marker genes like UCP1 in SC and DN derived differentiating adipocytes (not shown).

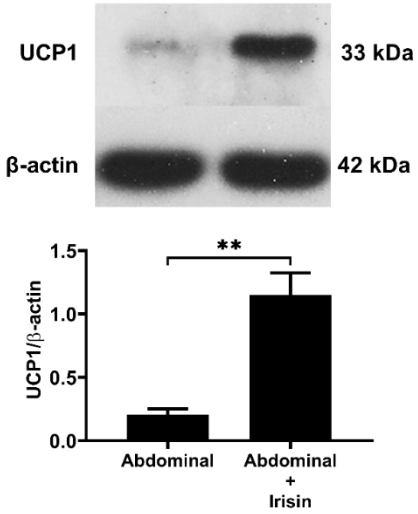

Figure 18: Irisin upregulates thermogenesis in human subcutaneous abdominal derived adipocytes. hADMSCs of abdominal origin were differentiated following the white adipogenic differentiation protocol with or without irisin treatment (250 ng/mL) for a period of 14 days. UCP1 protein expression normalized to β-actin (n=3). Results are expressed as mean ± SD. **p<0.01. Statistics: Welch's t-test.

4.2.3. Genes related to chemokine and interleukin signalling pathways are upregulated in response to irisin in SC and DN derived differentiating adipocytes

Panther enrichment analysis revealed that irisin treatment commonly upregulated pathways involving cytokine signalling (NFKB2, CXCL1, CXCL2, IL32, IL34, IL6, CCL2), interleukin-4 and 13 signalling (IL6, CCL2, JUNB, ICAM1), and class A/1 rhodopsin like receptors (CXCL3, CXCL5, CX3CL1, CXCL2, CCL2, CXCL1) in SC and DN adipocytes (Table 4). Gephi diagrams clearly illustrate the interactions of upregulated genes belonging to several pathways (Figure 19). IL10 signalling and G-alpha-I signalling pathways were amongst the upregulated pathways in SC and DN adipocytes respectively (Figure 19, Table 4).

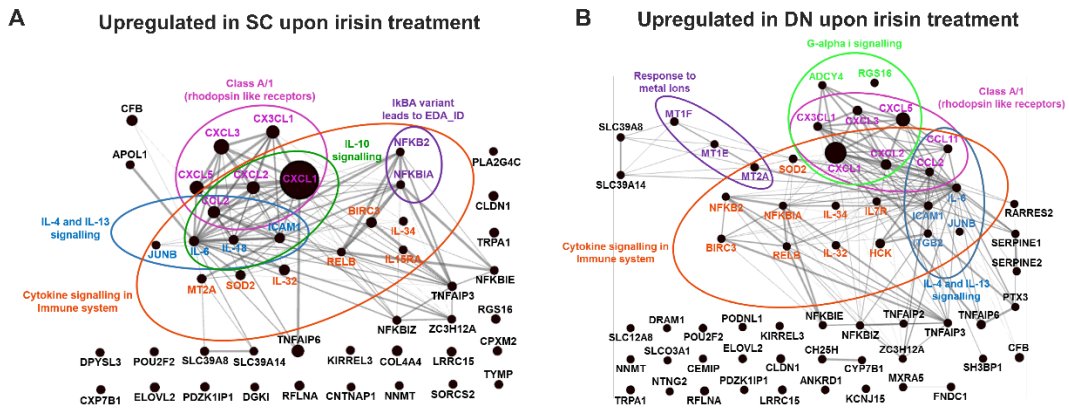

Figure 19: Irisin upregulates pathways relating to cytokine signalling in differentiating SC and DN derived adipocytes. Gephi diagrams highlighting the most important pathways upregulated by irisin treatment in SC (A) and DN (B) derived adipocytes.

Table 4: Pathways influenced by genes significantly upregulated by irisin treatment in SC and DN derived differentiated adipocytes

SC Irisin Upregulated		
Reactome Pathways	**Gene name**	**FDR**
IkBA variant leads to EDA-ID	NFKBIA, NFKB2	4.49×10^{-2}
Cytokine signalling in immune system	IL6, NFKBIA, JUNB, IL32, SOD2, MT2A, NFKB2, CXCL2, CCL2, IL15RA, IL18, IL34, ICAM1, CXCL1, RELB, BIRC3	5.23×10^{-8}
Interleukin-10 signalling	IL6, CXCL2, CCL2, IL18, ICAM1, CXCL1	1.65×10^{-6}
Class A/1 (Rhodopsin like receptors)	CXCL3, CXCL5, CX3CL1, CXCL2, CCL2, CXCL1	3.5×10^{-2}
Interleukin-4 and Interleukin-13 signalling	IL6, JUNB, CCL2, IL18, ICAM1	2.3×10^{-3}
DN Irisin Upregulated		
Reactome Pathways	**Gene name**	**FDR**
Response to metal ions	MT2A, MT1E, MT1F	4.74×10^{-3}
Class A/1 (Rhodopsin like receptors)	CCL11, CXCL3, CXCL5, CX3CL1, CXCL2, CCL2, CXCL1	1.85×10^{-2}
Cytokine signalling in immune system	IL6, CCL11, ITGB2, NFKBIA, JUNB, IL32, SOD2, MT2A, NFKB2, IL7R, CXCL2, CCL2, IL34, ICAM1, HCK, CXCL1, RELB, BIRC3	5.55×10^{-8}
Interleukin-4 and Interleukin-13 signalling	IL6, CCL11, ITGB2, JUNB, CCL2, ICAM1	6.33×10^{-4}
G-alpha (i) signalling events	CXCL3, CXCL5, CX3CL1, ADCY4, RGS16, CXCL2, CXCL1	5.07×10^{-2}

Genes commonly upregulated in both SC and DN depots are indicated in red colour

4.2.4. CXCL1 is primarily released from SC and DN derived differentiating adipocytes in response to irisin

The chemokine (C-X-C motif) ligand 1 (CXCL1) belonging to the CXC chemokine family acts as a chemoattractant for several immune cells, especially neutrophils (Schumacher et al., 1992). Earlier termed as GROα, in humans this protein is encoded by the gene CXCL1 (Haskill et al., 1990). CXCL1 was found to be the highest upregulated gene as per RNA-Sequencing, that was further validated by RT-qPCR to be significantly upregulated in both SC and DN adipocytes upon irisin treatment (Figure 20 A,B). CXCL1 was found to be released upon irisin treatment from the conditioned medium collected on days number 4 and 12 of the differentiation period of both SC and DN derived differentiating adipocytes (Figure 20C).

We aimed to further investigate the dependence of CXCL1 release on the presence of irisin. For this SC and DN derived hADMSCs were differentiated for a period of 21 days with or without irisin, along with a group where irisin treatment was discontinued for the last 7 days. CXCL1 was found to be consistently released on days number 4,12,18,21 of the differentiation period only in presence of irisin; removal of irisin on day 14 promptly lowered the release of CXCL1 on days number 18 and 21 (Figure 20D).

Inhibition of the proposed irisin receptors by RGDS, a pan integrin inhibitor (Kim et al., 2018), could reduce the irisin-stimulated CXCL1 release on day 12 of the differentiation period only for DN adipocytes (Figure 20E). This indicated presence of irisin stimulates the CXCL1 release but not prominently on its presumed integrin receptors.

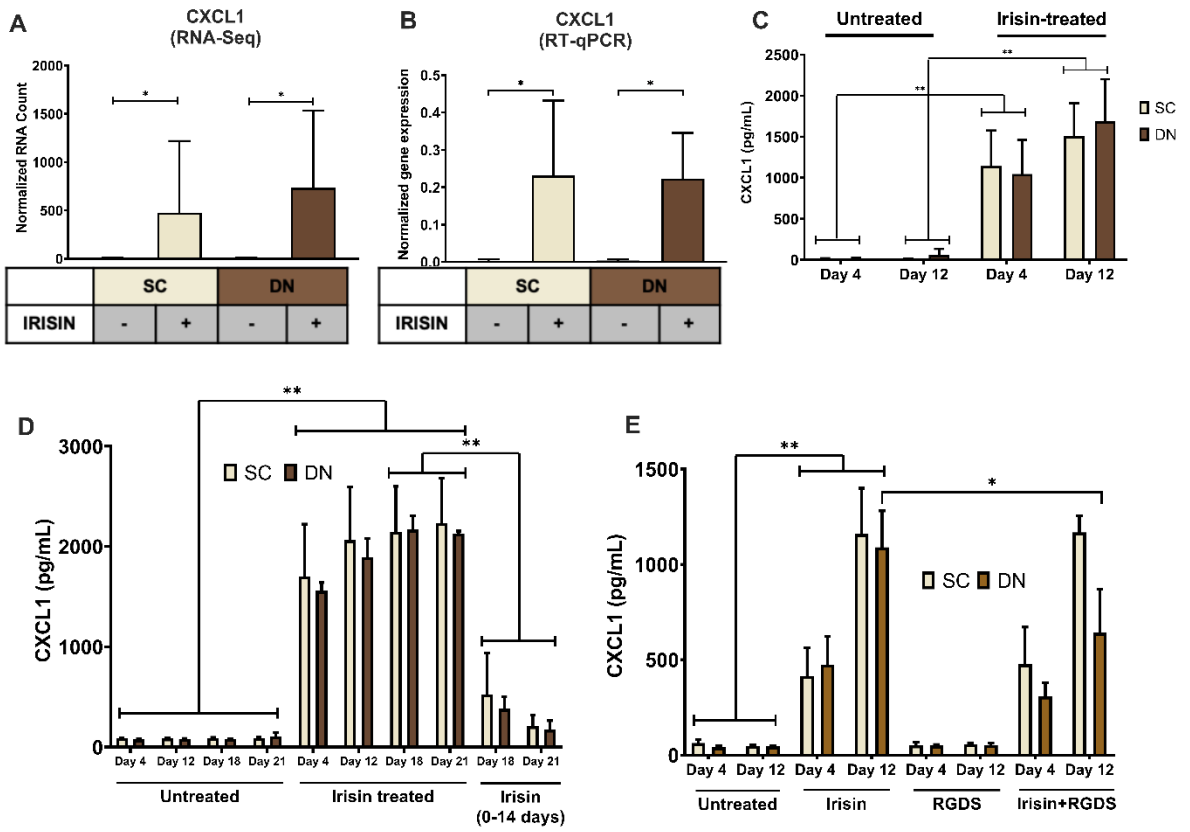

Figure 20: Irisin dependent release of CXCL1 from SC and DN derived differentiating adipocytes. SC and DN preadipocytes were differentiated and treated as per figure 15. Where indicated, irisin was omitted on day 14 from the differentiation medium. Quantification of CXCL1 gene expression by (A) RNA Sequencing (n=9) and (B) RT-qPCR (n=5). (C) CXCL1 release by SC and DN differentiating adipocytes quantified from conditioned media collected at the indicated intervals (n=4). (D) CXCL1 release in conditioned medium collected at indicated intervals from untreated (21 days) and irisin treated (14 and 21 days as indicated) cell-culture samples (n = 3), (E) Release of CXCL1 in presence or absence of irisin, with or without RGDS treatment at 10 µg/ml (n=4). RT-qPCR was normalized to GAPDH. Comparisons are for the respective days in case of ELISA. Data presented as Mean ± SD. $*p < 0.05$, $**p < 0.01$. Statistics: GLM (A), One-way ANOVA with Tukey's post-test (B), Two-way ANOVA with Tukey's post-test (C–E).

Release of CXCL1 throughout the differentiation period raised the possibility that both undifferentiated preadipocytes and differentiated adipocytes might release the chemokine. To investigate this, Brefeldin A was used to block the secretion machinery of the mixed cell population, followed by CXCL1 immunostaining and image acquisition by confocal microscopy. Irisin treatment resulted in accumulation of increased CXCL1 immunostaining in both SC and DN differentiated adipocytes than their preadipocyte counterparts (Figure 21). This clearly showed that the release of CXCL1 occurred primarily from SC and DN differentiated adipocytes.

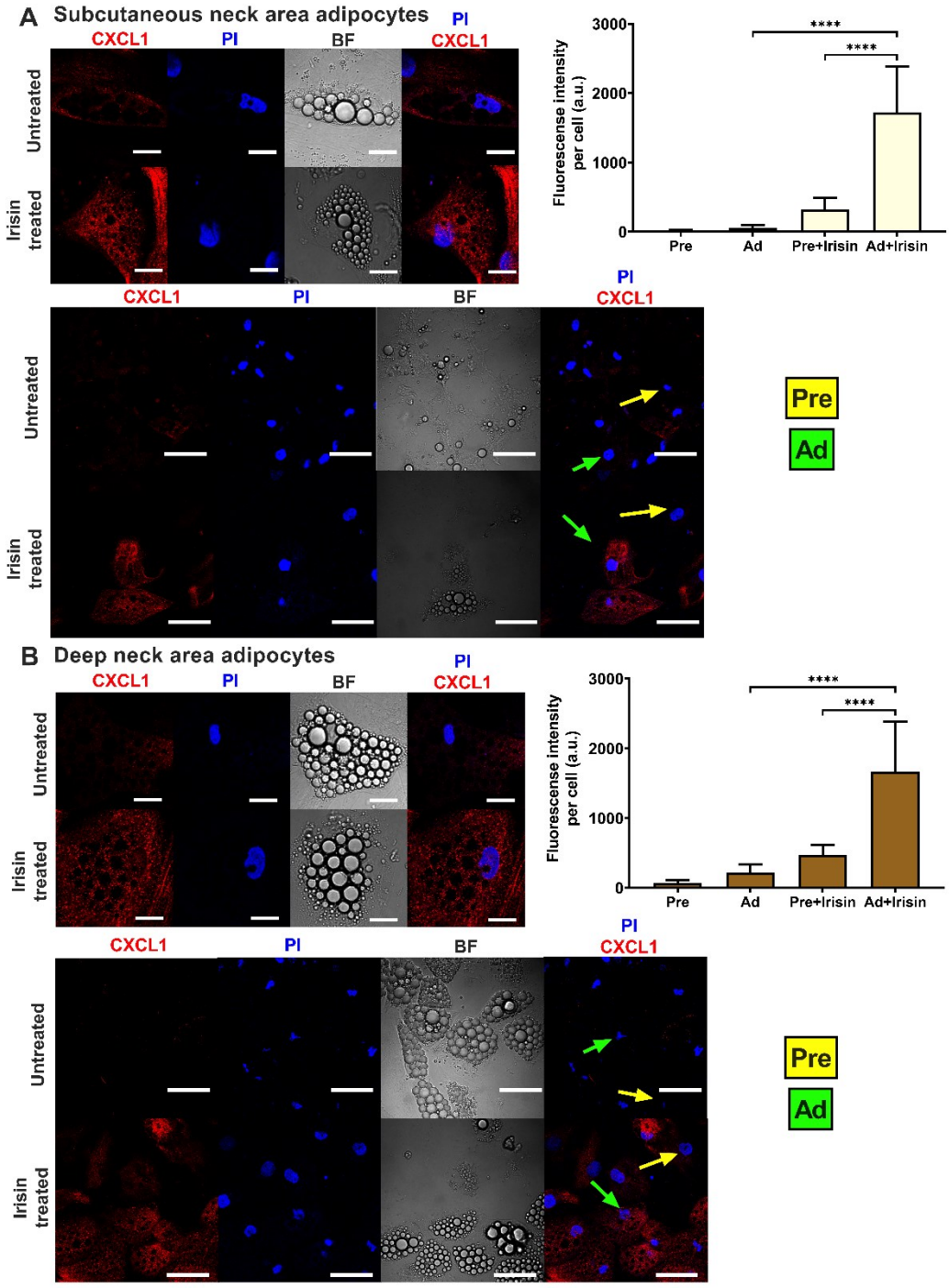

Figure 21: Irisin stimulates the release of CXCL1 predominantly from SC and DN derived differentiated adipocytes. Preadipocytes (Pre) were plated and differentiated into adipocytes (Ad) on Ibidi chambers, in presence or absence of irisin as in figure 15. Cells were treated with 100 ng/ml brefeldin-A for 24 hours to block the secretion of CXCL1, prior to fixation and image acquisition by confocal microscopy. BF represents the bright field image. Propidium Iodide (PI) was used to stain the nucleus. Confocal images of differentiated adipocytes were shown followed by wider coverage of undifferentiated and differentiated adipocytes. Scale bars represent 10 µm for single differentiated Ad and 30 µm for wider coverage of Pre and Ad. Yellow and green arrows point the undifferentiated preadipocytes and the differentiated adipocytes, respectively. Quantification of fluorescence intensity normalized to per cell are shown on the right bar graphs. n = 35 cells for SC (A) and 50 cells for DN (B) from two independent donors. Data presented as Mean ± SD. ****p < 0.0001. Statistics: One-way ANOVA with Tukey's post-test.

4.2.5. Irisin stimulates the CXCL1 release via upregulation of NFκB pathway

According to RNA-Sequencing data, irisin treatment significantly elevated NFKB2 and a very modest increasing trend was observed for NFKB1 and RELA that pointed towards the involvement of NFκB pathway (Figure 22).

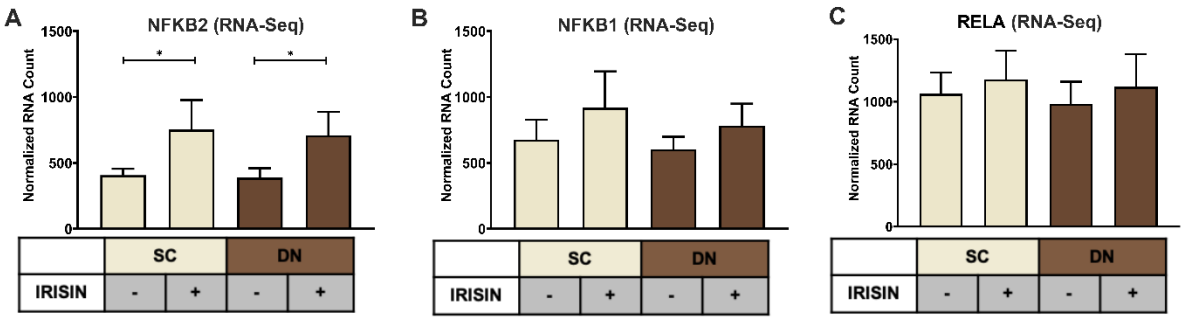

Figure 22: Irisin treatment upregulates genes related to NFκB pathway during the differentiation of SC and DN area adipocytes. SC and DN preadipocytes were differentiated and treated as per figure 15. Quantification of gene expression of NFKB2 (A), NFKB1 (B), RELA (C) as per RNA Sequencing (n=9). Data presented as Mean ± SD. *p<0.05. Statistics: GLM.

RT-qPCR validation confirmed a significant increase of NFKB1 (p50 subunit), RELA (p65 subunit) in DN and an increasing trend in SC adipocytes (Figure 23 A,B). Protein expression of p50 subunit was significantly elevated in DN, with an increasing trend in SC adipocytes (Figure 23C). IκBα (inhibitor of NFκB transcription factor) protein expression was significantly decreased by irisin treatment in SC, while a decreasing trend was observed in DN adipocytes (Figure 23D). These data collectively indicated an upregulation of the NFκB pathway.

To further prove the involvement of the NFκB pathway, a cell permeable inhibitor of NFκB nuclear translocation, SN50 was applied (Sárvári et al., 2015). SN50 significantly reduced the CXCL1 release from both SC and DN adipocytes treated with irisin (Figure 23E). Hence, irisin stimulates the release of CXCL1 via the upregulation of NFκB pathway.

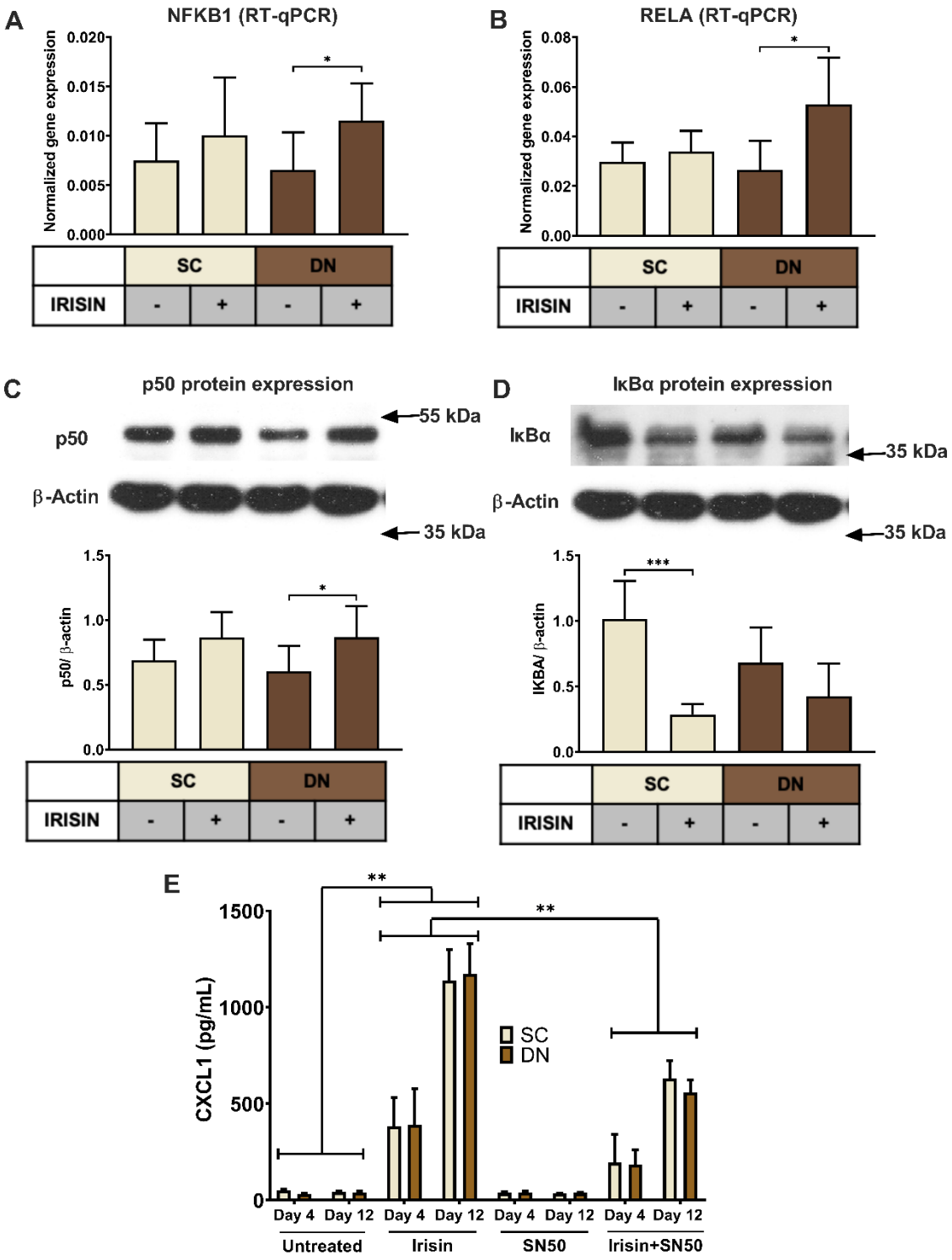

Figure 23: CXCL1 release is stimulated by irisin via NFκB pathway in SC and DN derived differentiating adipocytes. SC and DN preadipocytes were differentiated and treated as in figure 15. Quantification of gene expression for (A) NFKB1 and (B) RELA (n=5). (C) p50 and IκBα (D) protein expression (n = 6). (E) CXCL1 release from differentiating adipocytes with or without irisin treatment, in the presence or absence of 50 µg/ml SN50 (n = 4); comparisons are for the respective days. RT-qPCR was normalized to GAPDH and protein expression was normalized to β-actin. Data presented as Mean ± SD. ∗p < 0.05, ∗∗p < 0.01, and ∗∗∗p < 0.001. Statistics: One-way ANOVA with Tukey's post-test (A–D) and Two-way ANOVA with Tukey's post-test (E).

The observed effect of the CXCL1 release upon irisin treatment was not likely to be caused by an endotoxin contamination which was supported by the negligible expression of TNFα and CCL3 genes and decreasing trend for IL1β gene in irisin treated adipocytes (Figure 24). Furthermore, TNFα and IL1β could not be detected in the conditioned media of SC and DN derived differentiating adipocytes with or without irisin treatment (data not shown).

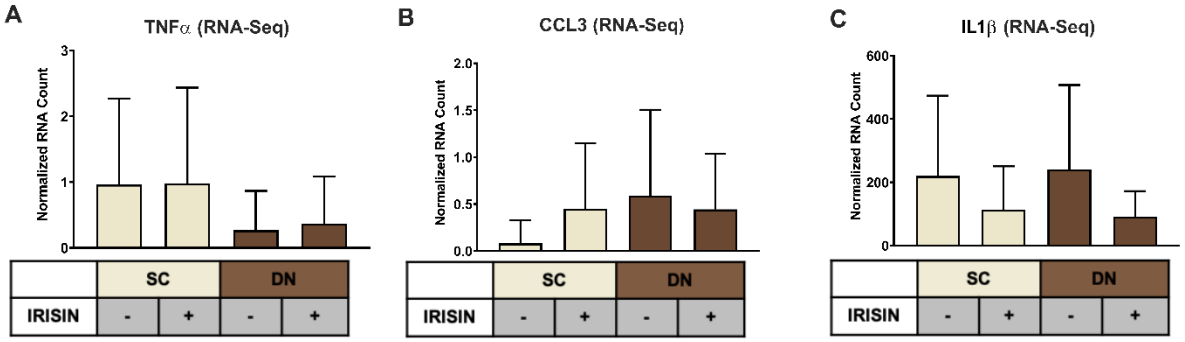

Figure 24: Irisin treatment of differentiating adipocytes does not influence the expression of pro-inflammatory marker genes. SC and DN preadipocytes were differentiated and treated as per figure 15. Quantification of gene expression of TNFα (A), CCL3 (B), and IL1β (C) as per RNA Sequencing (n=9). Data presented as Mean ± SD.

4.2.6. CXCL1 released from irisin stimulated adipocytes and adipose tissue improves adhesion property of human umbilical vein endothelial cells (HUVEC)

SC and DN tissue biopsies were floated for 24 hours in the presence or absence of irisin dissolved in empty media, followed by quantification of CXCL1 release from the conditioned media. CXCL1 release was found to be significantly stimulated from DN tissue biopsies upon irisin treatment (Figure 25A).

CXCL1 plays an important role in wound repair and angiogenesis (Gillitzer & Goebeler, 2001). Angiogenesis is vital for the thermogenic function of BAT (Cannon & Nedergaard, 2004). Therefore, we intended to detect the adhesion improving capacity of the released CXCL1. Conditioned media collected on the twelfth day of differentiation, from untreated and irisin treated SC and DN derived adipocytes, were added to HUVECs followed by a resorufin based adhesion assay. The conditioned medium from irisin treated adipocytes, containing various released factors (including CXCL1) significantly increased the number of attached viable HUVECs, compared to the medium collected from untreated adipocytes (Figure 25 B,C). HUVECs treated with recombinant CXCL1 at 2500 pg/mL (highest observed concentration of

CXCL1 from SC and DN differentiating adipocytes) significantly improved the adhesion property of the endothelial cells (Figure 25D). This suggested a potentially beneficial role of CXCL1 in promoting endothelial cell function and adipose tissue remodelling to indirectly promote efficient thermogenesis by enhanced vascularization.

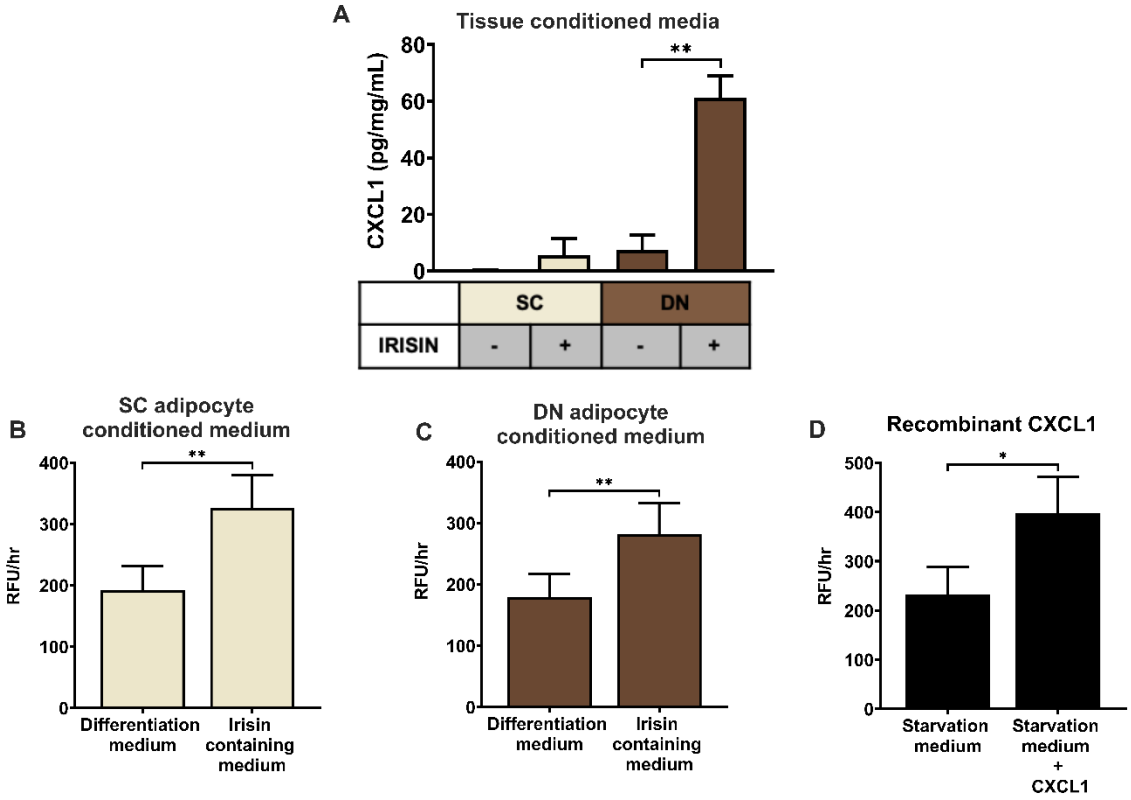

Figure 25: Irisin stimulates the release of CXCL1 from DN tissue biopsies, which has the capacity to improve the adhesion property of endothelial cells. (A) CXCL1 released into the conditioned media of paired SC and DN tissue biopsies 24 hours after incubation in the presence or absence of irisin (n = 4). Quantification of adhesion of endothelial cells upon incubation with the conditioned media (with or without irisin treatment) from *ex vivo* differentiated (incubation period from day 8–12 of differentiation) SC (B) and DN (C) area adipocytes (n = 5), (D) Quantification of endothelial cell adhesion upon incubation with recombinant CXCL1 in starvation medium (n = 3). Data presented as Mean ± SD. $*p < 0.05$, $**p < 0.01$. Statistics: One-way ANOVA with Tukey's post-test (A) and Welch's t-test (B–D).

4.3. BMP7 stimulates thermogenesis of deep neck derived adipocytes

4.3.1. Human primary SC and DN derived preadipocytes differentiated equally to mature white adipocytes irrespective of BMP7 treatment

hADMSCs were isolated from SVFs of SC and DN biopsies of nine independent donors, maintained and then differentiated following the white adipogenic differentiation protocol (Tóth et al., 2020) with or without the presence of BMP7 for 14 days. Samples were collected, followed by RNA isolation and RNA-Sequencing. Heatmap illustrating gene expression patterns of general adipocyte markers were elevated in all differentiated adipocytes compared to preadipocytes (Figure 26A). Adipocyte differentiation rate quantification by laser scanning cytometry showed that more than 50% cells were differentiated following the 14-day differentiation (Doan-Xuan et al., 2013; Kristóf et al., 2015); BMP7 did not exert any effect on the differentiation rate (Figure 26B). Gene expression of BMPR subunits (BMPR1A, BMPR1B, ACVR1, BMPR2, ACVR2A, ACVR2B) were abundant at the preadipocyte stage in both SC and DN adipocytes, BMP7 treatment did not alter their expression (Figure 26 C-H). Hence SC and DN derived preadipocytes differentiated equally irrespective of the BMP7 treatment.

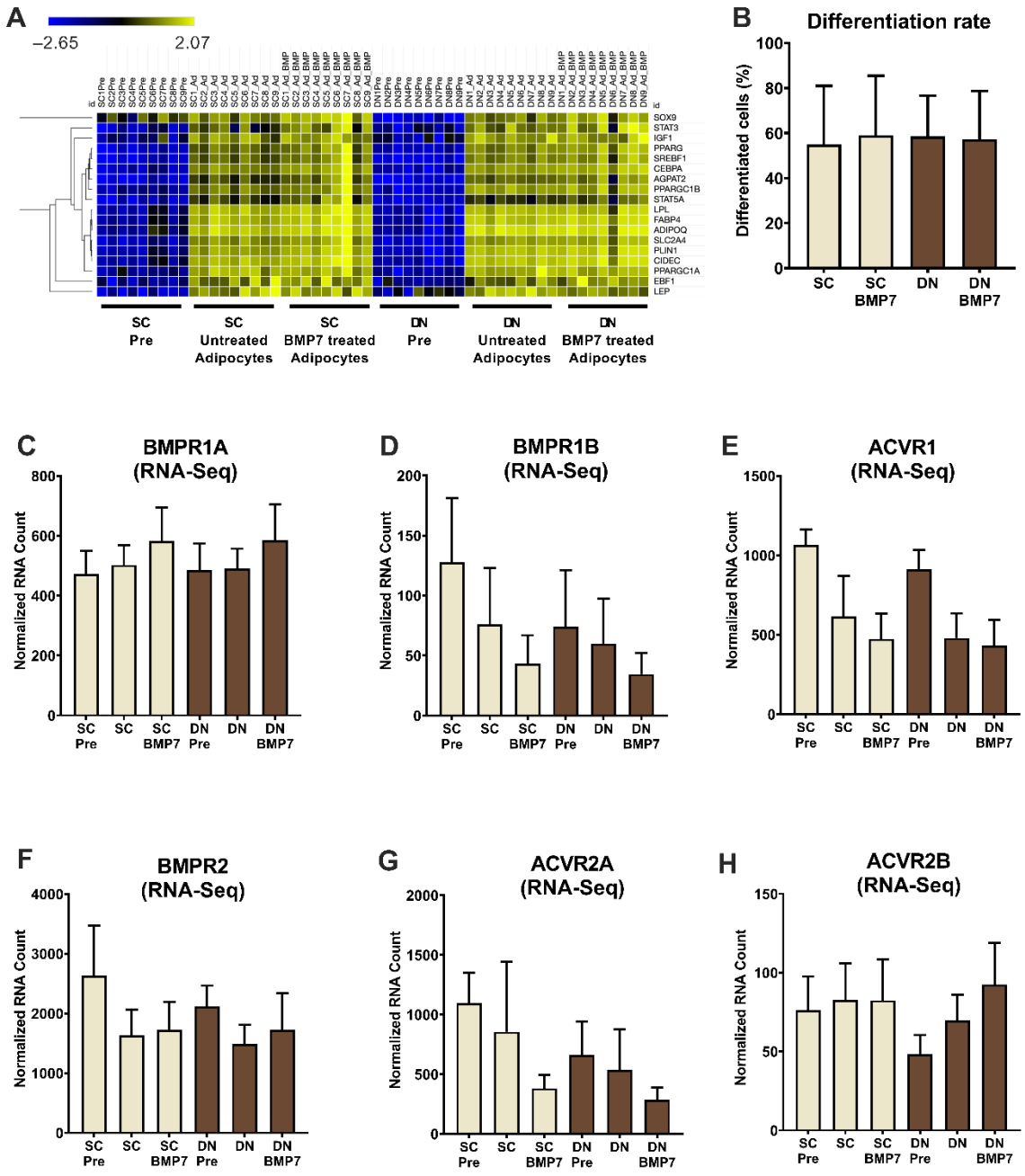

Figure 26: SC and DN derived preadipocytes differentiate equally in the presence or absence of BMP7 and express BMP7 receptors. SC and DN derived preadipocytes (Pre) were differentiated for two weeks following the white adipogenic differentiation protocol. BMP7 (50 ng/mL) was administered during the whole differentiation period as indicated. (A) Heatmap illustrating the expression of general adipogenic differentiation marker genes and (B) Differentiation rate quantification by laser-scanning cytometry. Quantification of gene expression of (C) BMPR1A, (D) BMPR1B, (E) ACVR1, (F) BMPR2, (G) ACVR2A, and (H) ACVR2B by RNA-sequencing. Data expressed as mean ± SD. n=9.

4.3.2. BMP7 elevates UCP1 dependent thermogenesis in SC and DN derived differentiating adipocytes

A recent in-depth analysis of murine and human white, beige and brown adipocyte transcriptomes has been utilized to develop BATLAS, an algorithm that can calculate brown/beige adipocyte content in cell and biopsy samples (Perdikari et al., 2018). Analysis of the RNA Sequencing data with BATLAS algorithm showed that browning content of DN adipocytes was significantly higher than SC (Figure 27A). BMP7 treatment significantly elevated browning content in both SC and DN derived differentiating adipocytes (Figure 27A). Quantification of texture sum variance by laser scanning cytometry (Doan-Xuan et al., 2013; Kristóf et al., 2015) revealed that BMP7 treatment slightly reduced the size of lipid droplets in both types of adipocytes, suggesting increased capacity for lipolysis and energy expenditure (Figure 27B). UCP1 gene expression showed a tendency to increase upon BMP7 treatment as per RNA Sequencing in both SC and DN adipocytes, that was found to be significant in DN adipocytes by RT-qPCR (Figure 27 C,D). UCP1 protein expression showed that DN adipocytes have a significantly higher UCP1 than SC (Figure 27E). BMP7 treatment significantly elevated UCP1 protein expression in both SC and DN adipocytes (Figure 27E). Confocal microscopy pictures of UCP1 immunostaining clearly showed that BMP7 increased the immunostaining intensity in neck derived adipocytes (Figure 27F). Laser-scanning cytometry assisted quantification of UCP1 immunostaining intensity (Kristóf et al., 2015) showed a significant increase of intensity in DN adipocytes upon BMP7 treatment (Figure 27G). Together these data suggest the upregulation of browning marker genes (including UCP1) in SC and DN adipocytes upon BMP7 treatment.

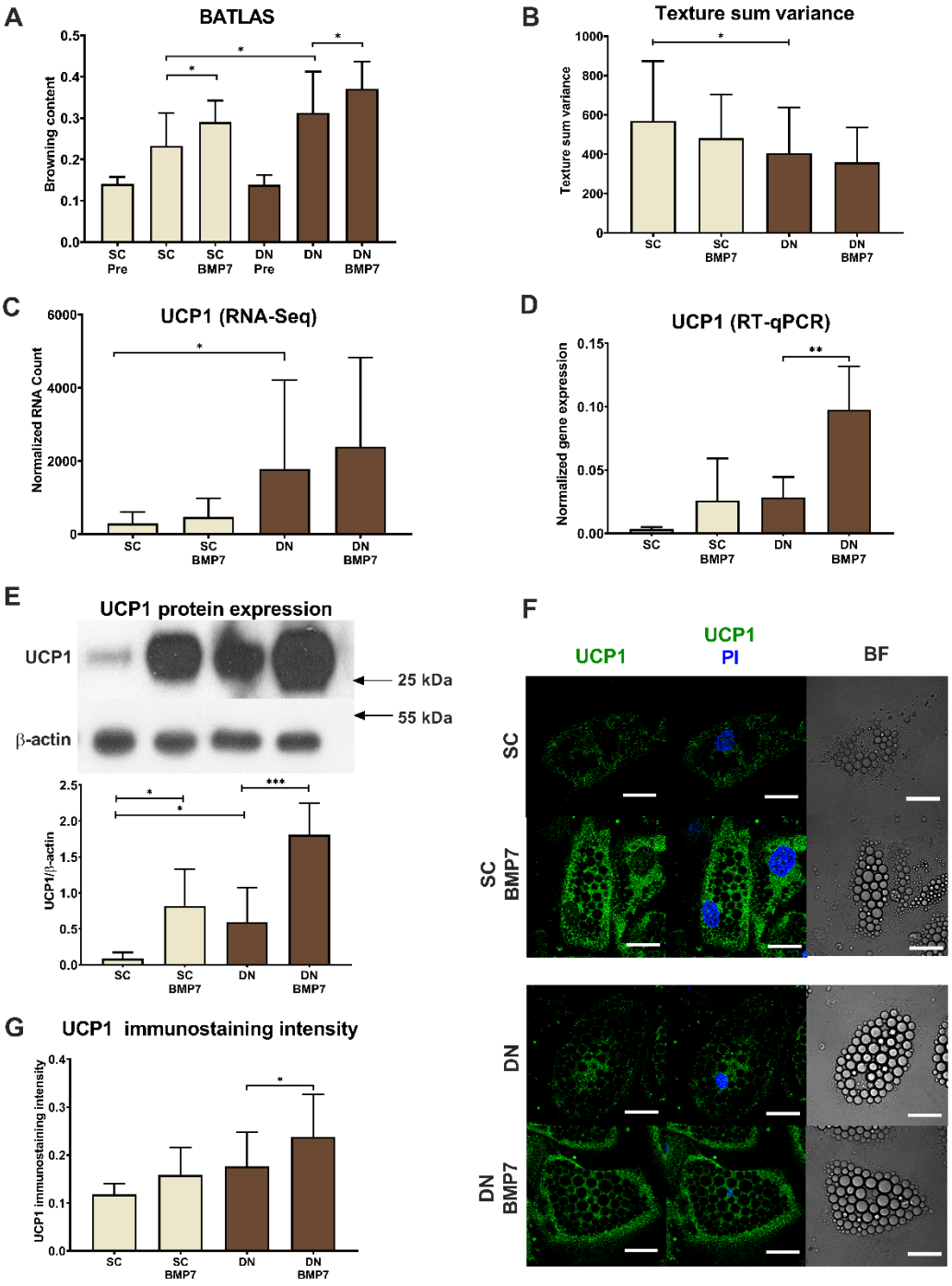

Figure 27: BMP7 upregulates UCP1-dependent thermogenesis in both SC and DN derived differentiated adipocytes. SC and DN preadipocytes were differentiated and treated as in figure 26. (A) Browning content estimated by BATLAS Webtool (n = 9), (B) texture sum variance as quantified by laser-scanning cytometry (n = 5). Quantification of UCP1 gene expression by (C) RNA-sequencing (n=9) and (D) RT-qPCR (n = 5). (E) UCP1 protein expression (n=5), (F) Representative UCP1 immunostaining images visualized by confocal microscopy. Nuclei was stained by PI, BF represents bright field image. Scale bars represent 10 µm. (G) Quantification of UCP1 immunostaining intensity assisted by laser-scanning cytometry (n = 4000 cells of 4 donors). RT-qPCR was normalized to GAPDH and protein expression was normalized to β-actin. Data expressed as mean ± SD. *p<0.05, **p<0.01, ***p<0.001. Statistics: Paired t-test (A, B, G), GLM (C), and one-way ANOVA with Tukey's post-test (D, E).

4.3.3. BMP7 elevated mitochondrial biogenesis leading to increased mitochondrial content, OXPHOS complex subunits and fragmented mitochondria

BMP7 treatment upregulated the protein expression of PGC1α in both SC and DN derived adipocytes (Figure 28A). PGC1α can be induced by the transcription factor CREB, that binds to a functional CRE in the PGC-1 promoter region (Puigserver et al., 1999). A significant induction of CREB phosphorylation (p-CREB) was observed in DN adipocytes (Figure 28B). Together the upregulation of PGC1α and p-CREB suggested an increase of mitochondrial biogenesis upon BMP7 treatment (Kelly & Scarpulla, 2004). This fact was further supported by an elevation of the protein expression of mitochondrial respiratory chain complexes upon BMP7 treatment; amongst which Complex I, II and III subunits showed a significant elevated level (Figure 28C).

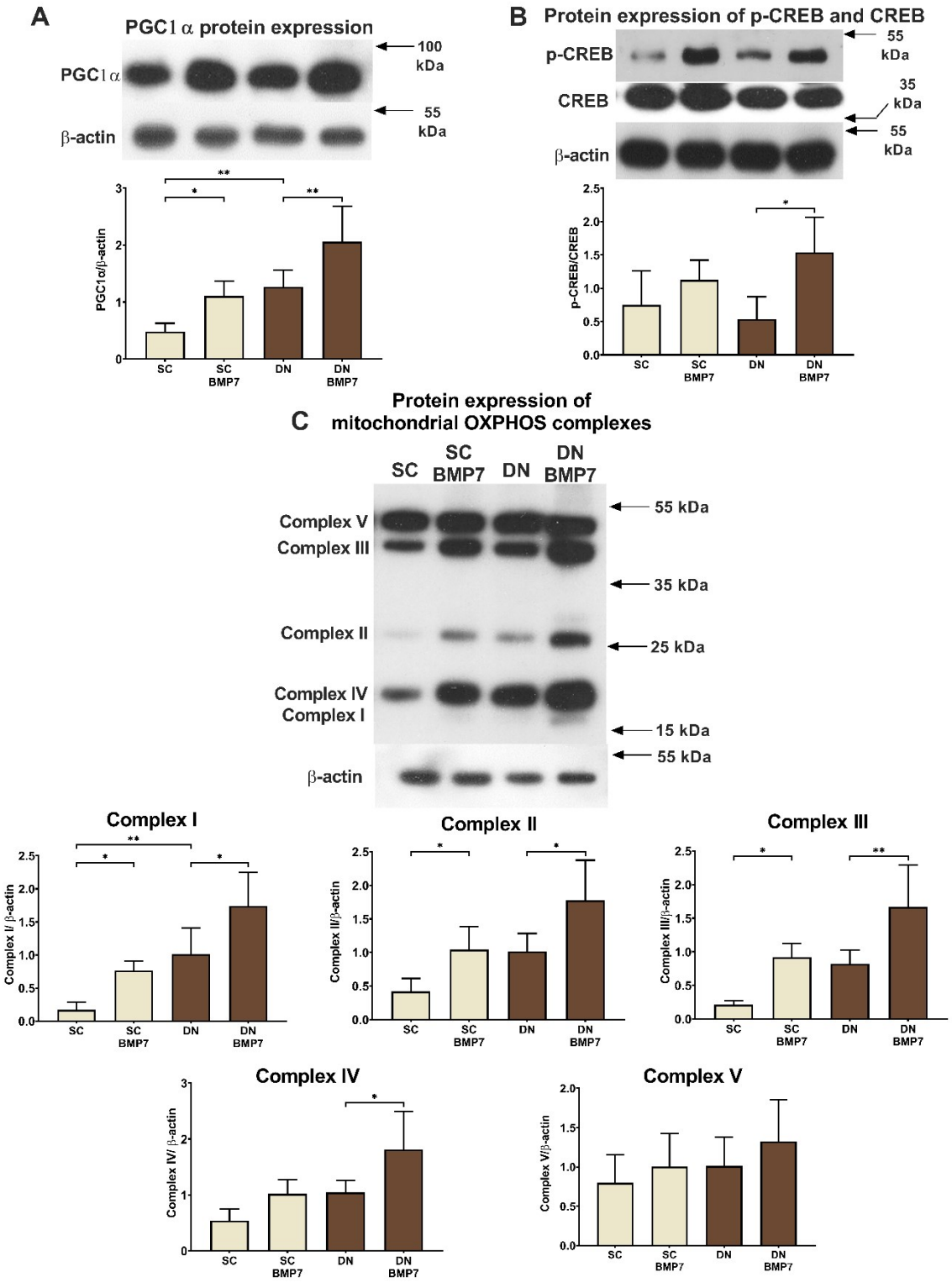

Figure 28: BMP7 treatment elevates mitochondrial biogenesis in neck derived differentiating adipocytes. SC and DN preadipocytes were differentiated and treated as in figure 26-27. Protein expression of (A) PGC1α, (B) pCREB:CREB and (C) mitochondrial OXPHOS complexes (I, II, III, IV, and V). n=5. Protein expression was normalized to β-actin. Data expressed as mean ± SD. *p<0.05, ** p<0.01. Statistics: one-way ANOVA with Tukey's post-test.

Quantification of fragmented mitochondria based on TOM20 immunostaining revealed a significant upregulation of its content following BMP7 treatment (Figure 29 A,B). The treatment also significantly increased the total mitochondrial DNA content in both types of adipocytes (Figure 29C). These data indicated that BMP7 treated differentiated adipocytes possess an enhanced thermogenic potential.

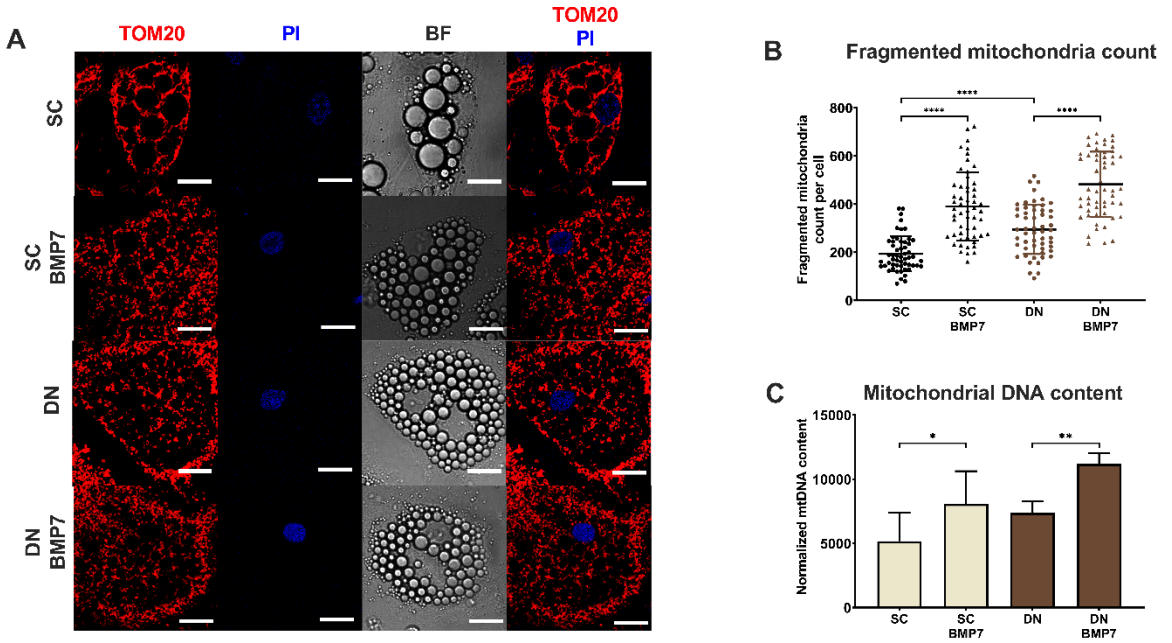

Figure 29: BMP7 treatment of differentiating adipocytes leads to elevated total and fragmented mitochondria content. SC and DN derived preadipocytes were differentiated and treated as in figure 26-28. (A) Representative confocal microscopy images of TOM20 immunostaining. Nuclei were stained by PI. Scale bars represent 10 µm. (B) Quantification of fragmented mitochondrial content normalized to per nuclei (n=55 cells, 3 donors), (C) total mitochondrial DNA content quantified by qPCR (n=5). mtDNA was normalized to SIRT1. Data expressed as mean ± SD. *p<0.05, **p<0.01, **** p<0.0001. Statistics: one-way ANOVA with Tukey's post-test.

Next, we intended to investigate the functional consequences of improved thermogenic potential. OCR data revealed that both basal and cAMP stimulated OCR was significantly elevated upon BMP7 treatment (Figure 30A). Importantly, proton leak related OCR was also significantly elevated following treatment in both SC and DN derived differentiated adipocytes; this indicated increased UCP1 mediated thermogenesis (Figure 30A). Basal ECAR showed an increasing trend, while cAMP stimulated ECAR was significantly elevated in DN derived adipocytes differentiated in the presence of BMP7 (Figure 30B). Together, the data suggests that BMP7 treatment can significantly upregulate thermogenesis in SC and DN derived differentiating adipocytes.

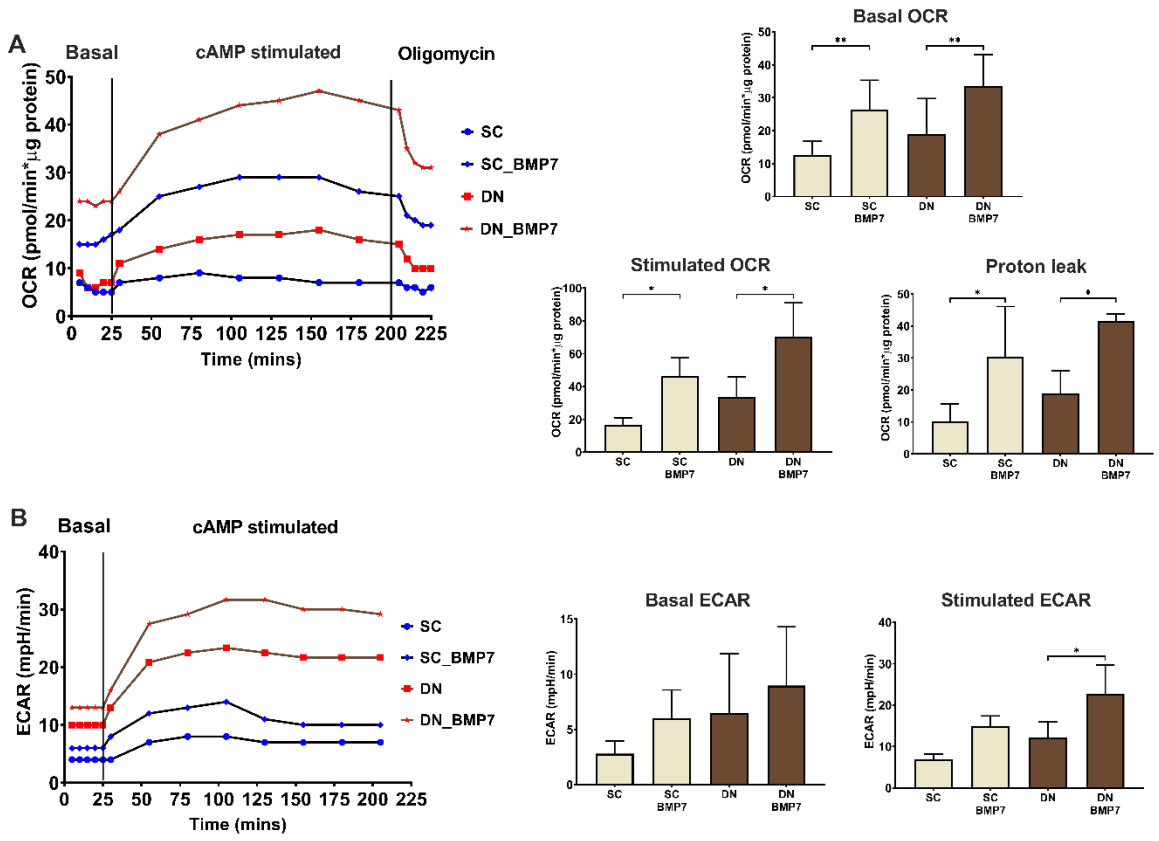

Figure 30: BMP7 treatment during differentiation results in increased oxygen consumption and acidification rates of differentiated adipocytes. SC and DN preadipocytes were differentiated and treated as in figure 26-29. (A) Representative time lapse curve for measured oxygen consumption rate (OCR) data after indicated treatments, followed by quantification of basal, stimulated, and proton leak OCR. Proton leak was calculated by administration of oligomycin and subtraction of OCR value for antimycin, (B) Representative time lapse curve for measured extracellular acidification rate (ECAR) data after the indicated treatment, followed by quantification of basal and stimulated ECAR. Data expressed as mean ± SD. n = 4. *p<0.05, **p<0.01. Statistics: one-way ANOVA with Tukey's post-test.

4.3.4. BMP7 elevated creatine driven substrate cycle related thermogenesis in neck area derived adipocytes

BMP7 treatment significantly increased the creatine driven substrate cycle related OCR in both SC and DN derived adipocytes (Figure 31A) (Kazak et al., 2015). RNA expression of mitochondrial creatine kinase 2 (CKMT2) (Kazak et al., 2015), one of the possible kinases acting in the futile cycle, was slightly elevated as per RNA-sequencing dataset and was found to be significantly elevated by RT-qPCR analysis in both types of BMP7 treated adipocytes (Figure 31B). CKMT2 protein expression followed a similar pattern (Figure 31B). RNA-sequencing data revealed an increasing trend for CKB gene expression (Rahbani et al., 2021) upon BMP7 treatment, that was found to be significant in terms of protein expression also in

both types of adipocytes (Figure 31C). TNAP, the phosphatase identified to hydrolyse phosphocreatine to creatine, was highly expressed in both types of adipocytes (Figure 31D) (Sun et al., 2021). Together, these data suggest that BMP7 upregulates thermogenesis via both UCP1 and futile creatine phosphate cycle in human neck area adipocytes.

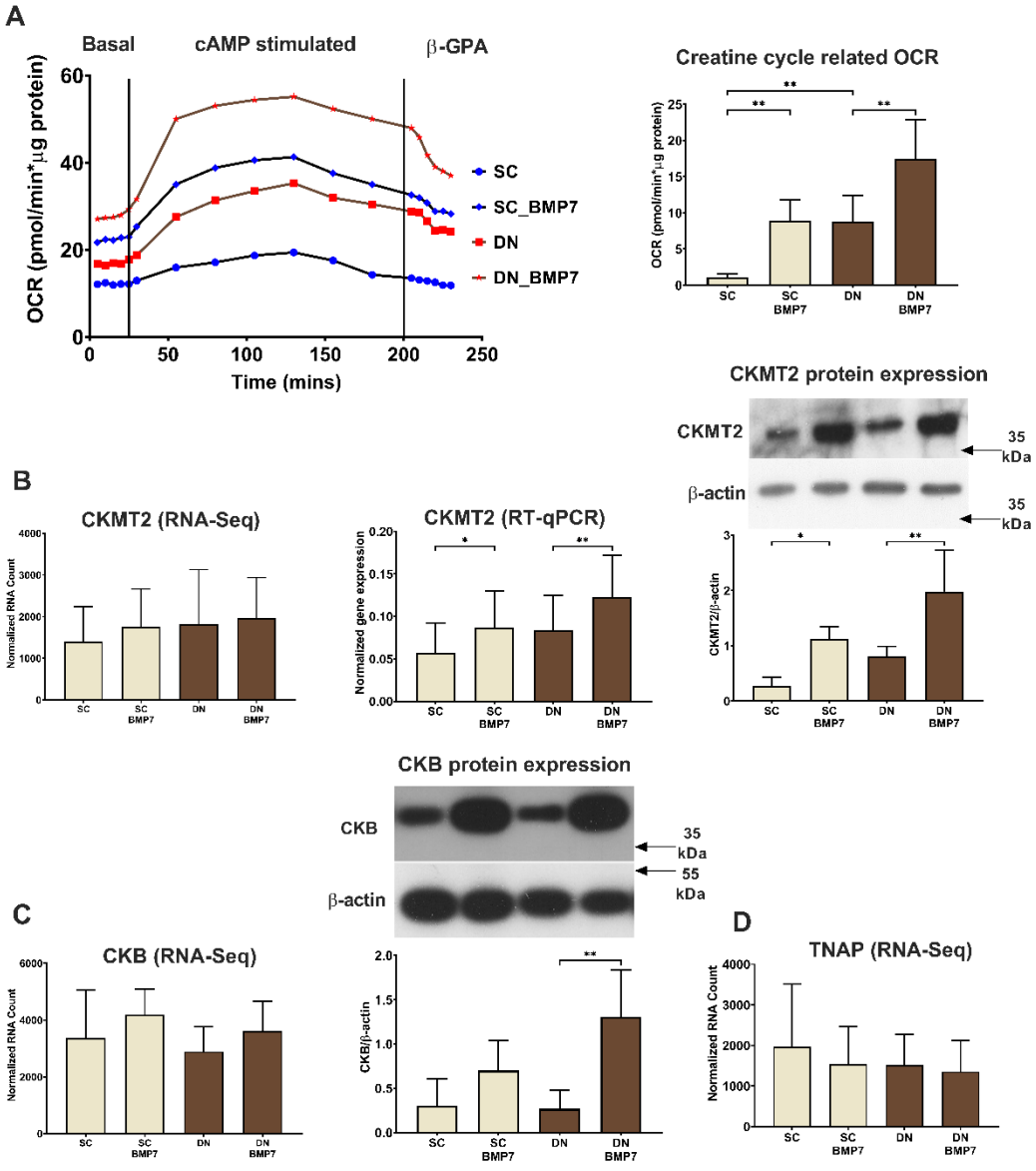

Figure 31: Creatine futile cycle-mediated thermogenesis is increased upon BMP7 treatment in neck area derived differentiated adipocytes. SC and DN preadipocytes were differentiated and treated as in figure 26-30. (A) Representative time lapse OCR curve after indicated treatments, followed by quantification of creatine cycle related (β-GPA inhibited) OCR (n=5). (B) Quantification of CKMT2 gene expression by RNA-sequencing (n=9) and RT-qPCR (n=5), followed by protein expression (n=5). (C) Quantification of CKB gene expression by RNA-sequencing (n=9), followed by protein expression (n=4). (D) Quantification of TNAP gene expression by RNA-sequencing (n=9). RT-qPCR was normalized to GAPDH and protein expression was normalized to β-actin. Data expressed as mean ± SD. *p<0.05, **p<0.01. Statistics: one-way ANOVA with Tukey's post-test.

4.3.5. BMP7 upregulated novel genes in SC and DN derived differentiating adipocytes that might play role in thermogenesis

Next, we aimed to further explore the BMP7 regulated pathways in neck area derived adipocytes that have so far not been linked to thermogenesis. RNA-sequencing data revealed that 121 and 60 genes were upregulated in BMP7 treated SC and DN derived adipocytes, while 190 and 87 genes were downregulated, respectively. BMP7 regulated genes are visualized by Volcano plot (Figure 32A) and the upregulated genes are listed in Table 5. Genes downregulated upon BMP7 treatment can be found at (Shaw, Tóth, Arianti, et al., 2021). 38 genes were commonly upregulated between SC and DN derived adipocytes, while 45 genes were commonly downregulated, respectively (Figure 32B). Panther pathway analysis illustrated that BMP signalling involving SMAD group of transcription factors (SMAD6, SMAD7, SMAD9) was commonly upregulated in both types of adipocytes, that is consistent with previous findings (Li & Wu, 2020). Integrin cell surface interactions (ITGA9, COMP, ITGA8), GPCR ligand binding (ADRA2A, ADRA2C, FZD1, FZD5, ACKR1) and extracellular matrix proteins (ACAN) were among the significantly elevated pathways only in SC derived adipocytes upon BMP7 treatment (Table 6).

Table 5: List of upregulated genes upon BMP7 treatment in SC and DN derived differentiating adipocytes

SC BMP7 Upregulated			
Gene symbol	**log2FoldChange**	**Gene symbol**	**log2FoldChange**
ID1	4.323910086	TMEM132C	1.676207435
MYOZ1	3.815257814	THBD	1.651241299
SAMD11	3.784625054	CABCOCO1	1.631222348
DES	3.554691177	RPL13AP25	1.628126529
CPNE5	3.309507889	SNCG	1.605034763
ACTC1	3.306069719	GLDN	1.592887743
ACAN	3.296401223	ADRA2A	1.574820332
DLX3	3.284339325	ONECUT2	1.573457918
LINC02600	3.186418672	KLHL23	1.544446163
ID3	3.16046663	DNAH9	1.465560789
COMP	3.108907299	A2M	1.462757238
ADRA2C	3.102683197	STOX1	1.446388329
CP	2.987441884	GRIK5	1.444671473
SCGN	2.819776974	MYOM1	1.44004003
LINC02593	2.813611147	SCN5A	1.41721036
SLC7A10	2.810247254	SYT17	1.391717843
PKD2L1	2.698658775	ITGA8	1.367114342

AL513523.1	2.683539568	NMUR1	1.335581269
RSPO2	2.626777174	REEP1	1.32984759
CADM3	2.57260893	CDK18	1.326750733
SOX8	2.560843947	FAM47E	1.31893393
ACKR1	2.524605317	NKD1	1.309467618
ATOH8	2.524303159	MYL3	1.297578592
PARM1	2.466669411	NPAS1	1.285051089
SOX18	2.41466829	PLPPR4	1.266329546
PTGDR	2.413106326	DMTN	1.260387229
AL645608.2	2.376186706	CRYAB	1.215425559
PLN	2.321543994	TMEM132B	1.203168431
CNR1	2.199495778	LGI4	1.202562633
CFAP221	2.169532573	PTH1R	1.200250783
REM1	2.113782599	C1QTNF1	1.190330752
ANGPT4	2.105206616	SHISAL1	1.159709646
NOG	2.104441062	LDB3	1.154500762
CADM3-AS1	2.099192777	TICRR	1.151449431
HPGD	2.080751198	KAZALD1	1.144952849
CDH22	2.051153334	SEZ6L2	1.142609772
COL26A1	1.960028377	PDZD7	1.126157135
SNAI1	1.953656146	AL590999.1	1.119495944
RELN	1.951226724	ITGA9	1.116605064
CDH20	1.93715909	PRUNE2	1.11027983
SLC38A11	1.931584893	CMYA5	1.10122402
OCA2	1.921927258	SMAD7	1.097474924
SMAD6	1.888147012	EDNRA	1.096823565
AF131216.3	1.830018607	SULT1A1	1.091532477
CD1D	1.822472003	GPD1L	1.080335373
FGF13	1.814904133	SOX5	1.076249272
COL9A3	1.809843487	AC115837.1	1.066296754
FNDC11	1.802770928	RIMS4	1.059059672
AC026469.1	1.796702366	MOCS1	1.044596893
HAAO	1.789572018	INAFM2	1.044446854
CHRM4	1.775738385	LEPR	1.028497206
COL9A2	1.747867605	HPD	1.021361988
SMAD9	1.745770338	FZD1	1.006403861
FCN2	1.739685418	KIF7	0.976720615
NPY1R	1.73663662	IL17RE	0.97165896
HSPB1P2	1.713445425	STBD1	0.971575003
HS3ST2	1.71204828	FZD5	0.965670843
CYP26B1	1.709335816	SLC6A8	0.952924339
AC005077.4	1.689437421	MATN2	0.943991767
GOLGA7B	1.682268174	PHOSPHO2	0.85854136
		HVCN1	0.85470841

DN BMP7 Upregulated			
Gene symbol	**log2FoldChange**	**Gene symbol**	**log2FoldChange**
ID1	3.852371514	CD1D	1.852039921
ACAN	3.825115247	SMAD9	1.786026121
SAMD11	3.648406106	COL9A2	1.777219922
CPNE5	3.625372971	ONECUT2	1.746618002
SAMD5	3.546433107	CFAP221	1.709276352
ACTC1	3.489450739	GDAP1L1	1.616393176
MYOZ1	2.997059593	SYNDIG1	1.606137257
ADRA2C	2.994785149	TMEM132B	1.558069466
AL645608.2	2.818377137	IL7R	1.550378741
NPTX2	2.691138574	PTH1R	1.461952975
SOX8	2.546407379	PLEKHA6	1.45512684
LINC02593	2.544341894	TRIM67	1.41517565
SOX18	2.518180935	SNAI1	1.391137702
MDFI	2.500496827	SMAD6	1.378591534
CABCOCO1	2.275778027	TNMD	1.371976192
RELN	2.264223218	TSPAN18	1.327019458
ID3	2.213056568	MYOM1	1.324118815
CDH22	2.119287966	PCA3	1.279184349
PARM1	2.113251223	GLDN	1.251295819
CADM3	2.091992884	KAZALD1	1.238911603
AL022068.1	2.068941949	CRYAB	1.176575401
CNTN4	2.044472392	PRUNE2	1.142913434
CD22	1.998432045	SPAG1	1.076299203
AC009041.2	1.991269877	EDNRA	1.067123926
ATOH8	1.979697576	MYL3	1.062148163
PGF	1.909710316	TICRR	1.049910116
STOX1	1.89968918	RSPO3	1.029570587
NOG	1.887943886	FOXD2AS1	0.97823264
MYOZ3	1.874786067	CETN2	0.884590041
CRTAC1	1.853633218	SMAD7	0.863214307

Table 6: Pathways influenced by genes significantly upregulated by BMP7 treatment in SC and DN derived differentiating adipocytes

SC BMP7 Upregulated		
Reactome Pathways	**Gene name**	**FDR**
Signalling by BMP	NOG, SMAD9, SMAD6, SMAD7	2.49×10^{-2}
ECM proteoglycans	ITGA9, AL645608, ITGA8, ACAN, COMP, COL9A3, COL9A2	1.87×10^{-3}
Integrin cell surface interactions	ITGA9, AL645608, ITGA8, COMP, COL9A3, COL9A2	2.3×10^{-2}
GPCR ligand binding	PLPPR4, NMUR1, ADRA2C, FZD5, ACKR1, ADRA2A, PTH1R, NPY1R, CHRM4, FZD1, EDNRA, PTGDR, CNR1	2.93×10^{-2}
DN BMP7 Upregulated		
Reactome Pathways	**Gene name**	**FDR**
Signalling by BMP	NOG, SMAD9, SMAD6, SMAD7	6.05×10^{-3}

Genes commonly upregulated in both SC and DN depots are indicated in red colour

According to the RNA-sequencing analysis, ACAN, CRYAB, and ID1 were strongly upregulated in BMP7 treated SC and DN derived adipocytes (Figure 32A, Table 5). Gene and protein expression of ACAN was confirmed to be significantly higher in BMP7 treated SC adipocytes (Figure 32C). Gene and protein expression of CRYAB, a member of small heat shock protein (HSP) 20 family, was significantly increased in BMP7 treated SC and DN adipocytes (Figure 32D). ID1 gene expression was also significantly higher in both types of BMP7 treated adipocytes, while in case of protein expression, ID1 was significantly elevated in SC and showed an increasing trend in DN treated adipocytes (Figure 32E).

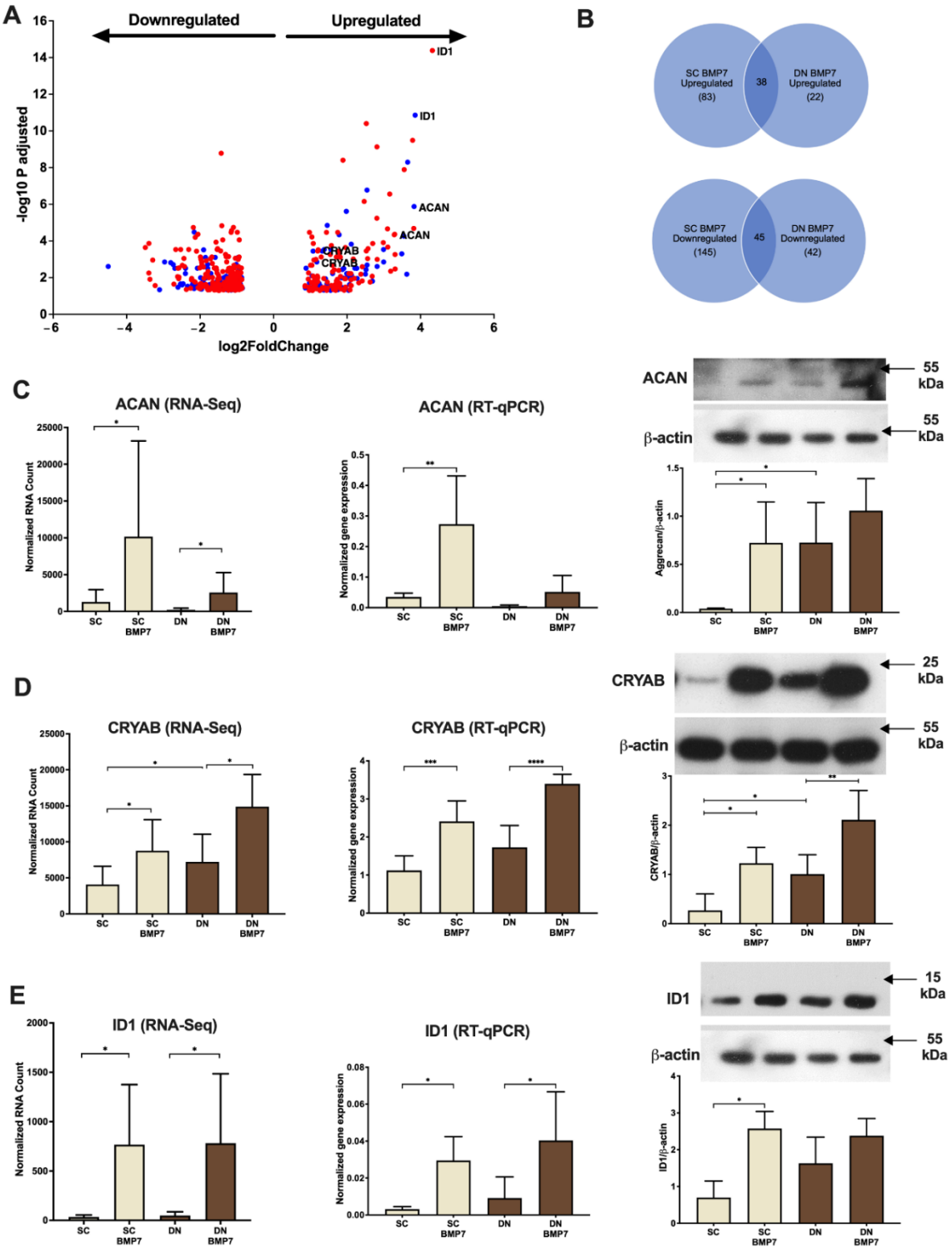

Figure 32: BMP7 treatment upregulates distinct genes in differentiating SC and DN adipocytes. SC and DN preadipocytes were differentiated and treated as in figure 26-31. (A) Volcano plot showing the up-or-downregulated genes in SC (red) and DN (blue) adipocytes upon BMP7 treatment. (B) Venn-diagram illustrating genes commonly up-or-downregulated by BMP7 between SC and DN derived adipocytes. Quantification of (C) ACAN, (D) CRYAB, and (E) ID1 gene expression by RNA-sequencing (n=9) and RT-qPCR (n=5), followed by their respective protein expression (n = 5). RT-qPCR was normalized to GAPDH, protein expression was normalized to β-actin. Data presented as mean ± SD. * $p < 0.05$, ** $p < 0.01$, *** $p < 0.001$, **** $p < 0.0001$. Statistics: GLM (RNA-sequencing), one-way ANOVA with Tukey's test (RT-qPCR and western blot densitometry).

5. Discussion

5.1. Downregulation of mitophagy contributes to the thermogenesis-inducing effect of cAMP mediated adrenergic stimulus in human abdominal white and beige differentiated adipocytes

Subcutaneous abdominal preadipocytes differentiated to white and beige adipocytes following a 14-day long differentiation protocol responded to cAMP mediated thermogenic stimulus starting 6 hours post exposure. The thermogenic stimulus led to increased UCP1 gene and protein expression both in white and beige differentiated adipocytes (Figure 9A). The total mitochondrial DNA content was also elevated following the cAMP stimulus, that partially resulted from an increased mitochondrial biogenesis driven by elevated PPARGC1A gene expression (Figure 9 B,C). The cAMP stimulus resulted in increased amount of mitochondria with fragmented morphology in both white and beige differentiated adipocytes, which possess the capacity to deliver thermogenesis on demand because of their increased UCP1 content (Figure 33).

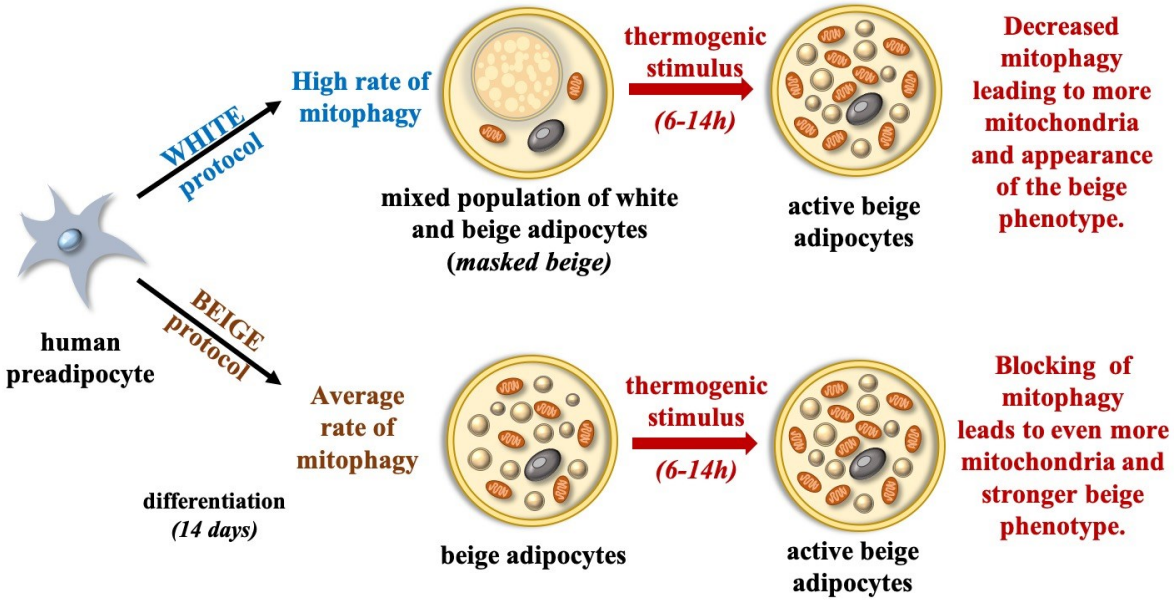

Figure 33: Mitophagy is repressed upon adrenergic stimulus leading to higher thermogenic potential in abdominal derived white and beige differentiated adipocytes (Szatmári-Tóth et al., 2020)

The increased fragmented mitochondria content may not be solely attributed to increased mitochondrial biogenesis, since mitophagy too plays an important role in the process (Altshuler-Keylin et al., 2016). The cAMP mediated thermogenic stimulus downregulated gene expression of general autophagy markers like ATG5, ATG7 and ATG12 (Figure 10A). It also resulted in decreased protein expression of LC3-II/LC3-I (Figure 10B), that was further verified by a reduced count of LC3 punctae upon immunostaining (Figure 11). This indicated a repression of the autophagy machinery upon thermogenic stimulus.

The binding of NA to adrenergic receptors increases intracellular cAMP levels, that in turn leads to activation of the cAMP-PKA signalling pathway (Cannon & Nedergaard, 2004; Kajimura & Saito, 2014). The activation of this pathway leads to the induction of mitochondrial biogenesis and genes related to thermogenesis. PKA has also shown to inhibit autophagy through various mechanisms in response to adrenergic stimulation in mammalian cells. PKA can directly phosphorylate LC3 (Cherra et al., 2010) or indirectly via activating the mammalian target of rapamycin complex 1 (mTORC1), that serves as a major repressor of autophagy (He & Klionsky, 2009; Liu et al., 2016). Consistent with recent mouse studies (Altshuler-Keylin et al., 2016; Cairó et al., 2016), we have shown that the cAMP mediated thermogenic stimulus represses the autophagic activity via activation of cAMP-dependent PKA pathway in primary human abdominal differentiated beige adipocytes (Szatmári-Tóth et al., 2020).

Altshuler-Keylin et al. identified autophagy-mediated removal of mitochondria as a novel mechanism for beige adipocyte maintenance and energy expenditure in mice (Altshuler-Keylin et al., 2016). Here, mitophagy rate was evaluated by colocalization of LC3 and TOM20 immunostaining, that indicated a repression of mitophagy upon thermogenic stimulus (Figure 11). Parkin is one of the major mediators of mitophagy, with decrease in parkin-dependent mitophagy reported to drive WAT browning in mouse 3T3-L1 adipocytes (Taylor & Gottlieb, 2017). Parkin downregulation was observed in response to thermogenic induction of mouse BAT, and high thermogenic activity was exhibited by parkin knockout mice (Cairó et al., 2019). However, Corsa et al. published opposing results, claiming parkin is dispensable for adipogenesis, differentiation and mitochondrial quality control in mice beige adipocytes (Corsa et al., 2019). In our study, parkin gene and protein expression were repressed upon thermogenic stimulus in human white and beige differentiated adipocytes (Figure 12A). Gene expression of parkin mediated mitophagy adapter proteins OPTN and NDP52 were also downregulated upon thermogenic stimulus (Figure 12 B,C). However, silencing of parkin could neither result in an improved thermogenic response nor it repressed autophagy, as was observed upon cAMP

mediated adrenergic stimulus (Figure 13). These results show that Parkin may not play a pivotal role in regulating mitophagy in white and beige adipocytes of abdominal origin. In addition to adapter proteins, parkin independent mitophagy pathways have also been shown to mediate adipose tissue specific thermogenic effects. BCL2L13 has been shown to contribute in beige adipocyte biogenesis (Ju et al., 2018) and BNIP3 in regulating mitochondrial fragmentation in mouse adipocytes (Tol et al., 2016). Here, gene expression of BCL2L13, FKBP8 and FUNDC1 were repressed upon thermogenic stimulus in white and beige adipocytes (Figure 14). Our results suggest that both parkin dependent and independent mitophagy mechanisms are important for mediating mitochondrial maintenance in white and beige adipocytes.

In addition to primary adipocytes, a non-immortalized human adipocyte cell line model, Simpson-Golabi-Behmel syndrome (SGBS) cells were used to rule out possible effects of heterogenicity and donor dependency (Wabitsch et al., 2001). All the experiments performed on primary adipocytes were subsequently repeated on SGBS adipocytes (Szatmári-Tóth et al., 2020). cAMP mediated adrenergic stimulus exerted similar effects on SGBS white and beige differentiated adipocytes. These further strengthened our findings that cAMP mediated adrenergic stimulus activates the thermogenic potential of subcutaneous abdominal fat by repressing mitophagy via both parkin dependent and independent mechanisms (Szatmári-Tóth et al., 2020).

The study raises the possibility of obtaining thermogenically active subcutaneous abdominal beige adipocytes from masked beige adipocytes in vivo by adipocyte specific inhibition of mitophagy. Recent studies indicated the presence of high amount of “brownable fat” in obese adults (Leitner et al., 2017). These depots might remain dormant as a result of high autophagy and mitophagy. Further studies are necessary for better understanding of the mechanisms regulating physiological mitophagy and its pathologic dysregulation that contribute to the cellular homeostasis of active beige adipocytes and the development of obesity, respectively.

5.2. Irisin as an inducer of browning

Irisin was discovered as a cleaved product of FNDC5 and primarily released by cardiac and skeletal muscles (Aydin et al., 2014; Boström et al., 2012). It has been shown to induce a beige differentiation program in mouse subcutaneous WAT. In human FNDC5 gene, adenine has shown to be replaced by guanine in the start codon, that might result in a shorter precursor protein lacking the part where irisin is cleaved (Raschke et al., 2013). Despite this, irisin has been detected from human blood plasma at 3-4 ng/mL by mass spectrometry (Jedrychowski et al., 2015). A recent publication determined the level of circulating irisin to be 0.3 ng/mL in mice, that was previously estimated to be 800 ng/mL (Maak et al., 2021). Irisin when applied at 25-1250 ng/mL, significantly increased UCP1 gene and protein expression in rat primary adipocytes (Zhang et al., 2014). The protein expression of BAT markers like PGC1α, PRDM16, and UCP1 were increased when irisin was applied at 250 ng/mL on 3T3L1 adipocytes (Tsai et al., 2020). Irisin (625 ng/mL) elevated mitochondrial respiration of human visceral and subcutaneous WAT-derived and perirenal BAT-derived adipocytes (Li et al., 2019). Our research group previously reported that recombinant irisin at above 50 ng/mL induced a beige program in human primary abdominal subcutaneous and SGBS adipocytes which were differentiated following the white adipogenic differentiation protocol (Klusóczki et al., 2019; Kristóf et al., 2015). Irisin treatment at 250 ng/ml significantly increased UCP1 protein expression in differentiating abdominal derived adipocytes (Figure 18). Adipocytes from the DN region has the ability to perform continuous non-shivering thermogenesis and hence play an important role in maintaining whole body energy expenditure (Cypess et al., 2013; Jespersen et al., 2013; Svensson et al., 2011; Wu et al., 2012). The effect of irisin treatment on differentiating human SC and DN derived adipocytes have not been fully elucidated. Recent publications indicated that irisin may induce a different degree of browning response in humans based on the adipose tissue origin (Buscemi et al., 2018; Li et al., 2019). As per our RNA-Sequencing results, irisin was unable to directly influence the expression of characteristic thermogenic marker genes in SC and DN area adipocytes.

5.3. Irisin plays a regulatory role, unrelated to thermogenesis upon acting on human neck derived differentiating adipocytes

In addition to their role in thermogenesis, active thermogenic adipose tissues secrete certain adipokines termed “batokines”, that act in an autocrine, paracrine or endocrine manner (Villarroya et al., 2017). Several recently discovered batokines, like NRG4, FGF21, CXCL14, BMP8b and adiponectin have been shown to exert a protective role against obesity by

enhancing beiging of WAT, sympathetic innervation, lipolysis and polarization of M2 macrophages (Ahmad et al., 2021). Our previous publication has shown that irisin treatment stimulated the release of batokines, like IL6 and MCP1 from human abdominal subcutaneous and neck area derived adipocytes (Kristóf et al., 2019). The released IL6 was shown to improve browning of human subcutaneous abdominal adipocytes (Kristóf et al., 2019). Here, using a RNA-Sequencing based approach, CXCL1 was found to be a novel adipokine released from both SC and DN derived differentiating adipocytes upon irisin treatment (Figure 17A, 20C and Table 3). The release of CXCL1 occurred primarily from differentiated adipocytes via upregulation of the NFκB pathway (Figure 21 and 23). Irisin has been shown to exert its effect on mouse osteocytes via a subset of integrin receptors, which are assembled from ITGAV and either of ITGB1, ITGB3 or ITGB5 (Kim et al., 2018). Our data showed a high expression of ITGAV, ITGB1, ITGB3 and ITGB5 in both preadipocytes and differentiated adipocytes. However, RGDS peptide (Kim et al., 2018) could exert only a mild effect on the irisin stimulated CXCL1 release only in DN adipocytes (Figure 20E). This suggests that irisin might exert its effect via receptors other than the proposed integrin receptors.

CXCL1 binds to CXCR2 (Silva et al., 2017) and act as a chemoattractant of several immune cells, majorly neutrophils (Schumacher et al., 1992). CXCL1 has been shown to initiate migration of immune and endothelial cells upon injury to facilitate tissue repair (Gillitzer & Goebeler, 2001). Conditioned medium containing CXCL1 collected from irisin treated SC and DN differentiating adipocytes significantly improved the adhesion of HUVECs. Similar observation was made when HUVECs were treated with recombinant CXCL1 (Figure 25). Together these showed a possible beneficial paracrine role of the released CXCL1 from irisin treated adipocytes.

5.4. BMP7 upregulates thermogenesis in human neck derived adipocytes via both UCP1 dependent and independent mechanisms

BMP7 acts as an auto/paracrine mediator which promotes murine beige and brown adipocyte differentiation (Schulz et al., 2013; Tseng et al., 2008). BMP7 pre-treatment before differentiation of immortalized human neck derived white and brown preadipocyte clones showed significant elevation of UCP1 gene expression (Xue et al., 2015). Our previous research showed that BMP7 can upregulate gene expression of UCP1 and other classical browning markers like ZIC1 in SGBS adipocytes (Klusóczki et al., 2019). BMP7 has been shown to exert its effect via activation of p38 MAPK and PGC1α that will upregulate mitochondrial biogenesis and UCP1 expression (Tseng et al., 2008). BMP7 also exerts its effect via phosphorylation of SMAD1, SMAD5 and SMAD8 (Li & Wu, 2020).

Our study showed that receptors involve in BMP signalling were abundantly expressed in the preadipocyte stage of human neck area derived adipocytes (Figure 26 C-H). BMP7 treatment could significantly upregulate UCP1 dependent thermogenesis in SC and DN derived adipocytes, that was clearly validated by an increase in UCP1 gene, protein expression and immunostaining intensity (Figure 27 C-G). BMP7 increased the total and fragmented mitochondria content in neck derived adipocytes via upregulation of the PGC1α and p-CREB pathways, that is in accord with previously published studies (Figure 28 A,B and 29). The increase of fragmented mitochondria content further indicated an increased thermogenic potential, the functional aspect of which was confirmed by an increased basal, stimulated, and proton leak OCR in the neck derived BMP7 treated adipocytes (Figure 30A).

A creatine mediated futile cycle was recently discovered that enhanced mitochondrial respiration in beige fat (Kazak et al., 2015). Further an adipose tissue specific knockout of glycine amidinotransferase, the rate limiting enzyme for creatine biosynthesis, made mice susceptible to diet-induced obesity (Kazak et al., 2017). Creatine driven thermogenesis was also shown to play an important in both UCP1 negative and positive murine beige adipocytes (Bertholet et al., 2017). Mitochondrial creatine kinases, CKMT1 A/B, CKMT2, and recently CKB have been shown to play an important role in the creatine cycle driven thermogenesis (Kazak et al., 2015; Rahbani et al., 2021). Our data showed an increase of CKMT2 and CKB protein expression in BMP7 treated neck derived adipocytes (Figure 31 B,C). As a functional consequence, creatine cycle related OCR was significantly elevated in both SC and DN adipocytes upon BMP7 treatment (Figure 31A). This clearly showed that BMP7 elevates thermogenesis by UCP1-independent mechanisms also.

BMP7 holds a strong potential in therapeutic approaches targeting obesity. A recent study in mouse has shown that, liver directed adeno-associated viral (AAV)-BMP7 vectors could increase long lasting presence of BMP7 in circulation. The increase in circulating BMP7 in high-fat-diet-fed and genetically obese mice induced browning of WAT and activation of BAT, which in turn normalized body weight and improved insulin resistance in these mice (Casana et al., 2022).

5.5. BMP7 upregulates certain novel genes that may serve as positive regulators of thermogenesis

Our results indicated that BMP7 upregulates certain genes, like ACAN, CRYAB and ID1 that are unrelated to browning of adipocytes so far but showed a strong corelation with increased thermogenesis.

ACAN encoding aggrecan protein, a chondroitin sulphated proteoglycan, functions as an important structural component of cartilage (Morawski, Brückner, Arendt, et al., 2012). It is also found in brain exclusively in the perineuronal net, where it assists in its formation and function (Brückner et al., 1993; Giamanco et al., 2010; Matthews et al., 2002; Morawski, Brückner, Jäger, et al., 2012). A similar function is also expected for the innervation of brown adipose tissue. ACAN gene and protein expression was significantly elevated in SC adipocytes upon BMP7 treatment (Figure 32C).

CRYAB (Crystallin Alpha B) is a major structural protein of eye lens but expressed in other tissues also. CRYAB belongs to the small HSP family and functions as a chaperone protecting against oxidative stress and apoptosis (Dubin et al., 1989; Horwitz, 1992; Iwaki et al., 1989; Kato et al., 1991; Raman & Rao, 1994; Rao et al., 1993). In eye lens, CRYAB serves as a substrate for TGM2 (transglutaminase 2) mediated crosslinking (Groenen et al., 1992; Shridas et al., 2001). Our group has previously shown that gonadal WAT from TGM2 KO mice showed reduced expression of characteristic beige marker genes, like UCP1 and TBX1 (Mádi et al., 2017). Our previous publication showed that CRYAB gene expression was higher in the thermogenic DN adipocytes as compared to SC (Tóth et al., 2020). In this study, CRYAB gene and protein expression was significantly increased in neck derived adipocytes upon BMP7 treatment (Figure 32D).

The ID family comprising of ID1, ID2, ID3 and ID4 belongs to the helix–loop–helix (HLH) transcription factor family. They act primarily via dimerization with transcriptional regulators like basic-HLH (bHLH) factors which fails to bind to DNA. Hence the ID proteins function as

negative regulators of bHLH proteins (Benezra et al., 1990). A recent study indicated that ID1 protein is highly expressed in both murine WAT and BAT, with BAT showing the highest expression (Patil et al., 2014). In our study, ID1 gene and protein expression was upregulated in BMP7 treated neck derived adipocytes (Figure 32E).

Further experiments are necessary to validate the direct effects of ACAN, CRYAB and ID1 in thermogenesis of human beige and brown adipocytes.

6. Summary

- Adrenergic stimulus elevates thermogenesis in human primary abdominal white and beige differentiated adipocytes. This effect was found to be mediated by increased availability of fragmented morphology mitochondria that possess higher thermogenic capacity. Adrenergic stimulus resulted in increased mitochondrial biogenesis and reduced mitophagy that protected the fragmented mitochondria from degradation, leading to their increased availability.
- cAMP mediated adrenergic stimulus resulted in repression of mitophagy via both parkin dependent and independent mechanisms.
- Human SC and DN derived preadipocytes differentiated equally in presence or absence of irisin. However, unlike in abdominal subcutaneous derived adipocytes, the presence of irisin failed to upregulate characteristic thermogenic genes in the neck derived adipocytes.
- Irisin upregulated several common genes in both SC and DN derived differentiating adipocytes which mostly pointed towards cytokine and interleukin signalling pathways. The topmost upregulated gene, CXCL1, was found to be released by both SC and DN adipocytes throughout the differentiation period upon irisin treatment. The release of CXCL1 occurred primarily from differentiated adipocytes via the upregulation of NFκB pathway. The released CXCL1 increased adhesion of HUVEC cells.
- Human SC and DN derived preadipocytes differentiated equally in presence or absence of BMP7. BMP7 upregulated thermogenesis in SC and DN derived differentiating adipocytes via both UCP1 dependent and independent (futile creatine cycle mediated thermogenesis) mechanisms.
- BMP7 treatment led to increased availability of thermogenically competent fragmented morphology of mitochondria. The increased amount of mitochondria was a result of upregulation of mitochondrial biogenesis via PGC1α and CREB pathways.
- BMP7 treatment upregulated certain genes like ID1, ACAN and CRYAB that correlated with increased thermogenesis and may represent a novel function in assisting thermogenesis.

7. References

Abelenda, M., & Puerta, M. L. (1992, Feb). Brown adipose tissue thermogenesis in T3-treated rats. *Horm Metab Res, 24*(2), 60-62. https://doi.org/10.1055/s-2007-1003256

Admiraal, W. M., Holleman, F., Bahler, L., Soeters, M. R., Hoekstra, J. B., & Verberne, H. J. (2013, Feb). Combining 123I-metaiodobenzylguanidine SPECT/CT and 18F-FDG PET/CT for the assessment of brown adipose tissue activity in humans during cold exposure. *J Nucl Med, 54*(2), 208-212. https://doi.org/10.2967/jnumed.112.111849

Ahmad, B., Vohra, M. S., Saleemi, M. A., Serpell, C. J., Fong, I. L., & Wong, E. H. (2021, May). Brown/Beige adipose tissues and the emerging role of their secretory factors in improving metabolic health: The batokines. *Biochimie, 184*, 26-39. https://doi.org/10.1016/j.biochi.2021.01.015

Altshuler-Keylin, S., & Kajimura, S. (2017, 02 28). Mitochondrial homeostasis in adipose tissue remodeling. *Sci Signal, 10*(468). https://doi.org/10.1126/scisignal.aai9248

Altshuler-Keylin, S., Shinoda, K., Hasegawa, Y., Ikeda, K., Hong, H., Kang, Q., Yang, Y., Perera, R. M., Debnath, J., & Kajimura, S. (2016, 09 13). Beige Adipocyte Maintenance Is Regulated by Autophagy-Induced Mitochondrial Clearance. *Cell Metab, 24*(3), 402-419. https://doi.org/10.1016/j.cmet.2016.08.002

Alvarez-Crespo, M., Csikasz, R. I., Martínez-Sánchez, N., Diéguez, C., Cannon, B., Nedergaard, J., & López, M. (2016, Apr). Essential role of UCP1 modulating the central effects of thyroid hormones on energy balance. *Mol Metab, 5*(4), 271-282. https://doi.org/10.1016/j.molmet.2016.01.008

Arianti, R., Vinnai, B., Tóth, B. B., Shaw, A., Csősz, É., Vámos, A., Győry, F., Fischer-Posovszky, P., Wabitsch, M., Kristóf, E., & Fésüs, L. (2021, 08). ASC-1 transporter-dependent amino acid uptake is required for the efficient thermogenic response of human adipocytes to adrenergic stimulation. *FEBS Lett, 595*(16), 2085-2098. https://doi.org/10.1002/1873-3468.14155

Aydin, S., Kuloglu, T., Eren, M. N., Celik, A., Yilmaz, M., Kalayci, M., Sahin, İ., Gungor, O., Gurel, A., Ogeturk, M., & Dabak, O. (2014, Feb). Cardiac, skeletal muscle and serum irisin responses to with or without water exercise in young and old male rats: cardiac muscle produces more irisin than skeletal muscle. *Peptides, 52*, 68-73. https://doi.org/10.1016/j.peptides.2013.11.024

Bal, N. C., Maurya, S. K., Sopariwala, D. H., Sahoo, S. K., Gupta, S. C., Shaikh, S. A., Pant, M., Rowland, L. A., Bombardier, E., Goonasekera, S. A., Tupling, A. R., Molkentin, J. D., & Periasamy, M. (2012, Oct). Sarcolipin is a newly identified regulator of muscle-based thermogenesis in mammals. *Nat Med, 18*(10), 1575-1579. https://doi.org/10.1038/nm.2897

Benezra, R., Davis, R. L., Lockshon, D., Turner, D. L., & Weintraub, H. (1990, Apr 06). The protein Id: a negative regulator of helix-loop-helix DNA binding proteins. *Cell, 61*(1), 49-59. https://doi.org/10.1016/0092-8674(90)90214-y

Bényi, M., Kéki, Z., Hangay, I., & Kókai, Z. (2012, May 20). [Obesity related increase in diseases in Hungary studied by the Health Interview Survey 2009]. *Orv Hetil, 153*(20), 768-775. https://doi.org/10.1556/OH.2012.29302

Bertholet, A. M., Kazak, L., Chouchani, E. T., Bogaczyńska, M. G., Paranjpe, I., Wainwright, G. L., Bétourné, A., Kajimura, S., Spiegelman, B. M., & Kirichok, Y. (2017, Apr 04). Mitochondrial Patch Clamp of Beige Adipocytes Reveals UCP1-Positive and UCP1-Negative Cells Both Exhibiting Futile Creatine Cycling. *Cell Metab, 25*(4), 811-822.e814. https://doi.org/10.1016/j.cmet.2017.03.002

Block, B. A. (1994). Thermogenesis in muscle. *Annu Rev Physiol, 56*, 535-577. https://doi.org/10.1146/annurev.ph.56.030194.002535

Block, B. A., O'Brien, J., & Meissner, G. (1994, Dec). Characterization of the sarcoplasmic reticulum proteins in the thermogenic muscles of fish. *J Cell Biol, 127*(5), 1275-1287. https://doi.org/10.1083/jcb.127.5.1275

Boström, P., Wu, J., Jedrychowski, M. P., Korde, A., Ye, L., Lo, J. C., Rasbach, K. A., Boström, E. A., Choi, J. H., Long, J. Z., Kajimura, S., Zingaretti, M. C., Vind, B. F., Tu, H., Cinti, S., Højlund, K., Gygi, S. P., & Spiegelman, B. M. (2012, Jan). A PGC1-α-dependent myokine that drives brown-fat-like development of white fat and thermogenesis. *Nature, 481*(7382), 463-468. https://doi.org/10.1038/nature10777

Branco, M., Ribeiro, M., Negrão, N., & Bianco, A. C. (1999, 01). 3,5,3'-Triiodothyronine actively stimulates UCP in brown fat under minimal sympathetic activity. *Am J Physiol, 276*(1), E179-187. https://doi.org/10.1152/ajpendo.1999.276.1.E179

Brandt, C., & Pedersen, B. K. (2010). The role of exercise-induced myokines in muscle homeostasis and the defense against chronic diseases. *J Biomed Biotechnol, 2010*, 520258. https://doi.org/10.1155/2010/520258

Brückner, G., Brauer, K., Härtig, W., Wolff, J. R., Rickmann, M. J., Derouiche, A., Delpech, B., Girard, N., Oertel, W. H., & Reichenbach, A. (1993, Jul). Perineuronal nets provide a polyanionic, glia-associated form of microenvironment around certain neurons in many parts of the rat brain. *Glia, 8*(3), 183-200. https://doi.org/10.1002/glia.440080306

Buscemi, S., Corleo, D., Buscemi, C., & Giordano, C. (2018, Aug). Does iris(in) bring bad news or good news? *Eat Weight Disord, 23*(4), 431-442. https://doi.org/10.1007/s40519-017-0431-8

Cairó, M., Campderrós, L., Gavaldà-Navarro, A., Cereijo, R., Delgado-Anglés, A., Quesada-López, T., Giralt, M., Villarroya, J., & Villarroya, F. (2019, 05). Parkin controls brown adipose tissue plasticity in response to adaptive thermogenesis. *EMBO Rep, 20*(5). https://doi.org/10.15252/embr.201846832

Cairó, M., Villarroya, J., Cereijo, R., Campderrós, L., Giralt, M., & Villarroya, F. (2016, 10). Thermogenic activation represses autophagy in brown adipose tissue. *Int J Obes (Lond), 40*(10), 1591-1599. https://doi.org/10.1038/ijo.2016.115

Cannon, B., & Nedergaard, J. (2004, Jan). Brown adipose tissue: function and physiological significance. *Physiol Rev, 84*(1), 277-359. https://doi.org/10.1152/physrev.00015.2003

Casana, E., Jimenez, V., Jambrina, C., Sacristan, V., Muñoz, S., Rodo, J., Grass, I., Garcia, M., Mallol, C., León, X., Casellas, A., Sánchez, V., Franckhauser, S., Ferré, T., Marcó, S., & Bosch, F. (2022, Jun 09). AAV-mediated BMP7 gene therapy counteracts insulin resistance and obesity. *Mol Ther Methods Clin Dev, 25*, 190-204. https://doi.org/10.1016/j.omtm.2022.03.007

Chaudhry, A., & Granneman, J. G. (1999, 07). Differential regulation of functional responses by beta-adrenergic receptor subtypes in brown adipocytes. *Am J Physiol, 277*(1), R147-153. https://doi.org/10.1152/ajpregu.1999.277.1.R147

Cherra, S. J., Kulich, S. M., Uechi, G., Balasubramani, M., Mountzouris, J., Day, B. W., & Chu, C. T. (2010, Aug 23). Regulation of the autophagy protein LC3 by phosphorylation. *J Cell Biol, 190*(4), 533-539. https://doi.org/10.1083/jcb.201002108

Chondronikola, M., Volpi, E., Børsheim, E., Porter, C., Annamalai, P., Enerbäck, S., Lidell, M. E., Saraf, M. K., Labbe, S. M., Hurren, N. M., Yfanti, C., Chao, T., Andersen, C. R., Cesani, F., Hawkins, H., & Sidossis, L. S. (2014, Dec). Brown adipose tissue improves whole-body glucose homeostasis and insulin sensitivity in humans. *Diabetes, 63*(12), 4089-4099. https://doi.org/10.2337/db14-0746

Cinti, S. (2005, Jul). The adipose organ. *Prostaglandins Leukot Essent Fatty Acids, 73*(1), 9-15. https://doi.org/10.1016/j.plefa.2005.04.010

Claussnitzer, M., Dankel, S. N., Kim, K. H., Quon, G., Meuleman, W., Haugen, C., Glunk, V., Sousa, I. S., Beaudry, J. L., Puviindran, V., Abdennur, N. A., Liu, J., Svensson, P. A., Hsu, Y. H., Drucker, D. J., Mellgren, G., Hui, C. C., Hauner, H., & Kellis, M. (2015, Sep 03). FTO Obesity Variant Circuitry and Adipocyte Browning in Humans. *N Engl J Med, 373*(10), 895-907. https://doi.org/10.1056/NEJMoa1502214

Commins, S. P., Watson, P. M., Frampton, I. C., & Gettys, T. W. (2001, Feb). Leptin selectively reduces white adipose tissue in mice via a UCP1-dependent mechanism in brown

adipose tissue. *Am J Physiol Endocrinol Metab, 280*(2), E372-377. https://doi.org/10.1152/ajpendo.2001.280.2.E372

Contreras, C., Gonzalez, F., Fernø, J., Diéguez, C., Rahmouni, K., Nogueiras, R., & López, M. (2015, Mar). The brain and brown fat. *Ann Med, 47*(2), 150-168. https://doi.org/10.3109/07853890.2014.919727

Corsa, C. A. S., Pearson, G. L., Renberg, A., Askar, M. M., Vozheiko, T., MacDougald, O. A., & Soleimanpour, S. A. (2019, 05 03). The E3 ubiquitin ligase parkin is dispensable for metabolic homeostasis in murine pancreatic β cells and adipocytes. *J Biol Chem, 294*(18), 7296-7307. https://doi.org/10.1074/jbc.RA118.006763

Counter, C. M., Hahn, W. C., Wei, W., Caddle, S. D., Beijersbergen, R. L., Lansdorp, P. M., Sedivy, J. M., & Weinberg, R. A. (1998, Dec). Dissociation among in vitro telomerase activity, telomere maintenance, and cellular immortalization. *Proc Natl Acad Sci U S A, 95*(25), 14723-14728. https://doi.org/10.1073/pnas.95.25.14723

Cousin, B., Cinti, S., Morroni, M., Raimbault, S., Ricquier, D., Pénicaud, L., & Casteilla, L. (1992, Dec). Occurrence of brown adipocytes in rat white adipose tissue: molecular and morphological characterization. *J Cell Sci, 103 (Pt 4)*, 931-942. https://doi.org/10.1242/jcs.103.4.931

Cuevas-Ramos, D., Mehta, R., & Aguilar-Salinas, C. A. (2019). Fibroblast Growth Factor 21 and Browning of White Adipose Tissue. *Front Physiol, 10*, 37. https://doi.org/10.3389/fphys.2019.00037

Cypess, A. M., Lehman, S., Williams, G., Tal, I., Rodman, D., Goldfine, A. B., Kuo, F. C., Palmer, E. L., Tseng, Y. H., Doria, A., Kolodny, G. M., & Kahn, C. R. (2009, Apr). Identification and importance of brown adipose tissue in adult humans. *N Engl J Med, 360*(15), 1509-1517. https://doi.org/10.1056/NEJMoa0810780

Cypess, A. M., White, A. P., Vernochet, C., Schulz, T. J., Xue, R., Sass, C. A., Huang, T. L., Roberts-Toler, C., Weiner, L. S., Sze, C., Chacko, A. T., Deschamps, L. N., Herder, L. M., Truchan, N., Glasgow, A. L., Holman, A. R., Gavrila, A., Hasselgren, P. O., Mori, M. A., Molla, M., & Tseng, Y. H. (2013, May). Anatomical localization, gene expression profiling and functional characterization of adult human neck brown fat. *Nat Med, 19*(5), 635-639. https://doi.org/10.1038/nm.3112

Czimmerer, Z., Daniel, B., Horvath, A., Rückerl, D., Nagy, G., Kiss, M., Peloquin, M., Budai, M. M., Cuaranta-Monroy, I., Simandi, Z., Steiner, L., Nagy, B., Poliska, S., Banko, C., Bacso, Z., Schulman, I. G., Sauer, S., Deleuze, J. F., Allen, J. E., Benko, S., & Nagy, L. (2018, 01 16). The Transcription Factor STAT6 Mediates Direct Repression of Inflammatory Enhancers and Limits Activation of Alternatively Polarized Macrophages. *Immunity, 48*(1), 75-90.e76. https://doi.org/10.1016/j.immuni.2017.12.010

De Matteis, R., Arch, J. R., Petroni, M. L., Ferrari, D., Cinti, S., & Stock, M. J. (2002, Nov). Immunohistochemical identification of the beta(3)-adrenoceptor in intact human adipocytes and ventricular myocardium: effect of obesity and treatment with ephedrine and caffeine. *Int J Obes Relat Metab Disord, 26*(11), 1442-1450. https://doi.org/10.1038/sj.ijo.0802148

de Meis, L., Arruda, A. P., da Costa, R. M., & Benchimol, M. (2006, Jun 16). Identification of a Ca2+-ATPase in brown adipose tissue mitochondria: regulation of thermogenesis by ATP and Ca2+. *J Biol Chem, 281*(24), 16384-16390. https://doi.org/10.1074/jbc.M600678200

Dhaka, A., Viswanath, V., & Patapoutian, A. (2006). Trp ion channels and temperature sensation. *Annu Rev Neurosci, 29*, 135-161. https://doi.org/10.1146/annurev.neuro.29.051605.112958

Doan-Xuan, Q. M., Sarvari, A. K., Fischer-Posovszky, P., Wabitsch, M., Balajthy, Z., Fesus, L., & Bacso, Z. (2013, Oct). High content analysis of differentiation and cell death in human adipocytes. *Cytometry A, 83*(10), 933-943. https://doi.org/10.1002/cyto.a.22333

Dobin, A., Davis, C. A., Schlesinger, F., Drenkow, J., Zaleski, C., Jha, S., Batut, P., Chaisson, M., & Gingeras, T. R. (2013, Jan 01). STAR: ultrafast universal RNA-seq aligner. *Bioinformatics, 29*(1), 15-21. https://doi.org/10.1093/bioinformatics/bts635

Dubin, R. A., Wawrousek, E. F., & Piatigorsky, J. (1989, Mar). Expression of the murine alpha B-crystallin gene is not restricted to the lens. *Mol Cell Biol, 9*(3), 1083-1091. https://doi.org/10.1128/mcb.9.3.1083-1091.1989

Febbraio, M. A., & Pedersen, B. K. (2002, Sep). Muscle-derived interleukin-6: mechanisms for activation and possible biological roles. *FASEB J, 16*(11), 1335-1347. https://doi.org/10.1096/fj.01-0876rev

Fedorenko, A., Lishko, P. V., & Kirichok, Y. (2012, Oct 12). Mechanism of fatty-acid-dependent UCP1 uncoupling in brown fat mitochondria. *Cell, 151*(2), 400-413. https://doi.org/10.1016/j.cell.2012.09.010

Füllgrabe, J., Klionsky, D. J., & Joseph, B. (2014, 01). The return of the nucleus: transcriptional and epigenetic control of autophagy. *Nat Rev Mol Cell Biol, 15*(1), 65-74. https://doi.org/10.1038/nrm3716

Gamas, L., Matafome, P., & Seiça, R. (2015). Irisin and Myonectin Regulation in the Insulin Resistant Muscle: Implications to Adipose Tissue: Muscle Crosstalk. *J Diabetes Res, 2015*, 359159. https://doi.org/10.1155/2015/359159

Gámez, B., Rodriguez-Carballo, E., & Ventura, F. (2013). BMP signaling in telencephalic neural cell specification and maturation. *Front Cell Neurosci, 7*, 87. https://doi.org/10.3389/fncel.2013.00087

Giamanco, K. A., Morawski, M., & Matthews, R. T. (2010, Nov 10). Perineuronal net formation and structure in aggrecan knockout mice. *Neuroscience, 170*(4), 1314-1327. https://doi.org/10.1016/j.neuroscience.2010.08.032

Gillitzer, R., & Goebeler, M. (2001, Apr). Chemokines in cutaneous wound healing. *J Leukoc Biol, 69*(4), 513-521. https://www.ncbi.nlm.nih.gov/pubmed/11310836

Golozoubova, V., Hohtola, E., Matthias, A., Jacobsson, A., Cannon, B., & Nedergaard, J. (2001, Sep). Only UCP1 can mediate adaptive nonshivering thermogenesis in the cold. *FASEB J, 15*(11), 2048-2050. https://doi.org/10.1096/fj.00-0536fje

Gomez-Puerto, M. C., Iyengar, P. V., García de Vinuesa, A., Ten Dijke, P., & Sanchez-Duffhues, G. (2019, 01). Bone morphogenetic protein receptor signal transduction in human disease. *J Pathol, 247*(1), 9-20. https://doi.org/10.1002/path.5170

González-Muniesa, P., Mártinez-González, M. A., Hu, F. B., Després, J. P., Matsuzawa, Y., Loos, R. J. F., Moreno, L. A., Bray, G. A., & Martinez, J. A. (2017, Jun 15). Obesity. *Nat Rev Dis Primers, 3*, 17034. https://doi.org/10.1038/nrdp.2017.34

Granneman, J. G., Li, P., Zhu, Z., & Lu, Y. (2005, Oct). Metabolic and cellular plasticity in white adipose tissue I: effects of beta3-adrenergic receptor activation. *Am J Physiol Endocrinol Metab, 289*(4), E608-616. https://doi.org/10.1152/ajpendo.00009.2005

Groenen, P. J., Bloemendal, H., & de Jong, W. W. (1992, Apr 15). The carboxy-terminal lysine of alpha B-crystallin is an amine-donor substrate for tissue transglutaminase. *Eur J Biochem, 205*(2), 671-674. https://doi.org/10.1111/j.1432-1033.1992.tb16827.x

Gyurina, K., Kárai, B., Ujfalusi, A., Hevessy, Z., Barna, G., Jáksó, P., Pálfi-Mészáros, G., Póliska, S., Scholtz, B., Kappelmayer, J., Zahuczky, G., & Kiss, C. (2019). Coagulation FXIII-A Protein Expression Defines Three Novel Sub-populations in Pediatric B-Cell Progenitor Acute Lymphoblastic Leukemia Characterized by Distinct Gene Expression Signatures. *Front Oncol, 9*, 1063. https://doi.org/10.3389/fonc.2019.01063

Haim, Y., Blüher, M., Slutsky, N., Goldstein, N., Klöting, N., Harman-Boehm, I., Kirshtein, B., Ginsberg, D., Gericke, M., Guiu Jurado, E., Kovsan, J., Tarnovscki, T., Kachko, L., Bashan, N., Gepner, Y., Shai, I., & Rudich, A. (2015, Nov 02). Elevated autophagy gene expression in adipose tissue of obese humans: A potential non-cell-cycle-dependent function of E2F1. *Autophagy, 11*(11), 2074-2088. https://doi.org/10.1080/15548627.2015.1094597

Halaas, J. L., Gajiwala, K. S., Maffei, M., Cohen, S. L., Chait, B. T., Rabinowitz, D., Lallone, R. L., Burley, S. K., & Friedman, J. M. (1995, Jul 28). Weight-reducing effects of the plasma protein encoded by the obese gene. *Science, 269*(5223), 543-546. https://doi.org/10.1126/science.7624777

Hamacher-Brady, A., & Brady, N. R. (2016, Feb). Mitophagy programs: mechanisms and physiological implications of mitochondrial targeting by autophagy. *Cell Mol Life Sci, 73*(4), 775-795. https://doi.org/10.1007/s00018-015-2087-8

Hany, T. F., Gharehpapagh, E., Kamel, E. M., Buck, A., Himms-Hagen, J., & von Schulthess, G. K. (2002, Oct). Brown adipose tissue: a factor to consider in symmetrical tracer uptake in the neck and upper chest region. *Eur J Nucl Med Mol Imaging, 29*(10), 1393-1398. https://doi.org/10.1007/s00259-002-0902-6

Harms, M., & Seale, P. (2013, Oct). Brown and beige fat: development, function and therapeutic potential. *Nat Med, 19*(10), 1252-1263. https://doi.org/10.1038/nm.3361

Haskill, S., Peace, A., Morris, J., Sporn, S. A., Anisowicz, A., Lee, S. W., Smith, T., Martin, G., Ralph, P., & Sager, R. (1990, Oct). Identification of three related human GRO genes encoding cytokine functions. *Proc Natl Acad Sci U S A, 87*(19), 7732-7736. https://doi.org/10.1073/pnas.87.19.7732

He, C., & Klionsky, D. J. (2009). Regulation mechanisms and signaling pathways of autophagy. *Annu Rev Genet, 43*, 67-93. https://doi.org/10.1146/annurev-genet-102808-114910

Heaton, G. M., Wagenvoord, R. J., Kemp, A., & Nicholls, D. G. (1978, Jan 16). Brown-adipose-tissue mitochondria: photoaffinity labelling of the regulatory site of energy dissipation. *Eur J Biochem, 82*(2), 515-521. https://doi.org/10.1111/j.1432-1033.1978.tb12045.x

Heick, H. M., Vachon, C., Kallai, M. A., Bégin-Heick, N., & LeBlanc, J. (1973, Oct). The effects of thyroxine and isopropylnoradrenaline on cytochrome oxidase activity in brown adipose tissue. *Can J Physiol Pharmacol, 51*(10), 751-758. https://doi.org/10.1139/y73-114

Himms-Hagen, J., Melnyk, A., Zingaretti, M. C., Ceresi, E., Barbatelli, G., & Cinti, S. (2000, Sep). Multilocular fat cells in WAT of CL-316243-treated rats derive directly from white adipocytes. *Am J Physiol Cell Physiol, 279*(3), C670-681. https://doi.org/10.1152/ajpcell.2000.279.3.C670

Hinck, A. P. (2012, Jul 04). Structural studies of the TGF-βs and their receptors - insights into evolution of the TGF-β superfamily. *FEBS Lett, 586*(14), 1860-1870. https://doi.org/10.1016/j.febslet.2012.05.028

Hondares, E., Iglesias, R., Giralt, A., Gonzalez, F. J., Giralt, M., Mampel, T., & Villarroya, F. (2011, Apr). Thermogenic activation induces FGF21 expression and release in brown adipose tissue. *J Biol Chem, 286*(15), 12983-12990. https://doi.org/10.1074/jbc.M110.215889

Horwitz, J. (1992, Nov 01). Alpha-crystallin can function as a molecular chaperone. *Proc Natl Acad Sci U S A, 89*(21), 10449-10453. https://doi.org/10.1073/pnas.89.21.10449

Inokuma, K., Ogura-Okamatsu, Y., Toda, C., Kimura, K., Yamashita, H., & Saito, M. (2005, May). Uncoupling protein 1 is necessary for norepinephrine-induced glucose utilization in brown adipose tissue. *Diabetes, 54*(5), 1385-1391. https://doi.org/10.2337/diabetes.54.5.1385

Iwaki, T., Kume-Iwaki, A., Liem, R. K., & Goldman, J. E. (1989, Apr 07). Alpha B-crystallin is expressed in non-lenticular tissues and accumulates in Alexander's disease brain. *Cell, 57*(1), 71-78. https://doi.org/10.1016/0092-8674(89)90173-6

Jacobsson, A., Stadler, U., Glotzer, M. A., & Kozak, L. P. (1985, Dec 25). Mitochondrial uncoupling protein from mouse brown fat. Molecular cloning, genetic mapping, and mRNA expression. *J Biol Chem, 260*(30), 16250-16254. https://www.ncbi.nlm.nih.gov/pubmed/2999153

Jedrychowski, M. P., Wrann, C. D., Paulo, J. A., Gerber, K. K., Szpyt, J., Robinson, M. M., Nair, K. S., Gygi, S. P., & Spiegelman, B. M. (2015, Oct). Detection and Quantitation of Circulating Human Irisin by Tandem Mass Spectrometry. *Cell Metab, 22*(4), 734-740. https://doi.org/10.1016/j.cmet.2015.08.001

Jespersen, N. Z., Larsen, T. J., Peijs, L., Daugaard, S., Homøe, P., Loft, A., de Jong, J., Mathur, N., Cannon, B., Nedergaard, J., Pedersen, B. K., Møller, K., & Scheele, C. (2013, May). A classical brown adipose tissue mRNA signature partly overlaps with brite in the supraclavicular region of adult humans. *Cell Metab, 17*(5), 798-805. https://doi.org/10.1016/j.cmet.2013.04.011

Ju, L., Chen, S., Alimujiang, M., Bai, N., Yan, H., Fang, Q., Han, J., Ma, X., Yang, Y., & Jia, W. (2018, 11 30). A novel role for Bcl2l13 in promoting beige adipocyte biogenesis. *Biochem Biophys Res Commun, 506*(3), 485-491. https://doi.org/10.1016/j.bbrc.2018.10.034

Kajimura, S., & Saito, M. (2014). A new era in brown adipose tissue biology: molecular control of brown fat development and energy homeostasis. *Annu Rev Physiol, 76*, 225-249. https://doi.org/10.1146/annurev-physiol-021113-170252

Kajimura, S., Spiegelman, B. M., & Seale, P. (2015, Oct). Brown and Beige Fat: Physiological Roles beyond Heat Generation. *Cell Metab, 22*(4), 546-559. https://doi.org/10.1016/j.cmet.2015.09.007

Katagiri, T., & Watabe, T. (2016, Jun 01). Bone Morphogenetic Proteins. *Cold Spring Harb Perspect Biol, 8*(6). https://doi.org/10.1101/cshperspect.a021899

Kato, K., Shinohara, H., Kurobe, N., Goto, S., Inaguma, Y., & Ohshima, K. (1991, Oct 25). Immunoreactive alpha A crystallin in rat non-lenticular tissues detected with a sensitive immunoassay method. *Biochim Biophys Acta, 1080*(2), 173-180. https://doi.org/10.1016/0167-4838(91)90146-q

Kazak, L., Chouchani, E. T., Jedrychowski, M. P., Erickson, B. K., Shinoda, K., Cohen, P., Vetrivelan, R., Lu, G. Z., Laznik-Bogoslavski, D., Hasenfuss, S. C., Kajimura, S., Gygi, S. P., & Spiegelman, B. M. (2015, Oct 22). A creatine-driven substrate cycle enhances energy expenditure and thermogenesis in beige fat. *Cell, 163*(3), 643-655. https://doi.org/10.1016/j.cell.2015.09.035

Kazak, L., Chouchani, E. T., Lu, G. Z., Jedrychowski, M. P., Bare, C. J., Mina, A. I., Kumari, M., Zhang, S., Vuckovic, I., Laznik-Bogoslavski, D., Dzeja, P., Banks, A. S., Rosen, E. D., & Spiegelman, B. M. (2017, Oct 03). Genetic Depletion of Adipocyte Creatine Metabolism Inhibits Diet-Induced Thermogenesis and Drives Obesity. *Cell Metab, 26*(4), 660-671.e663. https://doi.org/10.1016/j.cmet.2017.08.009

Kazak, L., & Cohen, P. (2020, 08). Creatine metabolism: energy homeostasis, immunity and cancer biology. *Nat Rev Endocrinol, 16*(8), 421-436. https://doi.org/10.1038/s41574-020-0365-5

Kelly, D. P. (2012, Apr 06). Medicine. Irisin, light my fire. *Science, 336*(6077), 42-43. https://doi.org/10.1126/science.1221688

Kelly, D. P., & Scarpulla, R. C. (2004, Feb 15). Transcriptional regulatory circuits controlling mitochondrial biogenesis and function. *Genes Dev, 18*(4), 357-368. https://doi.org/10.1101/gad.1177604

Kim, H., Wrann, C. D., Jedrychowski, M., Vidoni, S., Kitase, Y., Nagano, K., Zhou, C., Chou, J., Parkman, V. A., Novick, S. J., Strutzenberg, T. S., Pascal, B. D., Le, P. T., Brooks, D. J., Roche, A. M., Gerber, K. K., Mattheis, L., Chen, W., Tu, H., Bouxsein, M. L., Griffin, P. R., Baron, R., Rosen, C. J., Bonewald, L. F., & Spiegelman, B. M. (2018, 12). Irisin Mediates Effects on Bone and Fat via αV Integrin Receptors. *Cell, 175*(7), 1756-1768.e1717. https://doi.org/10.1016/j.cell.2018.10.025

Kim, I., Rodriguez-Enriquez, S., & Lemasters, J. J. (2007, Jun 15). Selective degradation of mitochondria by mitophagy. *Arch Biochem Biophys, 462*(2), 245-253. https://doi.org/10.1016/j.abb.2007.03.034

Klusóczki, Á., Veréb, Z., Vámos, A., Fischer-Posovszky, P., Wabitsch, M., Bacso, Z., Fésüs, L., & Kristóf, E. (2019, 04). Differentiating SGBS adipocytes respond to PPARγ

stimulation, irisin and BMP7 by functional browning and beige characteristics. *Sci Rep, 9*(1), 5823. https://doi.org/10.1038/s41598-019-42256-0

Kosacka, J., Kern, M., Klöting, N., Paeschke, S., Rudich, A., Haim, Y., Gericke, M., Serke, H., Stumvoll, M., Bechmann, I., Nowicki, M., & Blüher, M. (2015, Jul 05). Autophagy in adipose tissue of patients with obesity and type 2 diabetes. *Mol Cell Endocrinol, 409*, 21-32. https://doi.org/10.1016/j.mce.2015.03.015

Kristóf, E., Doan-Xuan, Q. M., Bai, P., Bacso, Z., & Fésüs, L. (2015, Jul). Laser-scanning cytometry can quantify human adipocyte browning and proves effectiveness of irisin. *Sci Rep, 5*, 12540. https://doi.org/10.1038/srep12540

Kristóf, E., Klusóczki, Á., Veress, R., Shaw, A., Combi, Z. S., Varga, K., Győry, F., Balajthy, Z., Bai, P., Bacso, Z., & Fésüs, L. (2019, 04). Interleukin-6 released from differentiating human beige adipocytes improves browning. *Exp Cell Res, 377*(1-2), 47-55. https://doi.org/10.1016/j.yexcr.2019.02.015

Lamb, C. A., Yoshimori, T., & Tooze, S. A. (2013, Dec). The autophagosome: origins unknown, biogenesis complex. *Nat Rev Mol Cell Biol, 14*(12), 759-774. https://doi.org/10.1038/nrm3696

Lazarou, M., Sliter, D. A., Kane, L. A., Sarraf, S. A., Wang, C., Burman, J. L., Sideris, D. P., Fogel, A. I., & Youle, R. J. (2015, Aug 20). The ubiquitin kinase PINK1 recruits autophagy receptors to induce mitophagy. *Nature, 524*(7565), 309-314. https://doi.org/10.1038/nature14893

Lee, P., Greenfield, J. R., Ho, K. K., & Fulham, M. J. (2010, Oct). A critical appraisal of the prevalence and metabolic significance of brown adipose tissue in adult humans. *Am J Physiol Endocrinol Metab, 299*(4), E601-606. https://doi.org/10.1152/ajpendo.00298.2010

Lee, P., Smith, S., Linderman, J., Courville, A. B., Brychta, R. J., Dieckmann, W., Werner, C. D., Chen, K. Y., & Celi, F. S. (2014, Nov). Temperature-acclimated brown adipose tissue modulates insulin sensitivity in humans. *Diabetes, 63*(11), 3686-3698. https://doi.org/10.2337/db14-0513

Lee, P., Swarbrick, M. M., & Ho, K. K. (2013, Jun). Brown adipose tissue in adult humans: a metabolic renaissance. *Endocr Rev, 34*(3), 413-438. https://doi.org/10.1210/er.2012-1081

Lee, Y. H., Petkova, A. P., Mottillo, E. P., & Granneman, J. G. (2012, Apr 04). In vivo identification of bipotential adipocyte progenitors recruited by β3-adrenoceptor activation and high-fat feeding. *Cell Metab, 15*(4), 480-491. https://doi.org/10.1016/j.cmet.2012.03.009

Leitner, B. P., Huang, S., Brychta, R. J., Duckworth, C. J., Baskin, A. S., McGehee, S., Tal, I., Dieckmann, W., Gupta, G., Kolodny, G. M., Pacak, K., Herscovitch, P., Cypess, A. M., & Chen, K. Y. (2017, 08). Mapping of human brown adipose tissue in lean and obese young men. *Proc Natl Acad Sci U S A, 114*(32), 8649-8654. https://doi.org/10.1073/pnas.1705287114

Li, H., Zhang, Y., Wang, F., Donelan, W., Zona, M. C., Li, S., Reeves, W., Ding, Y., Tang, D., & Yang, L. (2019). Effects of irisin on the differentiation and browning of human visceral white adipocytes. *Am J Transl Res, 11*(12), 7410-7421. https://www.ncbi.nlm.nih.gov/pubmed/31934288

Li, S. N., & Wu, J. F. (2020, 01 29). TGF-β/SMAD signaling regulation of mesenchymal stem cells in adipocyte commitment. *Stem Cell Res Ther, 11*(1), 41. https://doi.org/10.1186/s13287-020-1552-y

Liao, Y., Smyth, G. K., & Shi, W. (2014, Apr 01). featureCounts: an efficient general purpose program for assigning sequence reads to genomic features. *Bioinformatics, 30*(7), 923-930. https://doi.org/10.1093/bioinformatics/btt656

Lichtenbelt, W., Kingma, B., van der Lans, A., & Schellen, L. (2014, Apr). Cold exposure--an approach to increasing energy expenditure in humans. *Trends Endocrinol Metab, 25*(4), 165-167. https://doi.org/10.1016/j.tem.2014.01.001

Liesa, M., & Shirihai, O. S. (2013, Apr 02). Mitochondrial dynamics in the regulation of nutrient utilization and energy expenditure. *Cell Metab, 17*(4), 491-506. https://doi.org/10.1016/j.cmet.2013.03.002

Lin, C. S., & Klingenberg, M. (1980, May 05). Isolation of the uncoupling protein from brown adipose tissue mitochondria. *FEBS Lett, 113*(2), 299-303. https://doi.org/10.1016/0014-5793(80)80613-2

Liu, D., Bordicchia, M., Zhang, C., Fang, H., Wei, W., Li, J. L., Guilherme, A., Guntur, K., Czech, M. P., & Collins, S. (2016, 05 02). Activation of mTORC1 is essential for β-adrenergic stimulation of adipose browning. *J Clin Invest, 126*(5), 1704-1716. https://doi.org/10.1172/JCI83532

Liu, F., Ventura, F., Doody, J., & Massagué, J. (1995, Jul). Human type II receptor for bone morphogenic proteins (BMPs): extension of the two-kinase receptor model to the BMPs. *Mol Cell Biol, 15*(7), 3479-3486. https://doi.org/10.1128/MCB.15.7.3479

López, M., Varela, L., Vázquez, M. J., Rodríguez-Cuenca, S., González, C. R., Velagapudi, V. R., Morgan, D. A., Schoenmakers, E., Agassandian, K., Lage, R., Martínez de Morentin, P. B., Tovar, S., Nogueiras, R., Carling, D., Lelliott, C., Gallego, R., Oresic, M., Chatterjee, K., Saha, A. K., Rahmouni, K., Diéguez, C., & Vidal-Puig, A. (2010, Sep).

Hypothalamic AMPK and fatty acid metabolism mediate thyroid regulation of energy balance. *Nat Med, 16*(9), 1001-1008. https://doi.org/10.1038/nm.2207

Maak, S., Norheim, F., Drevon, C. A., & Erickson, H. P. (2021, Jul 16). Progress and Challenges in the Biology of FNDC5 and Irisin. *Endocr Rev, 42*(4), 436-456. https://doi.org/10.1210/endrev/bnab003

Mádi, A., Cuaranta-Monroy, I., Lénárt, K., Pap, A., Mezei, Z. A., Kristóf, E., Oláh, A., Vámosi, G., Bacsó, Z., Bai, P., & Fésüs, L. (2017, Dec). Browning deficiency and low mobilization of fatty acids in gonadal white adipose tissue leads to decreased cold-tolerance of transglutaminase 2 knock-out mice. *Biochim Biophys Acta Mol Cell Biol Lipids, 1862*(12), 1575-1586. https://doi.org/10.1016/j.bbalip.2017.07.014

Mahdaviani, K., Chess, D., Wu, Y., Shirihai, O., & Aprahamian, T. R. (2016, Jan). Autocrine effect of vascular endothelial growth factor-A is essential for mitochondrial function in brown adipocytes. *Metabolism, 65*(1), 26-35. https://doi.org/10.1016/j.metabol.2015.09.012

Mathur, N., & Pedersen, B. K. (2008). Exercise as a mean to control low-grade systemic inflammation. *Mediators Inflamm, 2008*, 109502. https://doi.org/10.1155/2008/109502

Matsuda, N., Sato, S., Shiba, K., Okatsu, K., Saisho, K., Gautier, C. A., Sou, Y. S., Saiki, S., Kawajiri, S., Sato, F., Kimura, M., Komatsu, M., Hattori, N., & Tanaka, K. (2010, Apr 19). PINK1 stabilized by mitochondrial depolarization recruits Parkin to damaged mitochondria and activates latent Parkin for mitophagy. *J Cell Biol, 189*(2), 211-221. https://doi.org/10.1083/jcb.200910140

Matsushita, M., Yoneshiro, T., Aita, S., Kameya, T., Sugie, H., & Saito, M. (2014, Jun). Impact of brown adipose tissue on body fatness and glucose metabolism in healthy humans. *Int J Obes (Lond), 38*(6), 812-817. https://doi.org/10.1038/ijo.2013.206

Matthews, R. T., Kelly, G. M., Zerillo, C. A., Gray, G., Tiemeyer, M., & Hockfield, S. (2002, Sep 01). Aggrecan glycoforms contribute to the molecular heterogeneity of perineuronal nets. *J Neurosci, 22*(17), 7536-7547. https://www.ncbi.nlm.nih.gov/pubmed/12196577

Matthias, A., Ohlson, K. B., Fredriksson, J. M., Jacobsson, A., Nedergaard, J., & Cannon, B. (2000, Aug 18). Thermogenic responses in brown fat cells are fully UCP1-dependent. UCP2 or UCP3 do not substitute for UCP1 in adrenergically or fatty scid-induced thermogenesis. *J Biol Chem, 275*(33), 25073-25081. https://doi.org/10.1074/jbc.M000547200

Meisinger, C., Döring, A., Thorand, B., Heier, M., & Löwel, H. (2006, Sep). Body fat distribution and risk of type 2 diabetes in the general population: are there differences between men and women? The MONICA/KORA Augsburg cohort study. *Am J Clin Nutr, 84*(3), 483-489. https://doi.org/10.1093/ajcn/84.3.483

Minokoshi, Y., Haque, M. S., & Shimazu, T. (1999, Feb). Microinjection of leptin into the ventromedial hypothalamus increases glucose uptake in peripheral tissues in rats. *Diabetes, 48*(2), 287-291. https://doi.org/10.2337/diabetes.48.2.287

Mizushima, N., Yoshimori, T., & Levine, B. (2010, Feb 05). Methods in mammalian autophagy research. *Cell, 140*(3), 313-326. https://doi.org/10.1016/j.cell.2010.01.028

Morawski, M., Brückner, G., Arendt, T., & Matthews, R. T. (2012, May). Aggrecan: Beyond cartilage and into the brain. *Int J Biochem Cell Biol, 44*(5), 690-693. https://doi.org/10.1016/j.biocel.2012.01.010

Morawski, M., Brückner, G., Jäger, C., Seeger, G., Matthews, R. T., & Arendt, T. (2012, Jul). Involvement of perineuronal and perisynaptic extracellular matrix in Alzheimer's disease neuropathology. *Brain Pathol, 22*(4), 547-561. https://doi.org/10.1111/j.1750-3639.2011.00557.x

Mueller, T. D., & Nickel, J. (2012, Jul 04). Promiscuity and specificity in BMP receptor activation. *FEBS Lett, 586*(14), 1846-1859. https://doi.org/10.1016/j.febslet.2012.02.043

Nakamura, K. (2011, Nov). Central circuitries for body temperature regulation and fever. *Am J Physiol Regul Integr Comp Physiol, 301*(5), R1207-1228. https://doi.org/10.1152/ajpregu.00109.2011

Narendra, D., Tanaka, A., Suen, D. F., & Youle, R. J. (2008, Dec 01). Parkin is recruited selectively to impaired mitochondria and promotes their autophagy. *J Cell Biol, 183*(5), 795-803. https://doi.org/10.1083/jcb.200809125

Nedergaard, J., Bengtsson, T., & Cannon, B. (2007, Aug). Unexpected evidence for active brown adipose tissue in adult humans. *Am J Physiol Endocrinol Metab, 293*(2), E444-452. https://doi.org/10.1152/ajpendo.00691.2006

Nedergaard, J., Dicker, A., & Cannon, B. (1997, Mar 15). The interaction between thyroid and brown-fat thermogenesis. Central or peripheral effects? *Ann N Y Acad Sci, 813*, 712-717. https://doi.org/10.1111/j.1749-6632.1997.tb51772.x

Nicholls, D. G. (1976, Jan 15). The bioenergetics of brown adipose tissue mitochondria. *FEBS Lett, 61*(2), 103-110. https://doi.org/10.1016/0014-5793(76)81014-9

Nicholls, D. G., & Locke, R. M. (1984, Jan). Thermogenic mechanisms in brown fat. *Physiol Rev, 64*(1), 1-64. https://doi.org/10.1152/physrev.1984.64.1.1

Nixon, R. A. (2013, Aug). The role of autophagy in neurodegenerative disease. *Nat Med, 19*(8), 983-997. https://doi.org/10.1038/nm.3232

Omatsu-Kanbe, M., Zarnowski, M. J., & Cushman, S. W. (1996, Apr 01). Hormonal regulation of glucose transport in a brown adipose cell preparation isolated from rats that shows a large response to insulin. *Biochem J, 315 (Pt 1)*, 25-31. https://doi.org/10.1042/bj3150025

Ouellet, V., Routhier-Labadie, A., Bellemare, W., Lakhal-Chaieb, L., Turcotte, E., Carpentier, A. C., & Richard, D. (2011, Jan). Outdoor temperature, age, sex, body mass index, and diabetic status determine the prevalence, mass, and glucose-uptake activity of 18F-FDG-detected BAT in humans. *J Clin Endocrinol Metab, 96*(1), 192-199. https://doi.org/10.1210/jc.2010-0989

Palatka, K., Serfozo, Z., Veréb, Z., Bátori, R., Lontay, B., Hargitay, Z., Nemes, Z., Udvardy, M., Erdodi, F., & Altorjay, I. (2006, Mar). Effect of IBD sera on expression of inducible and endothelial nitric oxide synthase in human umbilical vein endothelial cells. *World J Gastroenterol, 12*(11), 1730-1738. https://doi.org/10.3748/wjg.v12.i11.1730

Palikaras, K., Lionaki, E., & Tavernarakis, N. (2018, Sep). Mechanisms of mitophagy in cellular homeostasis, physiology and pathology. *Nat Cell Biol, 20*(9), 1013-1022. https://doi.org/10.1038/s41556-018-0176-2

Palikaras, K., & Tavernarakis, N. (2014, Aug). Mitochondrial homeostasis: the interplay between mitophagy and mitochondrial biogenesis. *Exp Gerontol, 56*, 182-188. https://doi.org/10.1016/j.exger.2014.01.021

Pankiv, S., Clausen, T. H., Lamark, T., Brech, A., Bruun, J. A., Outzen, H., Øvervatn, A., Bjørkøy, G., & Johansen, T. (2007, Aug 17). p62/SQSTM1 binds directly to Atg8/LC3 to facilitate degradation of ubiquitinated protein aggregates by autophagy. *J Biol Chem, 282*(33), 24131-24145. https://doi.org/10.1074/jbc.M702824200

Park, J., Euhus, D. M., & Scherer, P. E. (2011, Aug). Paracrine and endocrine effects of adipose tissue on cancer development and progression. *Endocr Rev, 32*(4), 550-570. https://doi.org/10.1210/er.2010-0030

Patil, M., Sharma, B. K., & Satyanarayana, A. (2014, Jun 01). Id transcriptional regulators in adipogenesis and adipose tissue metabolism. *Front Biosci (Landmark Ed), 19*, 1386-1397. https://doi.org/10.2741/4289

Pedersen, B. K., & Febbraio, M. A. (2012, Apr 03). Muscles, exercise and obesity: skeletal muscle as a secretory organ. *Nat Rev Endocrinol, 8*(8), 457-465. https://doi.org/10.1038/nrendo.2012.49

Pelleymounter, M. A., Cullen, M. J., Baker, M. B., Hecht, R., Winters, D., Boone, T., & Collins, F. (1995, Jul 28). Effects of the obese gene product on body weight regulation in ob/ob mice. *Science, 269*(5223), 540-543. https://doi.org/10.1126/science.7624776

Perdikari, A., Leparc, G. G., Balaz, M., Pires, N. D., Lidell, M. E., Sun, W., Fernandez-Albert, F., Müller, S., Akchiche, N., Dong, H., Balazova, L., Opitz, L., Röder, E., Klein, H., Stefanicka, P., Varga, L., Nuutila, P., Virtanen, K. A., Niemi, T., Taittonen, M., Rudofsky, G., Ukropec, J., Enerbäck, S., Stupka, E., Neubauer, H., & Wolfrum, C. (2018, 10 16). BATLAS: Deconvoluting Brown Adipose Tissue. *Cell Rep, 25*(3), 784-797.e784. https://doi.org/10.1016/j.celrep.2018.09.044

Petrovic, N., Walden, T. B., Shabalina, I. G., Timmons, J. A., Cannon, B., & Nedergaard, J. (2010, Mar 05). Chronic peroxisome proliferator-activated receptor gamma (PPARgamma) activation of epididymally derived white adipocyte cultures reveals a population of thermogenically competent, UCP1-containing adipocytes molecularly distinct from classic brown adipocytes. *J Biol Chem, 285*(10), 7153-7164. https://doi.org/10.1074/jbc.M109.053942

Pisani, D. F., Barquissau, V., Chambard, J. C., Beuzelin, D., Ghandour, R. A., Giroud, M., Mairal, A., Pagnotta, S., Cinti, S., Langin, D., & Amri, E. Z. (2018, 01). Mitochondrial fission is associated with UCP1 activity in human brite/beige adipocytes. *Mol Metab, 7*, 35-44. https://doi.org/10.1016/j.molmet.2017.11.007

Pischon, T., Boeing, H., Hoffmann, K., Bergmann, M., Schulze, M. B., Overvad, K., van der Schouw, Y. T., Spencer, E., Moons, K. G., Tjønneland, A., Halkjaer, J., Jensen, M. K., Stegger, J., Clavel-Chapelon, F., Boutron-Ruault, M. C., Chajes, V., Linseisen, J., Kaaks, R., Trichopoulou, A., Trichopoulos, D., Bamia, C., Sieri, S., Palli, D., Tumino, R., Vineis, P., Panico, S., Peeters, P. H., May, A. M., Bueno-de-Mesquita, H. B., van Duijnhoven, F. J., Hallmans, G., Weinehall, L., Manjer, J., Hedblad, B., Lund, E., Agudo, A., Arriola, L., Barricarte, A., Navarro, C., Martinez, C., Quirós, J. R., Key, T., Bingham, S., Khaw, K. T., Boffetta, P., Jenab, M., Ferrari, P., & Riboli, E. (2008, Nov 13). General and abdominal adiposity and risk of death in Europe. *N Engl J Med, 359*(20), 2105-2120. https://doi.org/10.1056/NEJMoa0801891

Prusiner, S. B., Cannon, B., & Lindberg, O. (1968, Oct 17). Oxidative metabolism in cells isolated from brown adipose tissue. 1. Catecholamine and fatty acid stimulation of respiration. *Eur J Biochem, 6*(1), 15-22. https://doi.org/10.1111/j.1432-1033.1968.tb00413.x

Puigserver, P., Adelmant, G., Wu, Z., Fan, M., Xu, J., O'Malley, B., & Spiegelman, B. M. (1999, Nov 12). Activation of PPARgamma coactivator-1 through transcription factor docking. *Science, 286*(5443), 1368-1371. https://doi.org/10.1126/science.286.5443.1368

Rahbani, J. F., Roesler, A., Hussain, M. F., Samborska, B., Dykstra, C. B., Tsai, L., Jedrychowski, M. P., Vergnes, L., Reue, K., Spiegelman, B. M., & Kazak, L. (2021,

02). Creatine kinase B controls futile creatine cycling in thermogenic fat. *Nature, 590*(7846), 480-485. https://doi.org/10.1038/s41586-021-03221-y

Raman, B., & Rao, C. M. (1994, Nov 04). Chaperone-like activity and quaternary structure of alpha-crystallin. *J Biol Chem, 269*(44), 27264-27268. https://www.ncbi.nlm.nih.gov/pubmed/7961635

Rao, P. V., Horwitz, J., & Zigler, J. S. (1993, Feb 15). Alpha-crystallin, a molecular chaperone, forms a stable complex with carbonic anhydrase upon heat denaturation. *Biochem Biophys Res Commun, 190*(3), 786-793. https://doi.org/10.1006/bbrc.1993.1118

Raschke, S., Elsen, M., Gassenhuber, H., Sommerfeld, M., Schwahn, U., Brockmann, B., Jung, R., Wisløff, U., Tjønna, A. E., Raastad, T., Hallén, J., Norheim, F., Drevon, C. A., Romacho, T., Eckardt, K., & Eckel, J. (2013). Evidence against a beneficial effect of irisin in humans. *PLoS One, 8*(9), e73680. https://doi.org/10.1371/journal.pone.0073680

Reilly, S. M., & Saltiel, A. R. (2015, Oct 22). A futile approach to fighting obesity? *Cell, 163*(3), 539-540. https://doi.org/10.1016/j.cell.2015.10.006

Ricquier, D., Mory, G., & Hemon, P. (1979, Nov). Changes induced by cold adaptation in the brown adipose tissue from several species of rodents, with special reference to the mitochondrial components. *Can J Biochem, 57*(11), 1262-1266. https://doi.org/10.1139/o79-167

Roesler, A., & Kazak, L. (2020, 02 14). UCP1-independent thermogenesis. *Biochem J, 477*(3), 709-725. https://doi.org/10.1042/BCJ20190463

Rosen, E. D., & Spiegelman, B. M. (2014, Jan). What we talk about when we talk about fat. *Cell, 156*(1-2), 20-44. https://doi.org/10.1016/j.cell.2013.12.012

Ruan, C. C., Kong, L. R., Chen, X. H., Ma, Y., Pan, X. X., Zhang, Z. B., & Gao, P. J. (2018, 09). A2A receptor activation attenuates hypertensive cardiac remodeling via promoting brown adipose tissue-derived FGF21. *Cell Metab, 28*(3), 476-489.e475. https://doi.org/10.1016/j.cmet.2018.06.013

Saito, M., Matsushita, M., Yoneshiro, T., & Okamatsu-Ogura, Y. (2020). Brown Adipose Tissue, Diet-Induced Thermogenesis, and Thermogenic Food Ingredients: From Mice to Men. *Front Endocrinol (Lausanne), 11*, 222. https://doi.org/10.3389/fendo.2020.00222

Saito, M., Okamatsu-Ogura, Y., Matsushita, M., Watanabe, K., Yoneshiro, T., Nio-Kobayashi, J., Iwanaga, T., Miyagawa, M., Kameya, T., Nakada, K., Kawai, Y., & Tsujisaki, M. (2009, Jul). High incidence of metabolically active brown adipose tissue in healthy adult

humans: effects of cold exposure and adiposity. *Diabetes, 58*(7), 1526-1531. https://doi.org/10.2337/db09-0530

Sanchez-Gurmaches, J., Hung, C. M., & Guertin, D. A. (2016, 05). Emerging Complexities in Adipocyte Origins and Identity. *Trends Cell Biol, 26*(5), 313-326. https://doi.org/10.1016/j.tcb.2016.01.004

Sárvári, A. K., Doan-Xuan, Q. M., Bacsó, Z., Csomós, I., Balajthy, Z., & Fésüs, L. (2015, Jan). Interaction of differentiated human adipocytes with macrophages leads to trogocytosis and selective IL-6 secretion. *Cell Death Dis, 6*, e1613. https://doi.org/10.1038/cddis.2014.579

Satoh, N., Ogawa, Y., Katsuura, G., Numata, Y., Masuzaki, H., Yoshimasa, Y., & Nakao, K. (1998, Jun 19). Satiety effect and sympathetic activation of leptin are mediated by hypothalamic melanocortin system. *Neurosci Lett, 249*(2-3), 107-110. https://doi.org/10.1016/s0304-3940(98)00401-7

Schrauwen, P., van Marken Lichtenbelt, W. D., & Spiegelman, B. M. (2015, Aug). The future of brown adipose tissues in the treatment of type 2 diabetes. *Diabetologia, 58*(8), 1704-1707. https://doi.org/10.1007/s00125-015-3611-y

Schulz, T. J., Huang, P., Huang, T. L., Xue, R., McDougall, L. E., Townsend, K. L., Cypess, A. M., Mishina, Y., Gussoni, E., & Tseng, Y. H. (2013, Mar 21). Brown-fat paucity due to impaired BMP signalling induces compensatory browning of white fat. *Nature, 495*(7441), 379-383. https://doi.org/10.1038/nature11943

Schumacher, C., Clark-Lewis, I., Baggiolini, M., & Moser, B. (1992, Nov). High- and low-affinity binding of GRO alpha and neutrophil-activating peptide 2 to interleukin 8 receptors on human neutrophils. *Proc Natl Acad Sci U S A, 89*(21), 10542-10546. https://doi.org/10.1073/pnas.89.21.10542

Seale, P., Conroe, H. M., Estall, J., Kajimura, S., Frontini, A., Ishibashi, J., Cohen, P., Cinti, S., & Spiegelman, B. M. (2011, Jan). Prdm16 determines the thermogenic program of subcutaneous white adipose tissue in mice. *J Clin Invest, 121*(1), 96-105. https://doi.org/10.1172/JCI44271

Shaw, A., Tóth, B. B., Arianti, R., Csomós, I., Póliska, S., Vámos, A., Bacso, Z., Győry, F., Fésüs, L., & Kristóf, E. (2021, Oct 25). BMP7 Increases UCP1-Dependent and Independent Thermogenesis with a Unique Gene Expression Program in Human Neck Area Derived Adipocytes. *Pharmaceuticals (Basel), 14*(11). https://doi.org/10.3390/ph14111078

Shaw, A., Tóth, B. B., Király, R., Arianti, R., Csomós, I., Póliska, S., Vámos, A., Korponay-Szabó, I. R., Bacso, Z., Győry, F., Fésüs, L., & Kristóf, E. (2021). Irisin Stimulates the

Release of CXCL1 From Differentiating Human Subcutaneous and Deep-Neck Derived Adipocytes. *Front Cell Dev Biol, 9*, 737872. https://doi.org/10.3389/fcell.2021.737872

Shih, M. F., & Taberner, P. V. (1995, Aug 25). Selective activation of brown adipocyte hormone-sensitive lipase and cAMP production in the mouse by beta 3-adrenoceptor agonists. *Biochem Pharmacol, 50*(5), 601-608. https://doi.org/10.1016/0006-2952(95)00185-3

Shridas, P., Sharma, Y., & Balasubramanian, D. (2001, Jun 22). Transglutaminase-mediated cross-linking of alpha-crystallin: structural and functional consequences. *FEBS Lett, 499*(3), 245-250. https://doi.org/10.1016/s0014-5793(01)02565-0

Silva, R. L., Lopes, A. H., Guimarães, R. M., & Cunha, T. M. (2017, Sep). CXCL1/CXCR2 signaling in pathological pain: Role in peripheral and central sensitization. *Neurobiol Dis, 105*, 109-116. https://doi.org/10.1016/j.nbd.2017.06.001

Slot, J. W., Geuze, H. J., Gigengack, S., Lienhard, G. E., & James, D. E. (1991, Apr). Immuno-localization of the insulin regulatable glucose transporter in brown adipose tissue of the rat. *J Cell Biol, 113*(1), 123-135. https://doi.org/10.1083/jcb.113.1.123

Sun, K., Kusminski, C. M., Luby-Phelps, K., Spurgin, S. B., An, Y. A., Wang, Q. A., Holland, W. L., & Scherer, P. E. (2014, Jul). Brown adipose tissue derived VEGF-A modulates cold tolerance and energy expenditure. *Mol Metab, 3*(4), 474-483. https://doi.org/10.1016/j.molmet.2014.03.010

Sun, Y., Rahbani, J. F., Jedrychowski, M. P., Riley, C. L., Vidoni, S., Bogoslavski, D., Hu, B., Dumesic, P. A., Zeng, X., Wang, A. B., Knudsen, N. H., Kim, C. R., Marasciullo, A., Millán, J. L., Chouchani, E. T., Kazak, L., & Spiegelman, B. M. (2021, May). Mitochondrial TNAP controls thermogenesis by hydrolysis of phosphocreatine. *Nature, 593*(7860), 580-585. https://doi.org/10.1038/s41586-021-03533-z

Sundin, U. (1981, Sep). GDP binding to rat brown fat mitochondria: effects of thyroxine at different ambient temperatures. *Am J Physiol, 241*(3), C134-139. https://doi.org/10.1152/ajpcell.1981.241.3.C134

Svensson, P. A., Jernås, M., Sjöholm, K., Hoffmann, J. M., Nilsson, B. E., Hansson, M., & Carlsson, L. M. (2011, Feb). Gene expression in human brown adipose tissue. *Int J Mol Med, 27*(2), 227-232. https://doi.org/10.3892/ijmm.2010.566

Szatmári-Tóth, M., Shaw, A., Csomós, I., Mocsár, G., Fischer-Posovszky, P., Wabitsch, M., Balajthy, Z., Lányi, C., Győry, F., Kristóf, E., & Fésüs, L. (2020, Sep). Thermogenic Activation Downregulates High Mitophagy Rate in Human Masked and Mature Beige Adipocytes. *Int J Mol Sci, 21*(18). https://doi.org/10.3390/ijms21186640

Taylor, D., & Gottlieb, R. A. (2017, 04). Parkin-mediated mitophagy is downregulated in browning of white adipose tissue. *Obesity (Silver Spring), 25*(4), 704-712. https://doi.org/10.1002/oby.21786

Teruel, T., Valverde, A. M., Benito, M., & Lorenzo, M. (1996, Oct 15). Insulin-like growth factor I and insulin induce adipogenic-related gene expression in fetal brown adipocyte primary cultures. *Biochem J, 319 (Pt 2)*, 627-632. https://doi.org/10.1042/bj3190627

Tol, M. J., Ottenhoff, R., van Eijk, M., Zelcer, N., Aten, J., Houten, S. M., Geerts, D., van Roomen, C., Bierlaagh, M. C., Scheij, S., Hoeksema, M. A., Aerts, J. M., Bogan, J. S., Dorn, G. W., Argmann, C. A., & Verhoeven, A. J. (2016, 09). A PPARγ-Bnip3 Axis Couples Adipose Mitochondrial Fusion-Fission Balance to Systemic Insulin Sensitivity. *Diabetes, 65*(9), 2591-2605. https://doi.org/10.2337/db16-0243

Tóth, B. B., Arianti, R., Shaw, A., Vámos, A., Veréb, Z., Póliska, S., Győry, F., Bacso, Z., Fésüs, L., & Kristóf, E. (2020, 04). FTO Intronic SNP Strongly Influences Human Neck Adipocyte Browning Determined by Tissue and PPARγ Specific Regulation: A Transcriptome Analysis. *Cells, 9*(4). https://doi.org/10.3390/cells9040987

Tsai, Y. C., Wang, C. W., Wen, B. Y., Hsieh, P. S., Lee, Y. M., Yen, M. H., & Cheng, P. Y. (2020, 08 20). Involvement of the p62/Nrf2/HO-1 pathway in the browning effect of irisin in 3T3-L1 adipocytes. *Mol Cell Endocrinol, 514*, 110915. https://doi.org/10.1016/j.mce.2020.110915

Tseng, Y. H., Kokkotou, E., Schulz, T. J., Huang, T. L., Winnay, J. N., Taniguchi, C. M., Tran, T. T., Suzuki, R., Espinoza, D. O., Yamamoto, Y., Ahrens, M. J., Dudley, A. T., Norris, A. W., Kulkarni, R. N., & Kahn, C. R. (2008, Aug 21). New role of bone morphogenetic protein 7 in brown adipogenesis and energy expenditure. *Nature, 454*(7207), 1000-1004. https://doi.org/10.1038/nature07221

van Marken Lichtenbelt, W. D., & Schrauwen, P. (2011, Aug). Implications of nonshivering thermogenesis for energy balance regulation in humans. *Am J Physiol Regul Integr Comp Physiol, 301*(2), R285-296. https://doi.org/10.1152/ajpregu.00652.2010

van Marken Lichtenbelt, W. D., Vanhommerig, J. W., Smulders, N. M., Drossaerts, J. M., Kemerink, G. J., Bouvy, N. D., Schrauwen, P., & Teule, G. J. (2009, Apr). Cold-activated brown adipose tissue in healthy men. *N Engl J Med, 360*(15), 1500-1508. https://doi.org/10.1056/NEJMoa0808718

Villarroya, F., Cereijo, R., Villarroya, J., & Giralt, M. (2017, 01). Brown adipose tissue as a secretory organ. *Nat Rev Endocrinol, 13*(1), 26-35. https://doi.org/10.1038/nrendo.2016.136

Villarroya, J., Cereijo, R., Gavaldà-Navarro, A., Peyrou, M., Giralt, M., & Villarroya, F. (2019, 11). New insights into the secretory functions of brown adipose tissue. *J Endocrinol, 243*(2), R19-R27. https://doi.org/10.1530/JOE-19-0295

Virtanen, K. A., Lidell, M. E., Orava, J., Heglind, M., Westergren, R., Niemi, T., Taittonen, M., Laine, J., Savisto, N. J., Enerbäck, S., & Nuutila, P. (2009, Apr). Functional brown adipose tissue in healthy adults. *N Engl J Med, 360*(15), 1518-1525. https://doi.org/10.1056/NEJMoa0808949

Wabitsch, M., Brenner, R. E., Melzner, I., Braun, M., Möller, P., Heinze, E., Debatin, K. M., & Hauner, H. (2001, Jan). Characterization of a human preadipocyte cell strain with high capacity for adipose differentiation. *Int J Obes Relat Metab Disord, 25*(1), 8-15. https://doi.org/10.1038/sj.ijo.0801520

Wang, Q. A., Tao, C., Gupta, R. K., & Scherer, P. E. (2013, Oct). Tracking adipogenesis during white adipose tissue development, expansion and regeneration. *Nat Med, 19*(10), 1338-1344. https://doi.org/10.1038/nm.3324

Wang, Q. A., Tao, C., Jiang, L., Shao, M., Ye, R., Zhu, Y., Gordillo, R., Ali, A., Lian, Y., Holland, W. L., Gupta, R. K., & Scherer, P. E. (2015, Sep). Distinct regulatory mechanisms governing embryonic versus adult adipocyte maturation. *Nat Cell Biol, 17*(9), 1099-1111. https://doi.org/10.1038/ncb3217

Whittle, A. J., López, M., & Vidal-Puig, A. (2011, Aug). Using brown adipose tissue to treat obesity - the central issue. *Trends Mol Med, 17*(8), 405-411. https://doi.org/10.1016/j.molmed.2011.04.001

Wikstrom, J. D., Mahdaviani, K., Liesa, M., Sereda, S. B., Si, Y., Las, G., Twig, G., Petrovic, N., Zingaretti, C., Graham, A., Cinti, S., Corkey, B. E., Cannon, B., Nedergaard, J., & Shirihai, O. S. (2014, Mar 03). Hormone-induced mitochondrial fission is utilized by brown adipocytes as an amplification pathway for energy expenditure. *EMBO J, 33*(5), 418-436. https://doi.org/10.1002/embj.201385014

Wu, J., Boström, P., Sparks, L. M., Ye, L., Choi, J. H., Giang, A. H., Khandekar, M., Virtanen, K. A., Nuutila, P., Schaart, G., Huang, K., Tu, H., van Marken Lichtenbelt, W. D., Hoeks, J., Enerbäck, S., Schrauwen, P., & Spiegelman, B. M. (2012, Jul). Beige adipocytes are a distinct type of thermogenic fat cell in mouse and human. *Cell, 150*(2), 366-376. https://doi.org/10.1016/j.cell.2012.05.016

Xue, R., Lynes, M. D., Dreyfuss, J. M., Shamsi, F., Schulz, T. J., Zhang, H., Huang, T. L., Townsend, K. L., Li, Y., Takahashi, H., Weiner, L. S., White, A. P., Lynes, M. S., Rubin, L. L., Goodyear, L. J., Cypess, A. M., & Tseng, Y. H. (2015, Jul). Clonal analyses and gene profiling identify genetic biomarkers of the thermogenic potential of human brown and white preadipocytes. *Nat Med, 21*(7), 760-768. https://doi.org/10.1038/nm.3881

Xue, Y., Petrovic, N., Cao, R., Larsson, O., Lim, S., Chen, S., Feldmann, H. M., Liang, Z., Zhu, Z., Nedergaard, J., Cannon, B., & Cao, Y. (2009, Jan). Hypoxia-independent angiogenesis in adipose tissues during cold acclimation. *Cell Metab, 9*(1), 99-109. https://doi.org/10.1016/j.cmet.2008.11.009

Yoneshiro, T., Aita, S., Matsushita, M., Kayahara, T., Kameya, T., Kawai, Y., Iwanaga, T., & Saito, M. (2013, Aug). Recruited brown adipose tissue as an antiobesity agent in humans. *J Clin Invest, 123*(8), 3404-3408. https://doi.org/10.1172/JCI67803

Yoshii, S. R., & Mizushima, N. (2017, Aug 28). Monitoring and Measuring Autophagy. *Int J Mol Sci, 18*(9). https://doi.org/10.3390/ijms18091865

Young, P., Arch, J. R., & Ashwell, M. (1984, Feb 13). Brown adipose tissue in the parametrial fat pad of the mouse. *FEBS Lett, 167*(1), 10-14. https://doi.org/10.1016/0014-5793(84)80822-4

Zhang, Y., Li, R., Meng, Y., Li, S., Donelan, W., Zhao, Y., Qi, L., Zhang, M., Wang, X., Cui, T., Yang, L. J., & Tang, D. (2014, Feb). Irisin stimulates browning of white adipocytes through mitogen-activated protein kinase p38 MAP kinase and ERK MAP kinase signaling. *Diabetes, 63*(2), 514-525. https://doi.org/10.2337/db13-1106

8. Acknowledgements

First of all, I would like to thank my supervisor, Prof. Dr. László Fésüs for giving me the opportunity to learn and work with his research group. I would like to express my sincere gratitude to Prof. Fésüs for the excellent training, continuous support, motivation, and scientific discussions during my Ph.D.

I am also thankful to Prof. Dr. József Tőzsér, Head, Department of Biochemistry and Molecular Biology for giving me the opportunity to work in the department.

I would also like to thank Dr. Endre Kristóf and Dr. Mária Szatmári-Tóth for teaching me and guiding me whenever I needed help.

I am especially grateful to Dr. Zsolt Bacsó and Dr. Péter Bai for their help in Laser-scanning image acquisition, analysis and in cellular respiration measurements.

I would also like to specially thank Dr. Ferenc Győry and the surgery group at the Auguszta Surgery Center for providing the adipose tissue samples.

Finally, I would like to thank all members of the lab for their continuous help throughout my years of PhD studies.

Lastly, I would like to thank my parents and all other members of the family, close friends for their continuous support and encouragement, without which this journey would have been impossible.

9. List of conferences

I) **Winter School Symposium of Doctoral School of Molecular, Cell and Immune biology, University of Debrecen (January 2022)**

Attended the conference and gave a short talk on “Irisin stimulates the release of CXCL1 via upregulation of NFκB pathway from human neck derived differentiating adipocytes”.

II) **Hungarian Molecular Life Sciences 2021 (October 2021)**

Attended the conference and presented a poster with title “BMP7 upregulates both UCP1 dependent and independent thermogenesis in human neck area derived adipocytes”.

III) **45th FEBS Congress and 20th FEBS Young Scientist Forum (July 2021)**

Selected for short talk on "Mitophagy is downregulated upon thermogenic stimulus in human beige adipocytes" and presented a poster in Young Scientist Forum.

IV) **Winter School Symposium of Doctoral School of Molecular, Cell and Immune biology, University of Debrecen (January 2021)**

Attended the conference and gave a short talk on “Irisin treatment stimulated the release of CXCL1 but prevented the upregulation of thermogenesis in human primary cervical subcutaneous and deep neck adipocytes”.

V) **Winter School Symposium of Doctoral School of Molecular, Cell and Immune biology, University of Debrecen (January 2020)**

Attended the conference and gave a short talk on “Mitophagy is downregulated upon thermogenic stimulus in human beige adipocytes”.

VI) **EMBO/FEBS Lecture Course on Mitochondria in life, death, and disease (September 2019)**

Attended the lecture course and presented a poster with title “Investigation of the role of mitophagy in primary human white and browning adipocytes”.

VII) **Hungarian Molecular Life Sciences 2019 (March 2019)**

Attended the conference and presented a poster with title “Distinct gene expression patterns, unrelated to thermogenesis, are induced in human adipocytes from the neck in response to Irisin and BMP7”.

VIII) **Winter School Symposium of Doctoral School of Molecular, Cell and Immune biology, University of Debrecen (January 2019)**

Attended the conference and gave a short talk on “Role of autophagy/mitophagy in primary human white and browning adipocytes upon cAMP stimulus”.

IX) **FEBS 3+ 2018 (September 2018, Siofok, Hungary)**

Attended the conference and presented a poster with title “Irisin and BMP7 induce distinct gene expression patterns but not the thermogenic genes in human adipocytes from the neck”.

UNIVERSITY AND NATIONAL LIBRARY
UNIVERSITY OF DEBRECEN
H-4002 Egyetem tér 1, Debrecen
Phone: +3652/410-443, email: publikaciok@lib.unideb.hu

Registry number: DEENK/230/2022.PL
Subject: PhD Publication List

Candidate: Abhirup Shaw
Doctoral School: Doctoral School of Molecular Cellular and Immune Biology
MTMT ID: 10067773

List of publications related to the dissertation

1. **Shaw, A.**, Bartáné Tóth, B., Arianti, R., Csomós, I., Póliska, S., Vámos, A., Bacsó, Z., Győry, F., Fésüs, L., Kristóf, E.: BMP7 increases UCP1-dependent and independent thermogenesis with a unique gene expression program in human neck area derived adipocytes. *Pharmaceuticals (Basel). 14* (11), 1-21, 2021.
DOI: http://dx.doi.org/10.3390/ph14111078
IF: 5.863 (2020)

2. **Shaw, A.**, Bartáné Tóth, B., Király, R., Arianti, R., Csomós, I., Póliska, S., Vámos, A., Korponay-Szabó, I., Bacsó, Z., Győry, F., Fésüs, L., Kristóf, E.: Irisin stimulates the release of CXCL1 from differentiating human subcutaneous and deep-neck derived adipocytes via upregulation of NF[kappa]B pathway.
Front. Cell. Dev. Biol. 9, 1-19, 2021.
DOI: http://dx.doi.org/10.3389/fcell.2021.737872
IF: 6.684 (2020)

3. Szatmári-Tóth, M., **Shaw, A.**, Csomós, I., Mocsár, G., Fischer-Posovszky, P., Wabitsch, M., Balajthy, Z., Lányi, C., Győry, F., Kristóf, E., Fésüs, L.: Thermogenic Activation Downregulates High Mitophagy Rate in Human Masked and Mature Beige Adipocytes.
Int. J. Mol. Sci. 21 (18), 1-21, 2020.
IF: 5.923

List of other publications

4. Vámos, A., **Shaw, A.**, Varga, K., Csomós, I., Mocsár, G., Balajthy, Z., Lányi, C., Bacsó, Z., Szatmári-Tóth, M., Kristóf, E.: Mitophagy Mediates the Beige to White Transition of Human Primary Subcutaneous Adipocytes Ex Vivo.
Pharmaceuticals (Basel). 15 (3), 1-21, 2022.
DOI: http://dx.doi.org/10.3390/ph15030363
IF: 5.863 (2020)

UNIVERSITY of DEBRECEN

UNIVERSITY AND NATIONAL LIBRARY
UNIVERSITY OF DEBRECEN
H-4002 Egyetem tér 1, Debrecen
Phone: +3652/410-443, email: publikaciok@lib.unideb.hu

5. Kapoor, I., **Shaw, A.**, Naha, A., Emam, E. A. F., Varshney, U.: Role of the nucleotide excision repair pathway proteins (UvrB and UvrD2) in recycling UdgB, a base excision repair enzyme in Mycobacterium smegmatis.
   DNA Repair. 113, 1-14, 2022.
   DOI: http://dx.doi.org/10.1016/j.dnarep.2022.103316
   IF: 4.913 (2020)

6. Arianti, R., Vinnai, B. Á., Bartáné Tóth, B., **Shaw, A.**, Csősz, É., Vámos, A., Győry, F., Fischer-Posovszky, P., Wabitsch, M., Kristóf, E., Fésüs, L.: ASC-1 transporter-dependent amino acid uptake is required for the efficient thermogenic response of human adipocytes to adrenergic stimulation.
   FEBS Lett. 595 (16), 2085-2098, 2021.
   DOI: http://dx.doi.org/10.1002/1873-3468.14155
   IF: 4.124 (2020)

7. Bartáné Tóth, B., Arianti, R., **Shaw, A.**, Vámos, A., Veréb, Z., Póliska, S., Győry, F., Bacsó, Z., Fésüs, L., Kristóf, E.: FTO intronic SNP strongly influences human neck adipocyte browning determined by tissue and PPARγ specific regulation: a transcriptome analysis.
   Cells. 9 (4), E987, 2020.
   DOI: https://doi.org/10.1101/2020.02.21.959593
   IF: 6.6

8. Kristóf, E., Klusóczki, Á., Veress, R., **Shaw, A.**, Combi, Z., Varga, K., Győry, F., Balajthy, Z., Bai, P., Bacsó, Z., Fésüs, L.: Interleukin-6 released from differentiating human beige adipocytes improves browning.
   Exp. Cell Res. 377 (1-2), 47-55, 2019.
   DOI: http://dx.doi.org/10.1016/j.yexcr.2019.02.015
   IF: 3.383

9. Kapoor, I., Emam, E. A. F., **Shaw, A.**, Varshney, U.: Nucleoside Diphosphate Kinase Escalates A-to-C Mutations in MutT-Deficient Strains of Escherichia coli.
   J. Bacteriol. 202 (1), 1-10, 2019.
   DOI: http://dx.doi.org/10.1128/JB.00567-19
   IF: 3.004

Total IF of journals (all publications): 46,357
Total IF of journals (publications related to the dissertation): 18,47

The Candidate's publication data submitted to the iDEa Tudóstér have been validated by DEENK on the basis of the Journal Citation Report (Impact Factor) database.

28 April, 2022